Article

Developmental Cell

# Hippo pathway and Bonus control developmental cell fate decisions in the *Drosophila* eye

## Graphical abstract

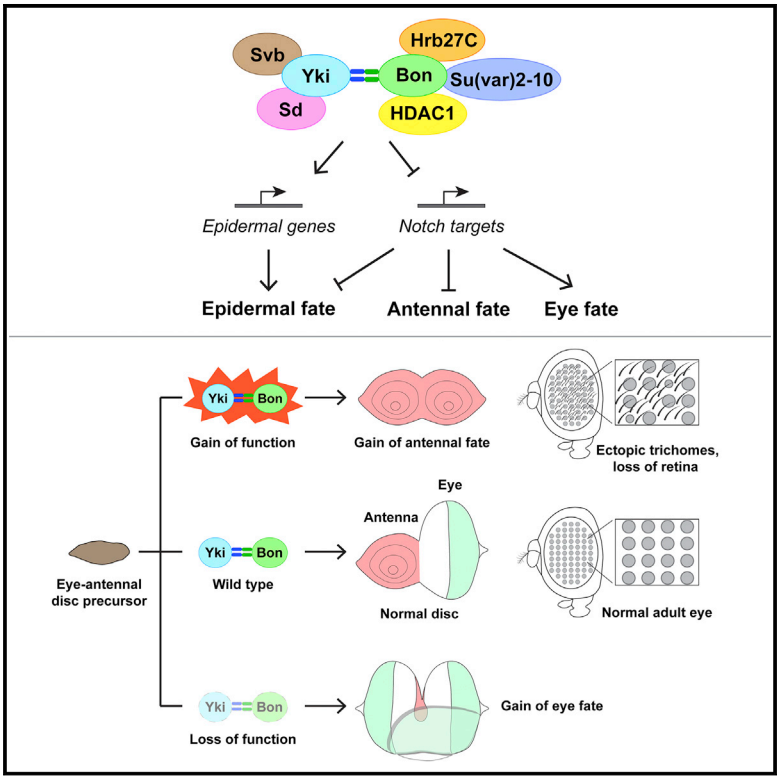


## Highlights

- In *Drosophila*, Bon interacts with Yki through the PPxY motif-WW domain interaction
- The Yki-Bon complex promotes epidermal and antennal fates and suppresses eye fate
- Yki and Bon recruit transcriptional co-regulators for cell-fate control
- Yki and Bon control cell fates via repressing Notch targets

## Authors

Heya Zhao, Kenneth H. Moberg, Alexey Veraksa

## Correspondence

alexey.veraksa@umb.edu

## In brief

Zhao et al. question how different cell fates are specified during *Drosophila* development and show that the Hippo pathway, which has previously been mainly implicated in growth regulation, controls major cell-fate decisions in the eye. This function engages a pathway member, Bonus, and involves a non-canonical transcriptional program.

Zhao et al., 2023, Developmental Cell *58*, 416–434
March 13, 2023 
https://doi.org/10.1016/j.devcel.2023.02.005

CellPress

CellPress

Developmental Cell

Article

# Hippo pathway and Bonus control developmental cell fate decisions in the *Drosophila* eye

Heya Zhao,[1] Kenneth H. Moberg,[2] and Alexey Veraksa[1,3,*]
[1]Department of Biology, University of Massachusetts Boston, Boston, MA 02125, USA
[2]Department of Cell Biology, Emory University School of Medicine, Atlanta, GA 30322, USA
[3]Lead contact
*Correspondence: alexey.veraksa@umb.edu
https://doi.org/10.1016/j.devcel.2023.02.005

## SUMMARY

The canonical function of the Hippo signaling pathway is the regulation of organ growth. How this pathway controls cell-fate determination is less well understood. Here, we identify a function of the Hippo pathway in cell-fate decisions in the developing *Drosophila* eye, exerted through the interaction of Yorkie (Yki) with the transcriptional regulator Bonus (Bon), an ortholog of mammalian transcriptional intermediary factor 1/tripartite motif (TIF1/TRIM) family proteins. Instead of controlling tissue growth, Yki and Bon promote epidermal and antennal fates at the expense of the eye fate. Proteomic, transcriptomic, and genetic analyses reveal that Yki and Bon control these cell-fate decisions by recruiting transcriptional and post-transcriptional co-regulators and by repressing Notch target genes and activating epidermal differentiation genes. Our work expands the range of functions and regulatory mechanisms under Hippo pathway control.

## INTRODUCTION

Tissue growth and cell-fate determination are critical developmental processes controlled by multiple signaling pathways, including the evolutionarily conserved Hippo pathway, whose dysregulation leads to developmental abnormalities and diseases.[1,2] The core Hippo (Hpo, MST1/2 in mammals)/Warts (Wts, LATS1/2 in mammals) kinase cascade inhibits the activity of the transcriptional coactivator Yorkie (Yki, YAP/TAZ in mammals) by phosphorylation and cytoplasmic retention, whereas unphosphorylated nuclear Yki associates with DNA-binding proteins such as Scalloped (Sd, TEAD1–4 in mammals) to activate gene expression.[3,4] The canonical transcriptional targets of the Yki-Sd complex in *Drosophila* include *Cyclin E* (*CycE*), *Death-associated inhibitor of apoptosis 1* (*Diap1*), *bantam* microRNA (*mir-ban*), and *expanded* (*ex*), which promote proliferation, inhibit apoptosis, and enable negative feedback regulation.[5] Although increasing evidence supports the essential role of the Hippo pathway in cell-fate determination,[5,6] the cellular mechanisms remain poorly understood.

The *Drosophila* eye is an excellent model to study gene regulatory networks controlling cell-fate determination.[7] Most of the *Drosophila* adult head structures develop from the larval eye-antennal disc, with the compound eye and ocelli originating from the eye disc compartment, the antenna and maxillary palp from the antennal compartment, and the head epidermis from the tissues surrounding the two compartments.[8] Segregation of the mutually antagonistic eye, antennal, and head epidermal fates, which begins at the second instar larval stage (L2), is regulated by several signaling pathways, including Notch, EGFR, Wingless, and Hedgehog, and retinal determination genes such as *eyeless* (*ey*) and *homothorax* (*hth*).[9,10] Alteration of these regulatory inputs can cause a switch from one fate to another, leading to partial or, in some cases, complete homeotic transformations of the affected structures.[11–14] Key patterning events in the eye are linked to a wave of differentiation called the morphogenetic furrow (MF) that starts in the early third instar larval stage (L3) and proceeds from the posterior to the anterior of the eye disc, resulting in the differentiation of an array of optical units called ommatidia, each consisting of photoreceptor cells, cone cells, primary pigment cells, interommatidial bristles, and secondary and tertiary pigment cells (also called interommatidial cells).[15,16]

Previous studies of the Hippo pathway in *Drosophila* eye differentiation focused on MF progression, terminal differentiation of photoreceptor cells, and formation of peripodial epithelium.[17–20] Mutant analyses of the Hippo pathway components *ex*, *Merlin* (*Mer*), and *mob as tumor suppressor* (*mats*) have suggested an earlier and broader impact of the Hippo pathway in eye specification.[21–24] However, the involvement of the Hippo pathway in controlling major cell-fate decisions among the eye, antenna, and head epidermis remains elusive, and the underlying transcriptional mechanisms are unknown.

We reasoned that the Hippo pathway may function in controlling the eye-antenna-epidermis fate determination through yet unknown interactors that regulate the transcriptional output of the Yki-Sd complex. To identify such interactors, we performed proteomic analyses and identified a Yki-interacting protein, Bonus (Bon). Bon is the only *Drosophila* ortholog of mammalian

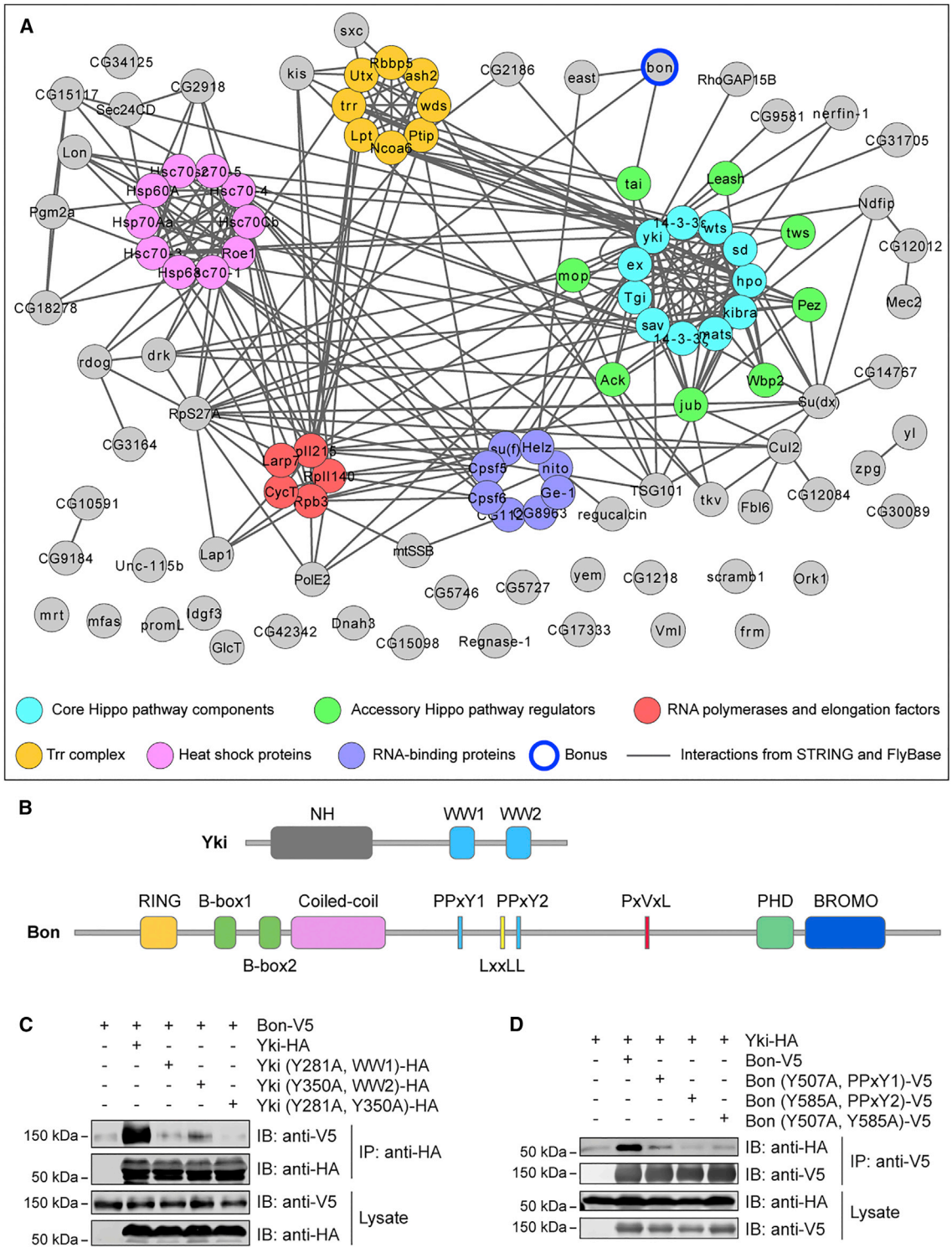


**Figure 1. Identification of Bonus as a Yorkie interactor**

(A) The Yki protein interaction network. AP-MS results of Yki-SBP from *Drosophila* S2 cells and Yki-EGFP from embryos were analyzed with significance analysis of interactome (SAINT).[36] Number of biological replicates: Yki-SBP, 4; blank S2, 4; Yki-EGFP, 3; *yw*, 5. All the interactors (nodes) in this network were identified as significant Yki interactors (SAINT score ≥ 0.8); these interactions (edges) are not shown to avoid clutter. The shown edges were incorporated from the STRING database and FlyBase and include various types of evidence.[37,38] See also method details.

*(legend continued on next page)*

TIF1 family proteins TIF1α (TRIM24), TIF1β (TRIM28/KAP1), TIF1γ (TRIM33), and TIF1δ (TRIM66).[25,26] TIF1/Bon proteins are chromatin-associated factors that activate or repress transcription by binding to co-regulators and controlling chromatin state.[25–28] TIF1 proteins play various roles during vertebrate development and are implicated in cancer.[29–31] *Drosophila* Bon is essential for nervous system development, embryo patterning, metamorphosis, and cell survival.[25,28,32–34]

Here, we present evidence that Bon and the Hippo pathway co-regulate major cell-fate decisions during the development of the *Drosophila* eye. Yki and Bon bind via WW domain-PPxY motif interactions and cooperate to produce epidermal cells in the eye at the expense of ommatidial cells, while the loss of *bon* induces ectopic eye markers, suggesting that the Hippo pathway and Bon control the choice between the eye and epidermal fates. The Hippo pathway and Bon also regulate the eye-antennal specification, with Yki and Bon inhibiting the eye fate and promoting the antennal fate. Through the analysis of Bon and Yki protein interactors, we have identified multiple transcriptional and post-transcriptional regulators that are necessary for their control of cell-fate decisions. Transcriptomic and genetic analyses have revealed that Bon and Yki exert their functions by jointly activating epidermal differentiation genes and, unexpectedly, repressing Notch target genes. Overall, we have identified a function of the Hippo pathway in the eye/antenna/epidermis cell-fate decisions during *Drosophila* eye development. This function requires the interaction of Yki with Bon, their recruitment of co-regulators, and the joint transcriptional control of a non-canonical set of target genes.

## RESULTS

### Bon is a Yki interactor

To identify regulators of the Hippo pathway, we performed affinity purification-mass spectrometry (AP-MS) using *Drosophila* embryos expressing Yki-EGFP with a ubiquitous driver, *da-GAL4*,[35] as well as cultured *Drosophila* S2 cells expressing streptavidin-binding peptide (SBP)-tagged Yki (see method details). We identified the core Hippo pathway components, accessory regulators, and several putative Yki interactors, including Bon (Figure 1A; Table S1). [5,39,40] We confirmed the interaction between Bon and Yki by co-immunoprecipitation (co-IP) of tagged Bon and Yki proteins in S2 cells (Figures 1C and 1D). We hypothesized that the Yki-Bon interaction may be mediated by the two PPxY motifs in Bon (PPLY$^{507}$ and PPSY$^{585}$) binding to the WW domains in Yki (Figure 1B), similar to other known Yki interactors.[40,41] Mutating the key tyrosine residue to alanine[42] in either single or both WW domains in Yki strongly reduced its binding to Bon, with the first WW domain (WW1) showing a stronger reduction in binding upon mutation (Figure 1C). Similarly, substituting tyrosine with alanine in one or both PPxY motifs in Bon also largely reduced its binding to Yki, with a stronger reduction by the mutation in the second PPxY motif (PPxY2) (Figure 1D). These results indicate that Bon interacts with Yki through PPxY motifs in Bon and WW domains in Yki.

### Activation of Bon or Yki induces epidermal trichomes in adult eyes

We next sought to investigate whether Bon is involved in Yki-mediated growth regulation. RNAi knockdown of *bon* did not affect the overgrowth or cell proliferation induced by Yki overexpression in adult eyes, larval eye discs, and wing discs (Figures S1A–S1D). In addition, RNAi knockdown of *bon* in wing discs did not affect the reporters of canonical Yki target genes *Diap1* and *ex* (Figure S1E). Loss-of-function *bon* mutants exhibit ectopic abdominal peripheral neurons in the embryo.[25,32] Null mutants of *wts* (*wts*$^{X1}$)[43] and *yki* (*yki*$^{B5}$)[44] did not show loss or gain of peripheral neurons and did not affect the ectopic neuron phenotype in null (*bon*$^{21B}$) or hypomorphic (*bon*$^{487}$) *bon* mutant embryos (Figure S1F). Collectively, these data argue that Yki and Bon have independent functions in growth regulation and embryonic peripheral nervous system (PNS) development.

Interestingly, overexpression of Bon with *GMR-GAL4*, which drives expression in all cells after the MF and persists through pupal eye development,[45–47] resulted in the formation of trichomes on the surface of adult eyes and disruption of the ommatidial array (Figures 2A, 2B, and S2A), which is consistent with a previous report.[48] Trichomes are actin-rich, non-neuronal apical extensions, which are present on *Drosophila* epidermal cells but not retinal cells.[49,50] This trichome induction suggests that Bon promotes epidermal fate in the eye.

To examine whether the Hippo pathway is involved in Bon trichome induction, we overexpressed or knocked down key components of the Hippo pathway in the Bon overexpression background and quantified trichome numbers. Yki overexpression or *wts* knockdown increased Bon-induced trichomes (Figures 2C, 2D, and 2H). In contrast, the knockdown of *yki* or *sd*[51] strongly suppressed Bon-induced trichomes, with only mild eye roughness observed in single knockdowns (Figures 2E, 2F, 2H, S2B, and S2R–S2T). Thus, the core Hippo pathway and Yki transcriptional activity are essential for Bon-induced trichomes in adult eyes. Furthermore, overexpression of Bon-PPxA, a Bon mutant with both PPxY motifs mutated to PPxA that cannot bind to Yki (see Figure 1D), resulted in significantly fewer trichomes and milder ommatidial defects (Figures 2G and 2H), indicating that Bon must bind Yki to efficiently induce eye trichomes.

We then investigated whether Yki activation is sufficient to induce trichomes in adult eyes. Indeed, Yki overexpression by *GMR-GAL4* resulted in trichome formation in the eye (Figures 2I, S2C, and S2D). Overexpression of constitutively active Yki-S168A, a Yki mutant insensitive to Wts phosphorylation and inhibition,[52] induced even more trichomes (Figures 2J, 2O, and S2G). Knockdown of *wts* also induced more trichomes than Yki overexpression (Figures 2K, 2O, and S2K). Therefore, Yki activation promotes trichome formation, with trichome

(B) Schematic diagram showing the major domains and motifs in Yki and Bon. Note two WW domains in Yki and two PPxY motifs in Bon.
(C) Co-IP of Bon-V5 and wild-type or mutant Yki-HA expressed in S2 cells.
(D) Co-IP of Yki-HA and wild-type or mutant Bon-V5 expressed in S2 cells.
See also Table S1.

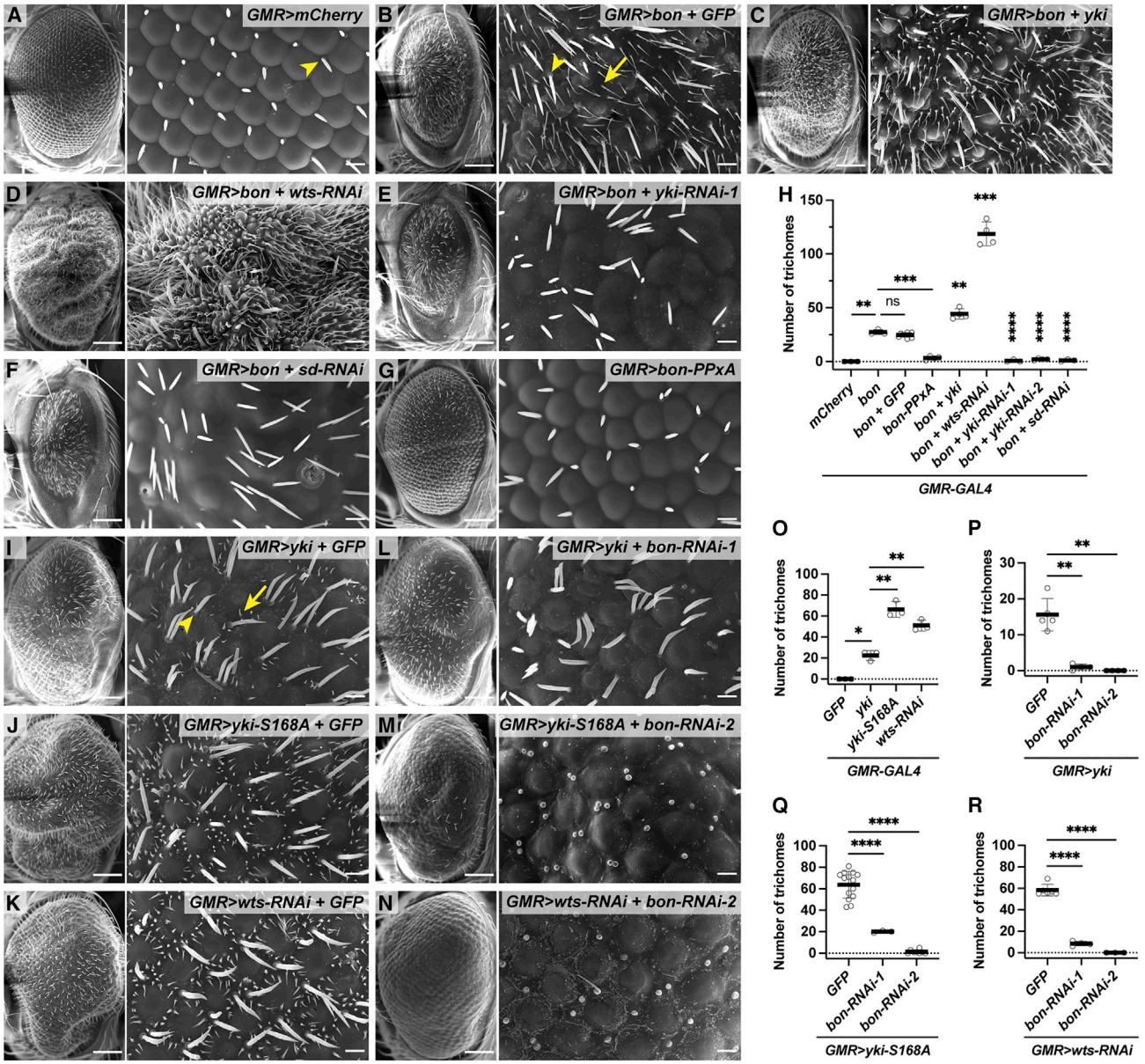


**Figure 2. Activation of Bon or Yki induces epidermal trichomes in adult eyes**

(A–G and I–N) SEM images of adult *Drosophila* eyes expressing indicated *UAS* transgenes with the *GMR-GAL4* driver. Crosses with Bon were carried out at 25°C, and crosses with Yki, Yki-S168A and *wts-RNAi* were set up at 25°C and shifted to 29°C after the emergence of first instar larvae. GFP was coexpressed for transgene dosage compensation. Arrowheads: interommatidial bristles, arrows: trichomes. Scale bars: 100 μm (left panels) and 10 μm (enlarged views).

(H and O–R) Quantification of trichome numbers: (H) for (A-G) and (O-R) for (I-N). Trichome numbers here and thereafter were counted in an area of 1,306 $\mu m^2$. Two additional *bon-RNAis* were used that significantly reduced trichome numbers (Figure S2; Table S5). All quantifications of the phenotypes here and thereafter are provided in Table S5. Data shown as mean ± SD of ≥3 adult eyes.

See also Figure S2 and Table S5.

number positively correlated with Yki activity. Knockdown of *bon* strongly suppressed trichome formation induced by wild-type Yki, Yki-S168A, and *wts*-RNAi, with only mild roughness when knocked down alone (Figures 2L–2N, 2P–2R, and S2D–S2Q), suggesting that Bon is necessary for trichome formation induced by activated Yki. Together, these results show that the Hippo pathway and Bon jointly regulate the ectopic trichome formation in the eye.

## Hippo pathway and Bon control the decision between eye and epidermal cell fates

Next, we investigated cell-fate changes underlying ectopic trichome induction in the retina. The establishment of trichomes occurs at 30–36 h after puparium formation (APF) in the wing and 38–39 h APF in the notum.[50,53] F-actin and cell boundary (Dlg) staining of pupal eyes revealed that Bon-induced trichomes are initiated at 40 h APF (Figures S3A–S3C) and are easily visible

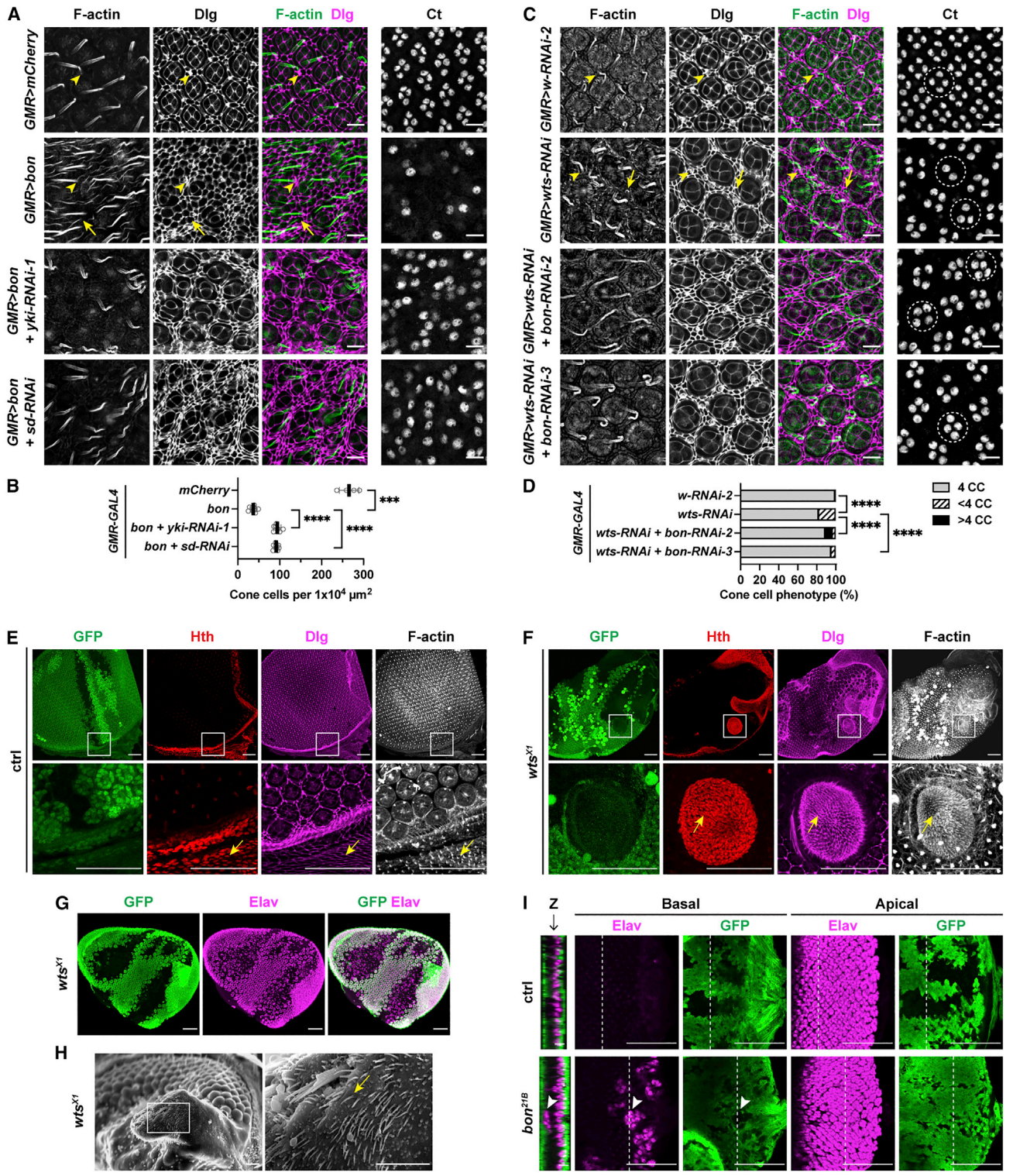


**Figure 3. Yki and Bon promote the epidermal fate at the expense of the eye fate**

(A and C) Pupal eyes expressing the indicated transgenes with *GMR-GAL4* were stained with phalloidin for F-actin and anti-disc large (Dlg) antibody for cell boundaries, or anti-Cut (Ct) antibody for cone cells. (A) 44 h APF grown at 25°C and (C) 40 h APF grown at 29°C (equivalent to 48 h APF at 25°C). Arrowheads: interommatidial bristles and sockets, arrows: trichomes and the corresponding cells, dashed circles in (C): individual cone cell clusters per ommatidium. Scale bars: 10 μm.

*(legend continued on next page)*

at 44 h APF (Figure 3A). Bon overexpression resulted in severe disruption of the ommatidia and produced extra interommatidial-like cells from which the trichomes derive (Figure 3A). Importantly, the excess interommatidial-like cells were generated without alteration in DNA synthesis (Figure S1D) or overall apical cell number (Figure S3D), suggesting a failure of differentiation rather than aberrant proliferation or survival. Interommatidial cells are believed to be the default state in retinal differentiation.[15,54] Trichomes on these cells indicate that they may be reprogrammed into epidermal-like cells. Knockdown of *yki* or *sd* strongly suppressed the initiation of Bon-induced trichomes in the eye and partially restored the ommatidia (Figure 3A). Therefore, Bon induces epidermal cell fate at the expense of the eye fate in a Yki- and Sd-dependent manner.

To determine more precisely which retinal cells were affected, we immunostained pupal eyes at 44 h APF for cone cell marker Ct, primary pigment cell marker BarH1, and photoreceptor cell and bristle group marker Elav.[15] Bon overexpression with *GMR-GAL4* strongly inhibited the formation of cone cells and primary pigment cells, and affected the patterning of photoreceptor cells and bristle groups (Figures 3A, 3B, and S3E). Knockdown of *yki* or *sd* partially rescued the loss of cone cells and the mispatterned photoreceptor cells and bristle groups resulting from Bon overexpression (Figures 3A, 3B, and S3E), but did not rescue the loss of primary pigment cells (Figure S3E), likely because the differentiation of primary pigment cells requires successful differentiation of cone cells.[55] These results demonstrate that Bon, Yki, and Sd jointly suppress eye fate.

*wts* knockdown by RNAi also induced trichomes on interommatidial cells at the mid-pupal stage, suggesting that these cells were reprogrammed into the epidermal fate (Figure 3C). Although the trichomes induced by *wts* RNAi were shorter and thicker than Bon-induced trichomes (Figures 2B and 2K), they were clearly distinguishable from the bristle shafts of the bristle groups, which have sockets (Figure 3C, Dlg staining) and neuronal input (Figure S3F, Elav staining).[15] *bon* knockdown strongly suppressed *wts* RNAi-induced trichome initiation, but not the excess interommatidial cells and bristles which result from overproliferation,[44,56] suggesting that Bon is specifically necessary for cell-fate reprogramming (Figure 3C). Consistent with previous studies, *wts* RNAi reduced the number of cone cells,[17,57] which was rescued by knockdown of *bon* (Figures 3C and 3D). Moreover, *bon* knockdown alone resulted in gain of cone cells, especially at the periphery of the retina (Figures S3H and S3I). Loss of *wts* and *bon* had a mild effect on photoreceptor patterning and showed a mixed outcome for primary pigment cells (either gain or loss per ommatidium) (Figure S3G). Together, these results show that either Bon activation or Wts inactivation behind the MF can induce epidermal fate at the expense of eye fate, as represented by trichome formation and inhibition of cone cells.

We further investigated endogenous control of cell-fate determination using loss-of-function clones of *wts* and *bon* alleles. Trichomes were apparent in $wts^{X1}$ eye clones at 46 h APF, and the trichome-making cells strongly expressed Hth, which normally marks the head epidermis at this stage (Figures 3E and 3F).[58,59] $wts^{X1}$ clones also suppressed eye fate, as evidenced by the loss of ommatidia (Dlg in Figure 3F) and photoreceptors (Elav in Figure 3G). In adult eyes, $wts^{X1}$ clones produced outgrowths of epidermal tissue covered with trichomes (Figure 3H). Interestingly, $bon^{21B}$ clones led to gain of neuronal eye marker Elav at the basal side of the larval eye disc without affecting the normal apical patterns of Elav, suggesting an induction of ectopic eye fate (Figure 3I). Altogether, our results using both loss- and gain-of-function analyses suggest that Bon and Yki suppress eye fate and promote epidermal fate.

## Hippo pathway and Bon regulate the choice between eye and antennal cell fates

Because eye fate is antagonistic to epidermal and antennal fates,[10] we asked whether Hippo and Bon also regulate the balance of eye-antennal fates. To explore this hypothesis, we used the early eye driver *ey-GAL4*, which is expressed in the entire eye disc beginning at the L2 stage, and examined L3 eye-antennal discs using Hth and Ct as antennal markers and Elav as the differentiated neuron/eye marker.[12,14,60,61] *wts* knockdown or Yki-S168A overexpression by *ey-GAL4* significantly suppressed the eye field, with the respective penetrance of 56% (*wts*-RNAi), 100% (*yki-S168A*-1), and 85% (*yki-S168A*-2), and even occasionally led to a complete eye-to-antenna transformation, with the respective penetrance of 11%, 5%, and 6% (Figures 4A–4C′, 4I, S4A–S4C′, S4E–S4E′, S4I–S4K′, and Table S5). Remarkably, *wts* knockdown or Yki-S168A overexpression also led to clear eye-to-antenna transformations in some adult flies (Figures 4E–4G). Wild-type Yki overexpression with *ey-GAL4* suppressed the eye field and resulted in extra epidermal bristles

(B and D) Quantification of cone cell numbers per area ($1 \times 10^4$ $\mu m^2$) due to a severe phenotype (B) or per ommatidium (D) for genotypes in (A) and (C), respectively. Data in (B) shown as mean ± SD of ≥4 pupal eyes. *p* values in (D) were determined by Fisher's exact test for ommatidia with ≥4 cone cells (CC) and those with <4 CC per ommatidium. Number of cone cell clusters quantified in (D): n ≥ 300 from ≥4 pupal eyes.
See also Table S5 for details.
(E and F) Pupal eyes at 46 h APF with mosaic clones generated by heat shock at 39 h after egg deposition (AED) and marked by absence of GFP were stained with anti-Hth antibody for head epidermis, anti-Dlg antibody for cell boundaries, and phalloidin for F-actin. Enlarged views of the boxed regions are shown in the bottom panels. Arrows: trichomes and the corresponding cells in wild-type head cuticle (E) or ectopic epidermis in the eye (F). Scale bars, 50 μm.
(G) Pupal eye at 46 h APF with mosaic clones of $wts^{X1}$ induced by heat shock at 42 h AED was immunostained with anti-GFP antibody to negatively mark the clones and anti-Elav antibody for neuronal eye fate. Scale bars, 50 μm.
(H) A representative adult eye with mosaic clones of $wts^{X1}$ generated with heat shock at 39 h AED. Right panel: enlarged view of the boxed region. Arrow: trichome. Scale bars, 20 μm.
(I) L3 eye discs with mosaic clones generated with *eyFLP* were immunostained with anti-GFP and anti-Elav antibodies. Z: orthogonal sections at the dashed lines of basal/apical views. Arrows: ectopic expression of the eye marker (Elav) and the corresponding clone (loss of GFP). The orthogonal sections and their scale bars were scaled 2× along the z axis for easier visualization. Scale bars: 5 μm in orthogonal views and 50 μm in basal/apical views.
Detailed genotypes of controls and mutants are given in method details.
See also Figure S3 and Table S5.

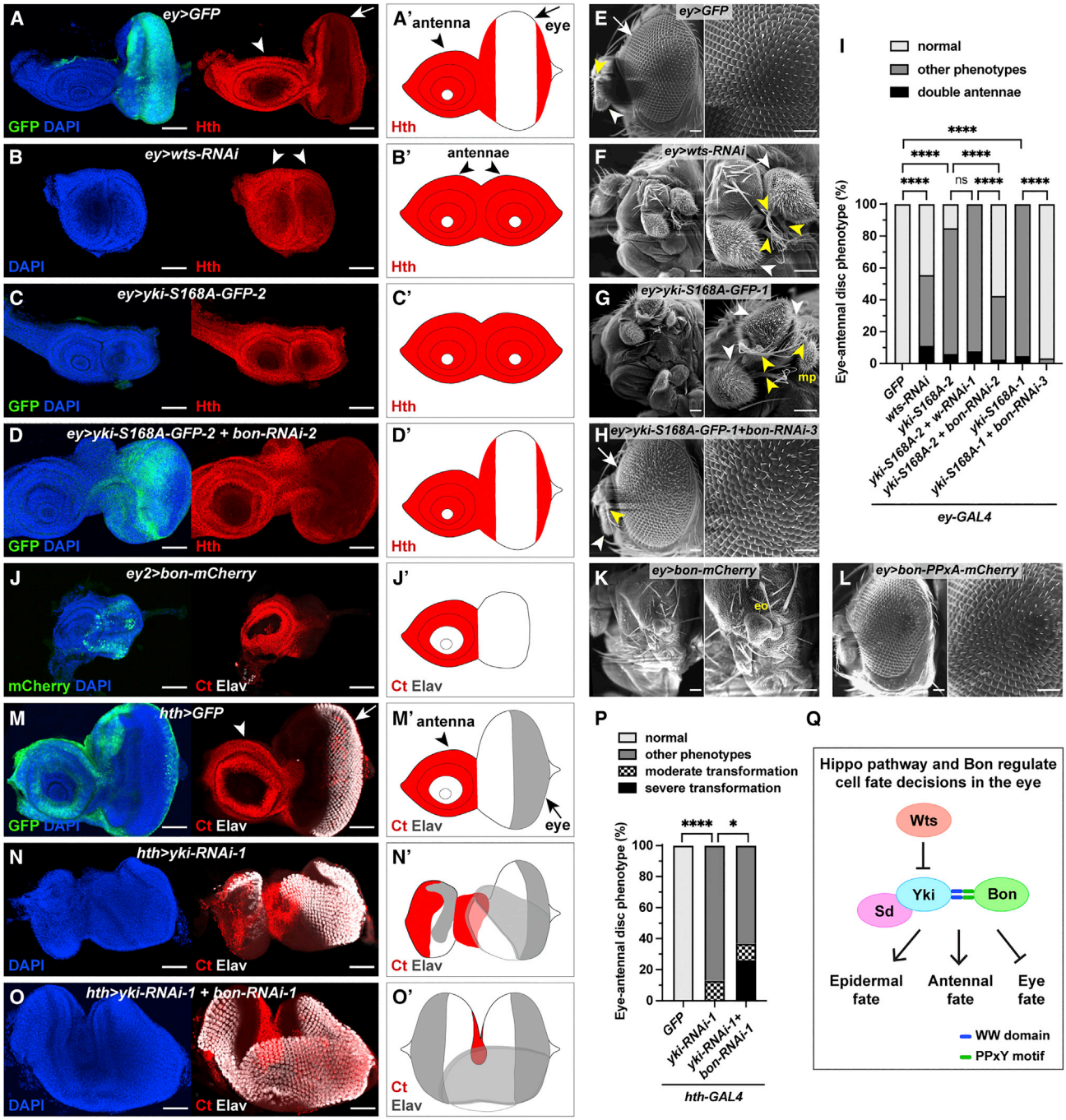


**Figure 4. Yki and Bon promote antennal fate and suppress eye fate**

(A–D′) L3 eye-antennal discs expressing indicated transgenes with *ey-GAL4* were immunostained with anti-Hth antibody for the antennal field. (A′–D′) Schematic illustrations for (A)–(D).

(E–H) Representative images of adult heads with indicated genotypes. *ey>wts-RNAi* had double antennae with three aristae (F). *ey>yki-S168A* had double or triple antennae with one arista each and an ectopic maxillary palp (mp) (G). Right panels: enlarged views of the phenotypes, arrows: eyes, white arrowheads: antennal a3 segments, yellow arrowheads: aristae.

(I) Quantification of the phenotypes in eye-antennal discs shown in (A)–(D), (S4A)–(S4F), and (S4I)–(S4K). *p* values were determined by Fisher's exact test for normal and abnormal eye discs. Number of discs quantified: n ≥ 18. See also Table S5 for details.

(J–J′) L3 eye-antennal disc expressing *bon-mCherry* with *ey-GAL4-2* was immunostained with anti-Ct antibody for the antennal field and anti-Elav antibody for the neuronal eye fate. mCherry and Ct signals were colored green and red, respectively. (J′) Schematic illustration of (J). Control with GFP expressed under the same driver is shown in (S4O)–(S4O'). Penetrance: 20% (n = 15).

*(legend continued on next page)*

(vibrissae) and occasional epidermal outgrowths, but without eye-to-antenna transformation (Figures S4G and S4H).

*bon* knockdown significantly rescued the smaller eye field resulting from Yki-S168A overexpression (from 100% to 3%, and 85% to 43%, with two lines) and suppressed the formation of double antennae (from 5% to 0%, and 6% to 2.5%, with two lines) (Figures 4D–4D′, 4I, S4D–S4D′, S4F–S4F′, and Table S5). In adults, *bon* knockdown also largely rescued Yki-S168A-induced eye loss (Figure 4H). Bon overexpression using *ey-GAL4* suppressed the differentiated eye field in eye-antennal discs with a penetrance of 20% (Figures 4J–4J′, S4O–S4O′, and Table S5), and led to a complete or partial loss of the eye with a penetrance of 18% and frequent epidermal outgrowths in adults (Figure 4K and Table S5), but without eye-to-antenna transformation. In contrast, Bon-PPxA overexpression led to largely normal eyes (Figure 4L and Table S5). Altogether, these results show that early and strong activation of Yki across the eye field can switch the eye fate to antennal fate in a Bon-dependent manner, while the weaker activation of Yki or Bon transforms the eye to the epidermis.

To determine whether the eye vs. antennal fate choice is under the control of endogenous *yki* and *bon*, we tested the effects of *yki*/*bon* loss in the antenna using the *hth-GAL4* driver.[14,58] Because eye and antennal fates are mutually antagonistic and reciprocally transformable,[14] we hypothesized that the loss of *yki* or *bon* in the antenna would promote eye fate. Indeed, *yki* knockdown alone resulted in variable degrees of antenna loss with 100% penetrance and moderate antenna-to-eye transformations (13% penetrance) (Figures 4M–4N′, 4P, S4L–S4N′, and Table S5). This partial antenna-to-eye transformation exhibited loss of Ct and gain of Elav in the antennal field, suggesting a suppression of the antennal fate and differentiation of ectopic eye tissue (Figure 4N). Strikingly, a double knockdown of *yki* and *bon* resulted in a severe antenna-to-eye transformation with a 26% penetrance in which the antennal field marked by Ct was restricted to the center of the eye-antennal disc and the ectopic Elav pattern resembled a mirror-image duplication of the endogenous eye field (Figures 4O and 4P). These results demonstrate that endogenous Yki and Bon are necessary for the specification of the antennal fate and the suppression of the eye fate. Altogether, our results support a model of eye specification regulated by the Hippo pathway and Bon, where Yki and Bon promote the epidermal and antennal fates and suppress the eye fate (Figure 4Q).

## Interactors of Bon and Yki are required for the eye-epidermal fate choice

We sought to further investigate the mechanism through which Yki and Bon regulate the eye-epidermal fate choice. One potential mechanism is that Bon enhances Yki activity by competing Yki away from Wts, given that both Bon and Wts bind to Yki through the PPxY-WW interaction. However, co-IP in S2 cells showed no competition between Bon and Wts for binding to Yki (Figure S5A). This result suggests that rather than competing with Wts, Bon may employ another mechanism, such as engaging a special set of interactors to mediate the eye-epidermal cell-fate decision together with Yki.

To identify Bon cofactors, we analyzed the Bon interactome by AP-MS using Bon-SBP expressed in S2 cells (Figure 5A and Table S2). Yki was identified as one of the top Bon interactors, further validating their interaction (Figure 5A). In addition, we identified Histone deacetylase 1 (HDAC1), Suppressor of variegation 2-10 (Su(var)2-10), and Heterogeneous nuclear ribonucleoprotein at 27C (Hrb27C) as top Bon interactors (Figure 5A). HDAC1 and its mammalian orthologs are key components of several transcriptional corepressor complexes, such as NuRD, Sin3, and CoRest.[62] Su(var)2-10 belongs to the PIAS family of SUMO ligases and controls gene transcription as well as *Drosophila* eye specification.[63–65] Hrb27C is an abundant hnRNP that is involved in various aspects of post-transcriptional mRNA regulation and is implicated in the modulation of Yki activity.[66–68] We tested whether these three Bon interactors are involved in trichome formation in adult eyes. Knockdown of *HDAC1* strongly suppressed—whereas its overexpression enhanced—both Bon- and Yki-S168A-induced trichomes (Figures 5B, 5C, 5G, 5H, 5L, S5B, and S5C), and knockdown of *Su(var)2-10* or *Hrb27C* suppressed these trichomes (Figures 5D, 5E, 5I, 5J, 5L, S5B, and S5C). Therefore, HDAC1, Su(var)2-10, and Hrb27C promote Bon- or Yki-induced epidermal fate in the eye.

The transcription factor Shavenbaby/Ovo (Svb/Ovo) plays a key role in the formation and patterning of epidermal trichomes.[50,69] Also, Svb interacts with Yki and regulates apoptosis through *Diap1*.[70] We tested whether Svb/Ovo was involved in the regulation of Bon- and Yki-induced trichomes in adult eyes. Overexpression of the constitutive activator OvoB enhanced Bon- and Yki-S168A-induced trichomes, while overexpression of the constitutive repressor OvoA, or knockdown of somatic *svb*, strongly suppressed Bon- and Yki-S168A-induced trichomes (Figures 5F, 5K, 5L, S5B, and S5C).[50,71] These results suggest that Svb/Ovo is required for ectopic trichome generation in the eye induced by Bon or Yki.

We then asked whether these interactors are involved in Bon- and Yki regulated suppression of eye fate. In pupal eyes, knockdown of *HDAC1* or *svb* with *GMR-GAL4* suppressed Bon-induced trichomes but did not rescue the loss of cone cells (Figures 5M and 5N). In contrast, knockdown of *Su(var)2-10* or *Hrb27C* not only suppressed the trichomes but also largely

(K and L) Representative images of adult heads with indicated genotypes. Right panels: enlarged views of the phenotypes, eo: epidermal outgrowth. Loss of eye penetrance: 18%, n = 56 (K); 0%, n = 35 (L).

(M–O′) L3 eye-antennal discs expressing indicated transgenes with *hth-GAL4* were immunostained with anti-Ct and anti-Elav antibodies. Representative moderate (N) and severe (O) antenna-to-eye transformations are shown. (M′–O′) Schematic illustrations of (M)–(O).

(P) Quantification of the phenotypes in eye-antennal discs shown in (M)–(O) and (S4L)–(S4N). *p* values were determined by Fisher's exact test for normal and abnormal antennal discs (*GFP* vs. *yki-RNAi-1*) or for severe transformation and non-severe phenotypes (*yki-RNAi-1* + *bon-RNAi-1* vs. *yki-RNAi-1*). Number of discs quantified: $n \geq 19$.

(Q) Model showing that the Yki-Bon complex promotes epidermal and antennal fates and suppresses eye fate.

All scale bars in Figure 4: 50 μm. See also Figure S4 and Table S5.

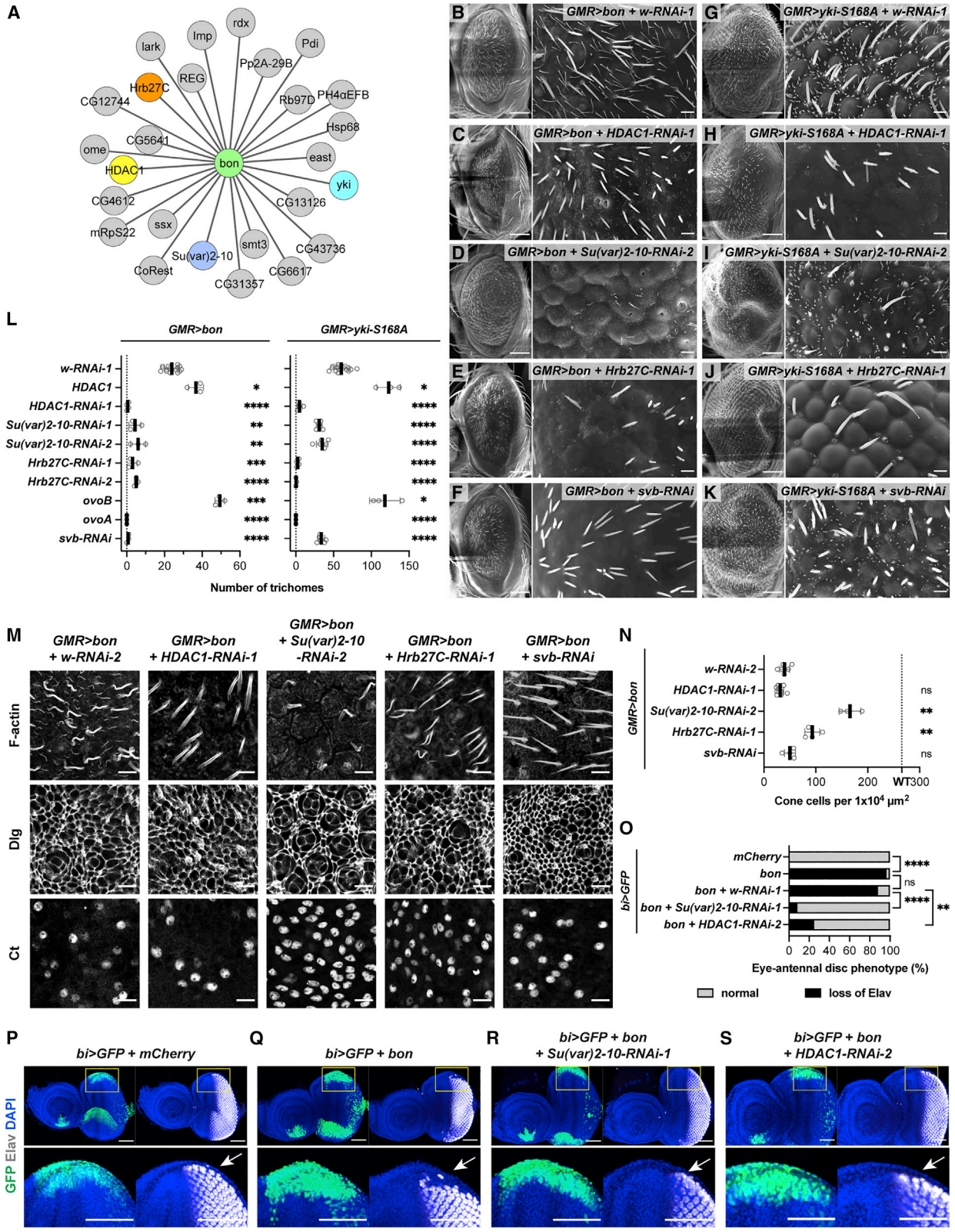


**Figure 5. Interactors of Bon and Yki are required for the eye-epidermis fate decision**

(A) Bon protein interactome showing significant interactors (SAINT score ≥ 0.8) identified from AP-MS of Bon-SBP in S2 cells. Highlighted interactors were tested in genetic experiments. Number of biological replicates: Bon-SBP, 2; blank S2, 3.

*(legend continued on next page)*

rescued the number of cone cells (Figures 5M and 5N). Interestingly, *Su(var)2-10* RNAi even partially restored the loss of primary pigment cells and mispatterned ommatidial array (Figure S5D). These results suggest that Su(var)2-10 and Hrb27C contribute to both eye fate suppression and epidermal fate promotion in the pupal eye, while HDAC1 and Svb/Ovo are only involved in the latter function at this stage. In L3 eye-antennal discs, Bon overexpression with the *bi-GAL4* driver, which drives expression at the dorsal and ventral margins of the eye disc from L2 stage,[72] inhibited Elav expression (Figures 5O–5Q), similar to Yki overexpression in a previous report.[17] Knockdown of *Su(var)2-10* or *HDAC1* suppressed the loss of Elav due to Bon overexpression (Figures 5R, 5S, and 5O). Furthermore, knockdown of *HDAC1* using *ey-GAL4* suppressed the loss of eye field due to Yki-S168A overexpression (Figures S5E–S5G). Collectively, these results suggest that Bon, Yki, Hrb27C, Su(var)2-10, and HDAC1 work together to suppress eye fate and promote epidermal fate, with the involvement of Svb/Ovo in the latter.

### Bon and Yki control cell-fate decisions in the eye through transcriptional regulation of joint target genes

Because Bon, Yki, and their interactors described above are all transcriptional or post-transcriptional regulators, we hypothesized that they mediate cell-fate choices in the eye by regulating a unique set of transcriptional targets. To identify these target genes, we performed RNA sequencing (RNA-seq) using pupal eyes at 40–41 h APF (when the trichomes initiate) that overexpressed Bon, with or without a simultaneous RNAi knockdown of *yki*. Through differential gene expression analysis, we identified 216 genes as Bon-activated/Yki-dependent genes, and 119 genes as Bon-repressed/Yki-dependent genes (Figures 6A, S6A, and S6B; Table S3). Correlation coefficient analysis revealed the significantly concordant regulation of gene expression by Bon and Yki (Figure 6B). Also, *ex* and *Rhodopsin 5* (*Rh5*), which are known targets of Yki in the pupal eye,[18,77] were among Bon-activated/Yki-dependent genes (Figures 6A, S6A, and S6B). These transcriptomic data suggest that Bon and Yki work together to regulate gene expression in pupal eyes, consistent with our genetic results.

We evaluated genes jointly regulated by Bon and Yki by Gene Ontology analysis of Biological Process (GO_BP, Table S4). Bon-activated/Yki-dependent genes were enriched for GO terms "epidermal cell differentiation," "cuticle development," and "sensory perception of taste," while Bon-repressed/Yki-dependent genes were enriched for GO terms "compound eye development" and "Notch signaling pathway," consistent with the genetic function of Bon and Yki in promoting epidermal/antennal fates and suppressing the eye fate (Figure 6C). Bon-activated/Yki-dependent epidermal genes, *shavenoid* (*sha*), *forked* (*f*), *nyobe* (*nyo*), and *neyo* (*neo*), are known Svb/Ovo target genes that are essential for the formation and patterning of epidermal trichomes, suggesting that they may mediate Bon- and Yki-induced trichome formation in the eye (Figures 6A and 6C).[69,78] Bon-repressed/Yki-dependent Notch pathway genes, *E(spl)mdelta-HLH*, *E(spl)m3-HLH*, and *E(spl)m2-BFM*, are members of the Enhancer of split gene complex (*E(spl)-C*), which is a major transcriptional target of Notch (Figures 6A and 6C).[79,80] Two other Notch target genes, *ct* and *Transcription factor AP-2* (*TfAP-2*), were also identified among Bon-repressed/Yki-dependent genes (Figure 6A).[81,82] Previous work showed that Notch signaling promotes eye fate and suppresses antennal fate and that Notch, E(spl)-C, Ct, and TfAP-2 are all critical for cell-fate establishment in the eye.[12,14,55,83–86] These observations raised an intriguing possibility that downregulation of Notch targets by Yki and Bon mediates the suppression of eye fate and the promotion of antennal fate. Finally, Bon-activated/Yki-dependent genes included sensory perception genes such as antenna-specific odorant receptor *Or47b*, as well as a group of gustatory receptors (*Gr64a-f*) that are expressed in multiple sensory organs, including the antenna, indicating the induction of antennal identity at the molecular level (Figures 6A, 6C, S6A, and S6B).[87–90]

We validated the transcriptional regulation of *sha*, *f*, *E(spl)m3-HLH*, *E(spl)m2-BFM*, and *E(spl)mdelta-HLH* by Bon and Yki using target-specific qRT-PCR, which generally confirmed the RNA-seq findings (Figure 6D). To determine whether the transcriptional targets of Yki and Bon are under their direct control, we analyzed published chromatin immunoprecipitation sequencing (ChIP-seq) datasets for Yki and Bon, and the DNA adenine methyltransferase identification sequencing (DamID-seq) dataset for Sd.[74–76] Pairwise overlaps of binding sites were significant, with 75 loci shared among all three proteins, including the *E(spl)-C* region, suggesting a general co-localization of Yki, Bon, and Sd on chromosomes and their direct control of *E(spl)-C* (Figures 6E and S6C). Yki and Sd also bound to *ct* and *TfAP-2*, raising the possibility of a direct regulation (Figure S6C). Yki, Sd, and Bon did not associate with the epidermal differentiation genes and antennal sensory receptor genes, except for Yki binding to *neo*, suggesting indirect activation of these genes by Bon and Yki (Figure S6C). To validate the binding of Bon to the *E(spl)mdelta-HLH* genomic locus, we performed ChIP-qPCR using L3 eye-antennal discs expressing Bon-mCherry with *GMR-GAL4*. We chose two DNA segments (P1 and P2) that overlapped the Yki and Sd binding regions (Figure 6F). Bon bound to

(B–K) SEM images of adult eyes with indicated genotypes. Scale bars: 100 μm (left panels) and 10 μm (enlarged views).
(L) Quantification of the trichome numbers for the indicated genotypes in (B)–(K) and (S5B) and (S5C). Data shown as mean ± SD of ≥3 adult eyes. See also Table S5 for details.
(M) Pupal eyes at 44 h APF with indicated genotypes were stained with phalloidin for F-actin and anti-Dlg antibody for cell boundaries, or anti-Ct antibody for cone cells. Scale bars: 10 μm.
(N) Quantification of the cone cell numbers per 1 × $10^4$ $\mu m^2$ area in (M). Dashed line indicates the mean cone cell number in WT (*GMR>mCherry*) shown in Figure 3B. Data shown as mean ± SD of ≥3 pupal eyes.
(O) Quantification of the phenotypes in eye-antennal discs shown in (P)–(S). *p* values were determined by Fisher's exact test for normal and loss-of-Elav populations. Number of discs quantified: n ≥ 8.
(P–S) L3 eye-antennal discs expressing indicated transgenes with the *bi-GAL4* driver were immunostained with anti-Elav antibody. Bottom panels: enlarged views of the dorsal margins (boxed). Arrows: Elav expression at the dorsal margins. Scale bars: 50 μm.
See also Figure S5 and Tables S2 and S5.

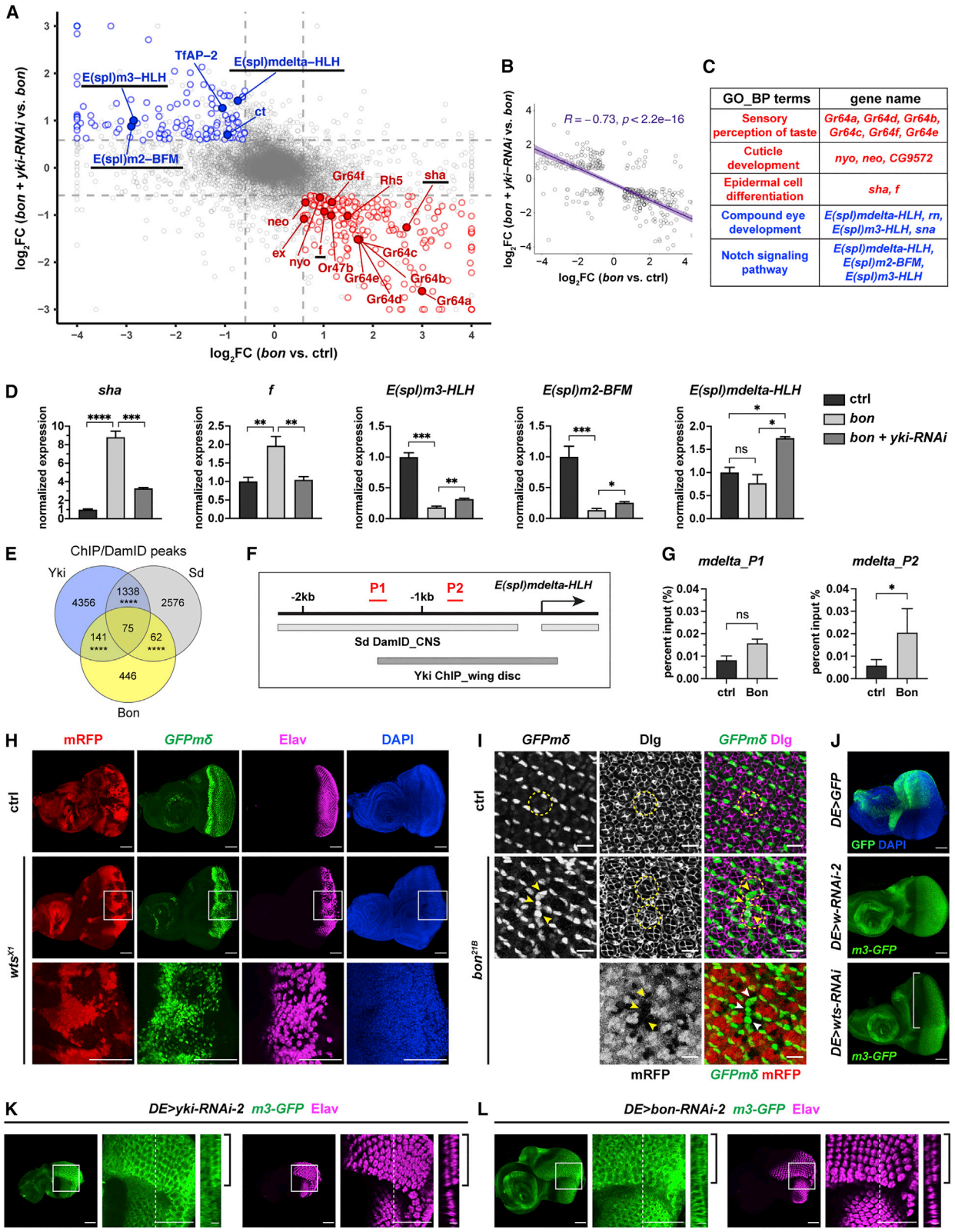


**Figure 6. Bon and Yki jointly regulate a set of non-canonical transcriptional target genes**

(A) Differential gene expression analysis of RNA-seq data from pupal eyes at 40-41 h APF. Output from DESeq2[73] from biological triplicates for each condition was plotted using $\log_2$ fold changes (FC) for *GMR>bon-mCherry + yki-RNAi-1* vs. *GMR>bon-mCherry* (y axis) and that for *GMR>bon-mCherry* vs. *GMR>mCherry*

*(legend continued on next page)*

P2 but did not significantly associate with P1 (Figure 6G). Together, these results suggest that Bon and Yki jointly and directly repress Notch targets and indirectly activate epidermal and antennal genes.

Identification of genes that are repressed by Yki and Bon was unexpected and suggests that binding by Bon may shift Yki activity toward repression. We further evaluated the repression of *E(spl)-C* by Bon and Yki using a transgene reporter expressing GFP-tagged E(spl)mdelta-HLH (*GFPmδ*) and a transcriptional reporter of *E(spl)m3-HLH* (*m3-GFP*).[91] In the L3 eye disc, both reporters are expressed within and posterior to the MF (Figures 6H and 6J). $wts^{X1}$ clones showed strongly reduced expression of *GFPmδ* and *m3-GFP* and moderately reduced Elav (Figures 6H and S6D). In pupal eyes at 25 h APF, *GFPmδ* is mainly expressed in primary pigment cells (Figure 6I). $bon^{21B}$ clones resulted in a gain of *GFPmδ*-positive cells, suggesting that Bon suppresses *E(spl)mdelta-HLH* expression and inhibits the primary pigment cell fate (Figure 6I). *wts* knockdown with the *DE-GAL4* driver, which is expressed in the dorsal eye in both columnar cells of the disc proper (DP) and squamous peripodial epithelium (PE) (Figure S6E),[92] reduced *GFPmδ*, *m3-GFP*, and Elav (Figures 6J and S6F). Knockdown of *yki* or *sd* expanded *GFPmδ*, *m3-GFP*, and Elav into the PE (Figures 6K and S6G–S6I), reminiscent of a PE-to-DP transformation previously reported for the loss of *yki* and *sd*.[19] *bon* knockdown also led to an occasional expansion of *m3-GFP* and Elav into the PE, with a penetrance of 8.3% and 12.5% for two RNAi lines (Figures 6L and S6J; Table S5). Together, these results show that Bon, Yki, and Sd repress, while Wts promotes, the expression of *E(spl)mdelta-HLH* and *E(spl)m3-HLH* during eye development.

We then asked whether the target genes we identified are involved in the eye-antenna-epidermis fate determination controlled by Bon and Yki. Sha overexpression enhanced, whereas *f* knockdown suppressed, trichomes induced by Bon and Yki-S168A in adult eyes (Figures 7A–7C, 7E–7G, 7I, and S6K–S6L). Therefore, *sha* and *f* promote Bon/Yki-induced epidermal fate in the eye, consistent with their transcriptional activation by Bon and Yki. In contrast, overexpression of E(spl) mdelta-HLH and E(spl)m3-HLH suppressed the trichomes induced by Bon and Yki-S168A, suggesting that they inhibit the epidermal fate in the eye, in agreement with their transcriptional repression by Bon and Yki (Figures 7D, 7H, 7I, S6M, and S6N). Overexpression of E(spl)m3-HLH significantly rescued the loss of eye field and completely suppressed the formation of double antennae due to Yki-S168A overexpression, suggesting that E(spl)-C promotes eye fate and suppresses antennal fate (Figures 7J–7K′, and S5G; Table S5). Therefore, Bon and Yki control cell-fate decisions in the eye through transcriptional regulation of a set of non-canonical target genes: activation of *sha* and *f* and repression of *E(spl)-C* genes.

## DISCUSSION

We have revealed a previously unappreciated and profound role of the Hippo pathway in controlling cell-fate determination in the *Drosophila* eye (Figure 7L). This function depends on a regulatory program in which Yki and Bon interact and likely function within larger multiprotein complexes that include other transcriptional and post-transcriptional regulators. Instead of mediating the previously described independent functions of Yki (growth control) and Bon (PNS differentiation), the Yki-Bon module regulates proper segregation of the eye, epidermal, and antennal fates in the developing eye. This function involves promotion of the epidermal and antennal fates, and suppression of the eye fate, via transcriptional regulation of a distinct set of target genes (Figure 7L). Our study thus provides a molecular mechanism for the

(ctrl) (x axis). Dashed lines: FC = 1.5 in both directions. Red circles: Bon-activated/Yki-dependent genes. Blue circles: Bon-repressed/Yki-dependent genes. All colored circles fulfill $p$ adj. $\leq$ 0.05. Solid circles with labels: genes of interest. Labels underlined: genes validated with qRT-PCR.

(B) Pearson correlation coefficient analysis of genes jointly regulated by Bon and Yki. Axes are the same as in (A). All genes with FC $\geq$ 1.5 in both directions and $p$ adj. $\leq$ 0.05 were included in the analysis.

(C) Terms of interest from GO_BP analysis of Bon-activated/Yki-dependent (red) and Bon-repressed/Yki-dependent (blue) genes. Complete GO_BP analysis is in Table S4.

(D) qRT-PCR validation for the genes of interest using 40–41 h APF pupal eyes with the genotypes *GMR>mCherry* (ctrl), *GMR>bon-mCherry*, and *GMR>bon-mCherry + yki-RNAi-1*. Data shown as mean ± SD of biological triplicates.

(E) Venn diagram showing the overlaps in chromatin binding sites among Yki, Bon, and Sd analyzed using published datasets: Yki ChIP-seq from wing discs,[74] Bon ChIP-seq from embryos,[75] and Sd DamID-seq from larval CNS.[76]

(F) Schematic diagram showing the genomic region around the transcription start site (arrow) of *E(spl)mdelta-HLH* (−2.2 to +0.5 kb). Yki and Sd binding regions from previous publications are indicated.[74,76] P1 and P2: amplicons for ChIP-qPCR.

(G) ChIP-qPCR analysis for the binding of Bon to P1 and P2 shown in (F), using L3 eye-antennal discs from *GMR>mCherry* (ctrl) and *GMR>bon-mCherry*. Data shown as mean ± SD of biological triplicates.

(H) L3 eye-antennal discs with mosaic clones generated by *eyFLP* and negatively marked by mRFP were immunostained with anti-GFP antibody for the *GFPmδ* reporter and anti-Elav antibody. Bottom panels for $wts^{X1}$: enlarged views of the boxed area. Scale bars: 50 μm.

(I) Pupal eyes at 25 h APF of control (*DE>w-RNAi*) and $bon^{21B}$ mosaic clones were immunostained with anti-GFP antibody for the *GFPmδ* reporter and anti-Dlg antibody for cell boundaries. $bon^{21B}$ clones were generated with *eyFLP* and marked by the absence of mRFP. Dashed circles: individual ommatidium, arrowheads: ectopic expression of *GFPmδ* in $bon^{21B}$ clones. Scale bars: 10 μm.

(J) L3 eye-antennal discs expressing indicated transgenes with *DE-GAL4*. The expression region of the driver is shown with GFP in the top panel here and in Figure S6E. Signal from the *m3-GFP* reporter was amplified by immunostaining with anti-GFP antibody. Bracket: loss of *m3-GFP* in the dorsal compartment of *DE>wts-RNAi*. Scale bars: 50 μm.

(K and L) L3 eye-antennal discs expressing indicated transgenes with *DE-GAL4* were immunostained with anti-GFP antibody for the *m3-GFP* reporter and anti-Elav antibody. Penetrance of (L): 8.3% (n = 12). Left and middle panels are focused on the PE layer. Middle panels: enlarged views of the boxed regions, right panels: orthogonal sections at the dashed lines, brackets: gain of *m3-GFP* and Elav in the PE layer of the dorsal compartment. The orthogonal sections and their scale bars were scaled 2× along the z axis for easier visualization. Scale bars: 5 μm in orthogonal views and 50 μm in others.

Detailed genotypes of controls and mutants are given in method details.

See also Figure S6 and Tables S3–S5.

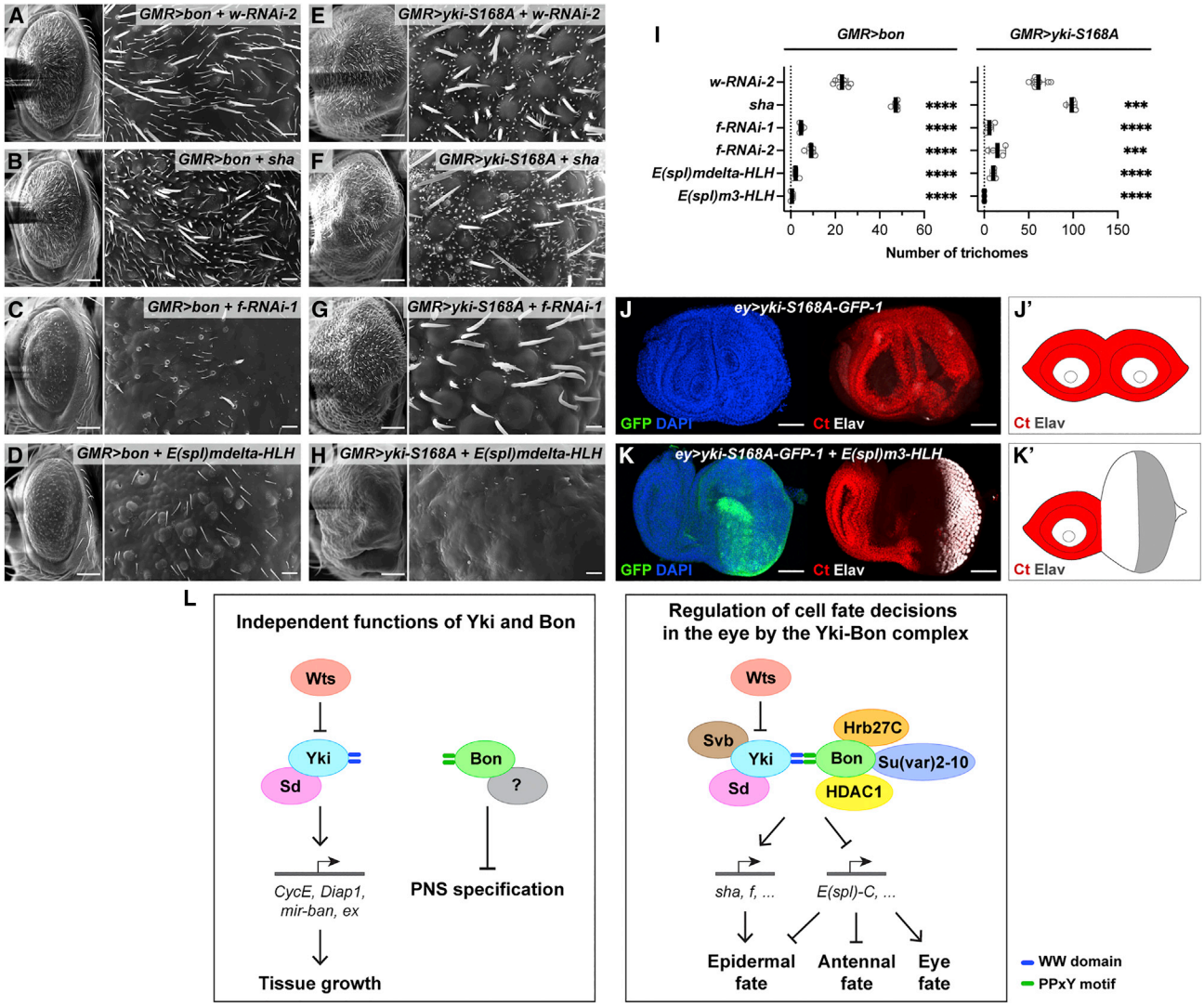


**Figure 7. Bon and Yki control the eye-antenna-epidermis fate determination through their joint transcriptional targets**

(A–H) SEM images of adult eyes with indicated genotypes. Scale bars: 100 μm (left panels) and 10 μm (enlarged views).

(I) Quantification of trichome numbers for the indicated genotypes in (A)–(H) and (S6K)–(S6N). Data shown as mean ± SD of ≥3 adult eyes. See also Table S5 for details.

(J–K′) L3 eye-antennal discs with indicated genotypes were immunostained with anti-Ct and anti-Elav antibodies. (J′–K′) Schematic illustrations of (J) and (K). Scale bars: 50 μm. Quantification of the phenotypes is shown in (S5G) and detailed in Table S5; number of discs quantified for each was ≥36.

(L) Left: independent functions of Yki and Bon in growth regulation and embryonic PNS specification. Right: Yki and Bon jointly regulate cell-fate decisions in the eye through recruitment of transcriptional and post-transcriptional regulators and transcriptional control of a set of non-canonical target genes.

See also Figures S5–S7 and Table S5.

biological function of the Hippo pathway and Bon in cell-fate determination during eye development.

## Hippo pathway and Bon control eye-antenna-epidermis cell-fate decisions at two levels

Our results suggest that the Hippo pathway and Bon regulate the developmental cell-fate decisions in the eye at two levels (Figure S7). First, the Yki-Bon complex promotes antennal and epidermal fates and suppresses the eye fate during early eye field specification, before the L3 larval stage. This is supported by the phenotypes observed under various genetic manipulations of Bon, Wts, Yki, and Sd during the L1 and L2 larval stages, including the reciprocal transformations of eye and antenna, epidermal outgrowths in the eye, and ectopic eye fate (Figures 3, 4, 6, S4, and S6). The Yki-Bon module is thus an essential component of the extensive gene regulatory network that controls these cell-fate decisions in early eye development.[9,12] Previous studies showed that *ex*, *Mer*, and *mats* mutants exhibit eye-to-epidermal transformation and an occasional eye-to-antenna transformation (in an *ex* mutant combination), suggesting that the upstream Hippo pathway may also regulate the Yki-Bon module in fate determination at this stage.[21–24]

Second, after the segregation of the eye/antenna/epidermis fields and the start of MF in L3, the Yki-Bon complex promotes the epidermal cell fate while suppressing ommatidia, whereas Wts counteracts this activity. This is evidenced by the formation of epidermal trichomes in the retina and the suppression of ommatidial cell types, especially cone cells, upon knockdown of *wts* or overexpression of Bon or Yki with the late eye driver *GMR-GAL4* (Figures 2, 3, and S3). Furthermore, our RNA-seq data also revealed cell-fate regulation at the molecular level: the Yki-Bon complex activates epidermal differentiation genes (*sha*, *f*, *nyo*, and *neo*) and represses Notch targets (*E(spl)-C*, *ct*, and *TfAP-2*) that are required for eye fate establishment and are expressed in ommatidial cells (e.g., *ct* in cone cells and *E(spl)mdelta-HLH* in primary pigment cells) (Figure 6). Although activation of the Yki-Bon complex at this stage did not exhibit an eye-to-antenna transformation phenotype, certain antennal genes (*Gr64s* and *Or47b*) were upregulated, suggesting transformation at the level of gene expression.

The eye-antenna-epidermis fate determination was previously studied during the early stages of eye-antennal disc development.[10] Our work shows that these fates are not completely defined during the early stages, as the retina could still transform into epidermal tissue and express epidermal and even antennal genes when the Hippo pathway and Bon were modulated after MF formation. Notably, conditional knockout of *eya* after the MF results in suppression of ommatidia and formation of trichomes in the eye.[93] This suggests that the retinal determination genes are also involved in eye-epidermal fate decisions during later stages of eye development and that trichome induction may be a general biological outcome of interference with the eye vs. epidermis specification after the start of MF. Thus, we conclude that the eye is still developmentally plastic at late stages, with a latent epidermal fate that is normally inhibited. Interestingly, this fate is revealed in the insect order Strepsiptera, whose compound eyes are composed of optical units that are separated by epidermal tissue bearing trichome-like extensions.[94]

Given Bon's role in promoting the epidermal fate in the eye, we asked whether it is involved in epidermal differentiation in other tissues. Knockdown of *bon* by RNAi in the wing with the *C5-GAL4* driver[95] did not affect the number of trichomes, but trichome morphology was abnormal, with *bon*-RNAi wing cells growing thinner trichomes (Figures S3J and S3K). $bon^{21B}$ mutant sensory bristles on the notum showed a similar thinning effect, although the *Sb* clonal marker precluded genotyping surrounding epidermal cells (Figures S3L–S3M″). These results suggest that Bon may contribute to epidermal differentiation in other contexts in addition to its role in the eye.

### Yki and Bon control cell-fate decisions in the eye by recruiting cofactors and regulating a distinct set of target genes

We have identified an unexpected layer of control over eye specification exerted by Yki and Bon at the level of Notch target genes. The Hippo pathway has been reported to control cell-fate determination in other biological contexts through regulation of the Notch receptor or ligands.[96–98] Although we have identified several Notch targets that are repressed by Bon and Yki, Notch and its ligands, Serrate and Delta, were not jointly regulated or found in high-confidence Yki or Bon protein interactomes (Tables S1–S3). Therefore, we propose that during cell-fate determination in the eye, Bon and Yki repress Notch targets (such as *E(spl)-C* genes) independently from upstream Notch signaling. We note that not all *E(spl)-C* genes are under Bon and Yki control, implying context-dependent regulation and functional divergence of *E(spl)-C* genes, as suggested by previous studies (Table S3).[91,99] Both Hippo and Notch contribute to cell proliferation and growth of the eye.[8,100] Our data suggest that Bon is not required for the growth-controlling function of the Hippo pathway (Figure S1). Instead, the Bon-Yki complex directs the acquisition of appropriate cell fates in the eye through the regulation of Notch targets. We speculate that Bon may function as a switch that redirects some of Hippo pathway activities from growth regulation to cell-fate determination.

So far, *Drosophila* Yki has only been implicated in transcriptional activation.[5] However, studies in mammalian systems have shown that the YAP/TAZ-TEAD complex can also function as a transcriptional repressor on non-canonical target genes.[101–103] The repression of Notch targets reported here suggests that *Drosophila* Yki can also function in transcriptional repression, likely via the recruitment of corepressors mediated by Bon. HDAC1 and its associated corepressor complexes repress gene transcription, including Notch targets.[62,104] We identified HDAC1 and its corepressor, CoRest, in the Bon interactome (Figure 5A), raising the possibility that Bon and Yki repress Notch target genes in part via recruiting this repressor complex. The involvement of epigenetic regulators is further exemplified by Su(var)2-10, which has a role in chromatin SUMOylation and piRNA target silencing.[65] Interestingly, Su(var)2-10 can suppress eye fate and even induce antennal fate in a sensitized background.[64] Due to the strong genetic interaction between Su(var)2-10 and the Bon-Yki complex (Figures 5 and S5), and the identification of the *Drosophila* SUMO (smt3) in the Bon interactome (Figure 5A), chromatin SUMOylation may be involved in gene repression by Bon and Yki. Future studies of chromatin status and epigenetic marks may reveal the mechanistic details of gene repression by Bon and Yki.

The Hippo pathway and TIF1 family proteins are conserved and broadly expressed in higher eukaryotes,[5,26] raising the possibility that they may also function together in other species and developmental processes, such as retinogenesis and hematopoiesis.[105–108] Thus, the biological functions controlled by the Hippo pathway and Bon, and the underlying molecular mechanisms we report here, may be evolutionarily conserved.

### Limitations of the study

RNA-seq was performed using pupal eyes when trichomes initiate; however, the pupal eye patterning defects were detectable before trichome initiation (Figures S3A–S3C). Thus, there might be additional differentially expressed genes at earlier stages of cell-fate determination that we have missed. Cells mutant for a null allele of *bon* tend to be eliminated,[25] potentially masking additional cell differentiation defects in *bon* mutant clones. Although our study has largely focused on eye development, it is possible that Bon and Yki interaction has additional functions in other tissues. Further studies are needed to analyze

the precise composition of multiprotein complexes involving Yki and Bon, as well as their effects on the target genes we identified here.

## STAR★METHODS

Detailed methods are provided in the online version of this paper and include the following:

- KEY RESOURCES TABLE
- RESOURCE AVAILABILITY
  - Lead contact
  - Materials availability
  - Data and code availability
- EXPERIMENTAL MODEL AND SUBJECT DETAILS
  - Cell lines
  - Drosophila strains
- METHOD DETAILS
  - Plasmid construction
  - Stable cell lines
  - Transgenic fly lines
  - Genetic crosses
  - Affinity Purification
  - Mass Spectrometry and data analysis
  - Co-immunoprecipitation
  - EdU incorporation assay
  - Tissue staining
  - Fluorescence and bright-field microscopy
  - Scanning electron microscopy (SEM)
  - Total RNA preparation
  - RNA-sequencing, data analysis, and qRT-PCR validation
  - DNA binding analysis and ChIP-qPCR
- QUANTIFICATION AND STATISTICAL ANALYSIS

## SUPPLEMENTAL INFORMATION

Suppletal information can be found online at https://doi.org/10.1016/j.devcel.2023.02.005.

## ACKNOWLEDGMENTS

We thank Spyros Artavanis-Tsakonas, Hugo Bellen, Kwang-Wook Choi, Claude Desplan, Maxim Frolov, Jin Jiang, Eric Lai, Duojia Pan, François Schweisguth, Alexei Tulin, BDSC, VDRC, DGRC, and DSHB for fly stocks and reagents. We thank Georg Halder, Kieran Harvey, Tony Ip, Kenneth Irvine, Ruth Johnson, Donald Ready, Nicolas Tapon, Barry Thompson, Can Zhang, and Lei Zhang for helpful discussions. We thank Alexander Letizia and Katerina Heath for helping with plasmid construction. We also thank Jens Rister and Claire Jackan for helpful comments on the manuscript. Part of the SEM work was supported by award #S10RR021043 from the National Center for Research Resources to the UMass Chan EM Core Facility. This work was funded by NIH grants GM105813 and GM123136 to K.H.M. and A.V.

## AUTHOR CONTRIBUTIONS

Conceptualization, H.Z., K.H.M., and A.V.; methodology, H.Z., K.H.M., and A.V.; formal analysis, H.Z.; investigation, H.Z.; resources, K.H.M. and A.V.; data curation, H.Z.; writing—original draft, H.Z.; writing—review and editing, H.Z., K.H.M., and A.V.; visualization, H.Z.; supervision, A.V.; funding acquisition, K.H.M. and A.V.

## DECLARATION OF INTERESTS

The authors declare no competing interests.

Received: September 8, 2021
Revised: August 10, 2022
Accepted: February 6, 2023
Published: March 2, 2023

## REFERENCES

1. Kulkarni, A., Chang, M.T., Vissers, J.H.A., Dey, A., and Harvey, K.F. (2020). The hippo pathway as a driver of select human cancers. Trends Cancer *6*, 781–796. https://doi.org/10.1016/j.trecan.2020.04.004.
2. Ma, S., Meng, Z., Chen, R., and Guan, K.L. (2019). The hippo pathway: biology and pathophysiology. Annu. Rev. Biochem. *88*, 577–604. https://doi.org/10.1146/annurev-biochem-013118-111829.
3. Misra, J.R., and Irvine, K.D. (2018). The hippo signaling network and its biological functions. Annu. Rev. Genet. *52*, 65–87. https://doi.org/10.1146/annurev-genet-120417-031621.
4. Manning, S.A., Kroeger, B., and Harvey, K.F. (2020). The regulation of Yorkie, YAP and TAZ: new insights into the Hippo pathway. Development *147*. https://doi.org/10.1242/dev.179069.
5. Zheng, Y., and Pan, D. (2019). The hippo signaling pathway in development and disease. Dev. Cell *50*, 264–282. https://doi.org/10.1016/j.devcel.2019.06.003.
6. Davis, J.R., and Tapon, N. (2019). Hippo signalling during development. Development *146*. https://doi.org/10.1242/dev.167106.
7. Weasner, B.P., and Kumar, J.P. (2022). The early history of the eye-antennal disc of Drosophila melanogaster. Genetics *221*. https://doi.org/10.1093/genetics/iyac041.
8. Domínguez, M., and Casares, F. (2005). Organ specification-growth control connection: new in-sights from the Drosophila eye-antennal disc. Dev. Dyn. *232*, 673–684. https://doi.org/10.1002/dvdy.20311.
9. Kumar, J.P. (2010). Retinal determination the beginning of eye development. Curr. Top. Dev. Biol. *93*, 1–28. https://doi.org/10.1016/B978-0-12-385044-7.00001-1.
10. Kumar, J.P. (2018). The fly eye: through the looking glass. Dev. Dyn. *247*, 111–123. https://doi.org/10.1002/dvdy.24585.
11. Ordway, A.J., Teeters, G.M., Weasner, B.M., Weasner, B.P., Policastro, R., and Kumar, J.P. (2021). A multi-gene knockdown approach reveals a new role for Pax6 in controlling organ number in Drosophila. Development *148*. https://doi.org/10.1242/dev.198796.
12. Kumar, J.P., and Moses, K. (2001). EGF receptor and Notch signaling act upstream of Eyeless/Pax6 to control eye specification. Cell *104*, 687–697. https://doi.org/10.1016/s0092-8674(01)00265-3.
13. Weasner, B.M., and Kumar, J.P. (2013). Competition among gene regulatory networks imposes order within the eye-antennal disc of Drosophila. Development *140*, 205–215. https://doi.org/10.1242/dev.085423.
14. Wang, C.W., and Sun, Y.H. (2012). Segregation of eye and antenna fates maintained by mutual antagonism in Drosophila. Development *139*, 3413–3421. https://doi.org/10.1242/dev.078857.
15. Charlton-Perkins, M., and Cook, T.A. (2010). Building a fly eye: terminal differentiation events of the retina, corneal lens, and pigmented epithelia. Curr. Top. Dev. Biol. *93*, 129–173. https://doi.org/10.1016/B978-0-12-385044-7.00005-9.
16. Cagan, R.L., and Ready, D.F. (1989). The emergence of order in the Drosophila pupal retina. Dev. Biol. *136*, 346–362. https://doi.org/10.1016/0012-1606(89)90261-3.
17. Wittkorn, E., Sarkar, A., Garcia, K., Kango-Singh, M., and Singh, A. (2015). The Hippo pathway effector Yki downregulates Wg signaling to promote retinal differentiation in the Drosophila eye. Development *142*, 2002–2013. https://doi.org/10.1242/dev.117358.

18. Jukam, D., Xie, B., Rister, J., Terrell, D., Charlton-Perkins, M., Pistillo, D., Gebelein, B., Desplan, C., and Cook, T. (2013). Opposite feedbacks in the Hippo pathway for growth control and neural fate. Science *342*, 1238016. https://doi.org/10.1126/science.1238016.

19. Zhang, T., Zhou, Q., and Pignoni, F. (2011). Yki/YAP, Sd/TEAD and Hth/MEIS control tissue specification in the Drosophila eye disc epithelium. PLoS One *6*, e22278. https://doi.org/10.1371/journal.pone.0022278.

20. Pojer, J.M., Manning, S.A., Kroeger, B., Kondo, S., and Harvey, K.F. (2021). The Hippo pathway uses different machinery to control cell fate and organ size. iScience *24*, 102830. https://doi.org/10.1016/j.isci.2021.102830.

21. Boedigheimer, M., and Laughon, A. (1993). Expanded: a gene involved in the control of cell proliferation in imaginal discs. Development *118*, 1291–1301.

22. Lai, Z.C., Wei, X., Shimizu, T., Ramos, E., Rohrbaugh, M., Nikolaidis, N., Ho, L.L., and Li, Y. (2005). Control of cell proliferation and apoptosis by mob as tumor suppressor, mats. Cell *120*, 675–685. https://doi.org/10.1016/j.cell.2004.12.036.

23. McCartney, B.M., Kulikauskas, R.M., LaJeunesse, D.R., and Fehon, R.G. (2000). The neurofibromatosis-2 homologue, Merlin, and the tumor suppressor expanded function together in Drosophila to regulate cell proliferation and differentiation. Development *127*, 1315–1324.

24. Pellock, B.J., Buff, E., White, K., and Hariharan, I.K. (2007). The Drosophila tumor suppressors Expanded and Merlin differentially regulate cell cycle exit, apoptosis, and Wingless signaling. Dev. Biol. *304*, 102–115. https://doi.org/10.1016/j.ydbio.2006.12.021.

25. Beckstead, R., Ortiz, J.A., Sanchez, C., Prokopenko, S.N., Chambon, P., Losson, R., and Bellen, H.J. (2001). Bonus, a Drosophila homolog of TIF1 proteins, interacts with nuclear receptors and can inhibit betaFTZ-F1-dependent transcription. Mol. Cell *7*, 753–765.

26. Cammas, F., Khetchoumian, K., Chambon, P., and Losson, R. (2012). TRIM involvement in transcriptional regulation. Adv. Exp. Med. Biol. *770*, 59–76. https://doi.org/10.1007/978-1-4614-5398-7_5.

27. Beckstead, R.B., Ner, S.S., Hales, K.G., Grigliatti, T.A., Baker, B.S., and Bellen, H.J. (2005). Bonus, a Drosophila TIF1 homolog, is a chromatin-associated protein that acts as a modifier of position-effect variegation. Genetics *169*, 783–794. https://doi.org/10.1534/genetics.104.037085.

28. Ito, H., Sato, K., Koganezawa, M., Ote, M., Matsumoto, K., Hama, C., and Yamamoto, D. (2012). Fruitless recruits two antagonistic chromatin factors to establish single-neuron sexual dimorphism. Cell *149*, 1327–1338. https://doi.org/10.1016/j.cell.2012.04.025.

29. Petrera, F., and Meroni, G. (2012). TRIM proteins in development. Adv. Exp. Med. Biol. *770*, 131–141. https://doi.org/10.1007/978-1-4614-5398-7_10.

30. Cambiaghi, V., Giuliani, V., Lombardi, S., Marinelli, C., Toffalorio, F., and Pelicci, P.G. (2012). TRIM proteins in cancer. Adv. Exp. Med. Biol. *770*, 77–91. https://doi.org/10.1007/978-1-4614-5398-7_6.

31. McAvera, R.M., and Crawford, L.J. (2020). TIF1 proteins in genome stability and cancer. Cancers (Basel) 12. 10.3390/cancers12082094.

32. Salzberg, A., Prokopenko, S.N., He, Y., Tsai, P., Pál, M., Maróy, P., Glover, D.M., Deák, P., and Bellen, H.J. (1997). P-element insertion alleles of essential genes on the third chromosome of Drosophila melanogaster: mutations affecting embryonic PNS development. Genetics *147*, 1723–1741.

33. Allton, K., Jain, A.K., Herz, H.M., Tsai, W.W., Jung, S.Y., Qin, J., Bergmann, A., Johnson, R.L., and Barton, M.C. (2009). Trim24 targets endogenous p53 for degradation. Proc. Natl. Acad. Sci. USA *106*, 11612–11616. https://doi.org/10.1073/pnas.0813177106.

34. Wisotzkey, R.G., Quijano, J.C., Stinchfield, M.J., and Newfeld, S.J. (2014). New gene evolution in the bonus-TIF1-gamma/TRIM33 family impacted the architecture of the vertebrate dorsal-ventral patterning network. Mol. Biol. Evol. *31*, 2309–2321. https://doi.org/10.1093/molbev/msu175.

35. Wodarz, A., Hinz, U., Engelbert, M., and Knust, E. (1995). Expression of crumbs confers apical character on plasma membrane domains of ectodermal epithelia of Drosophila. Cell *82*, 67–76. https://doi.org/10.1016/0092-8674(95)90053-5.

36. Choi, H., Larsen, B., Lin, Z.Y., Breitkreutz, A., Mellacheruvu, D., Fermin, D., Qin, Z.S., Tyers, M., Gingras, A.C., and Nesvizhskii, A.I. (2011). SAINT: probabilistic scoring of affinity purification-mass spectrometry data. Nat. Methods *8*, 70–73. https://doi.org/10.1038/nmeth.1541.

37. Szklarczyk, D., Gable, A.L., Lyon, D., Junge, A., Wyder, S., Huerta-Cepas, J., Simonovic, M., Doncheva, N.T., Morris, J.H., Bork, P., et al. (2019). STRING v11: protein-protein association networks with increased coverage, supporting functional discovery in genome-wide experimental datasets. Nucleic Acids Res. *47*, D607–D613. https://doi.org/10.1093/nar/gky1131.

38. Thurmond, J., Goodman, J.L., Strelets, V.B., Attrill, H., Gramates, L.S., Marygold, S.J., Matthews, B.B., Millburn, G., Antonazzo, G., Trovisco, V., et al. (2019). FlyBase 2.0: the next generation. Nucleic Acids Res. *47*, D759–D765. https://doi.org/10.1093/nar/gky1003.

39. Kwon, Y., Vinayagam, A., Sun, X., Dephoure, N., Gygi, S.P., Hong, P., and Perrimon, N. (2013). The Hippo signaling pathway interactome. Science *342*, 737–740. https://doi.org/10.1126/science.1243971.

40. Oh, H., Slattery, M., Ma, L., White, K.P., Mann, R.S., and Irvine, K.D. (2014). Yorkie promotes transcription by recruiting a histone methyltransferase complex. Cell Rep. *8*, 449–459. https://doi.org/10.1016/j.celrep.2014.06.017.

41. Oh, H., Reddy, B.V., and Irvine, K.D. (2009). Phosphorylation-independent repression of Yorkie in Fat-Hippo signaling. Dev. Biol. *335*, 188–197. https://doi.org/10.1016/j.ydbio.2009.08.026.

42. Zhang, C., Robinson, B.S., Xu, W., Yang, L., Yao, B., Zhao, H., Byun, P.K., Jin, P., Veraksa, A., and Moberg, K.H. (2015). The ecdysone receptor coactivator Taiman links Yorkie to transcriptional control of germline stem cell factors in somatic tissue. Dev. Cell *34*, 168–180. https://doi.org/10.1016/j.devcel.2015.05.010.

43. Xu, T., Wang, W., Zhang, S., Stewart, R.A., and Yu, W. (1995). Identifying tumor suppressors in genetic mosaics: the Drosophila lats gene encodes a putative protein kinase. Development *121*, 1053–1063.

44. Huang, J., Wu, S., Barrera, J., Matthews, K., and Pan, D. (2005). The Hippo signaling pathway coordinately regulates cell proliferation and apoptosis by inactivating Yorkie, the Drosophila Homolog of YAP. Cell *122*, 421–434. https://doi.org/10.1016/j.cell.2005.06.007.

45. Hay, B.A., Wolff, T., and Rubin, G.M. (1994). Expression of baculovirus P35 prevents cell death in Drosophila. Development *120*, 2121–2129.

46. Ellis, M.C., O'Neill, E.M., and Rubin, G.M. (1993). Expression of Drosophila glass protein and evidence for negative regulation of its activity in non-neuronal cells by another DNA-binding protein. Development *119*, 855–865.

47. Freeman, M. (1996). Reiterative use of the EGF receptor triggers differentiation of all cell types in the Drosophila eye. Cell *87*, 651–660. https://doi.org/10.1016/s0092-8674(00)81385-9.

48. Tardi, N.J., Cook, M.E., and Edwards, K.A. (2012). Rapid phenotypic analysis of uncoated Drosophila samples with low-vacuum scanning electron microscopy. Fly (Austin) *6*, 184–192. https://doi.org/10.4161/fly.20525.

49. Arif, S., Kittelmann, S., and McGregor, A.P. (2015). From shavenbaby to the naked valley: trichome formation as a model for evolutionary developmental biology. Evol. Dev. *17*, 120–126. https://doi.org/10.1111/ede.12113.

50. Delon, I., Chanut-Delalande, H., and Payre, F. (2003). The Ovo/Shavenbaby transcription factor specifies actin remodelling during epidermal differentiation in Drosophila. Mech. Dev. *120*, 747–758. https://doi.org/10.1016/s0925-4773(03)00081-9.

51. Zhang, L., Ren, F., Zhang, Q., Chen, Y., Wang, B., and Jiang, J. (2008). The TEAD/TEF family of transcription factor Scalloped mediates Hippo

signaling in organ size control. Dev. Cell *14*, 377–387. https://doi.org/10.1016/j.devcel.2008.01.006.

52. Oh, H., and Irvine, K.D. (2008). In vivo regulation of Yorkie phosphorylation and localization. Development *135*, 1081–1088. https://doi.org/10.1242/dev.015255.

53. Chanut-Delalande, H., Hashimoto, Y., Pelissier-Monier, A., Spokony, R., Dib, A., Kondo, T., Bohère, J., Niimi, K., Latapie, Y., Inagaki, S., et al. (2014). Pri peptides are mediators of ecdysone for the temporal control of development. Nat. Cell Biol. *16*, 1035–1044. https://doi.org/10.1038/ncb3052.

54. Kumar, J.P. (2012). Building an ommatidium one cell at a time. Dev. Dyn. *241*, 136–149. https://doi.org/10.1002/dvdy.23707.

55. Nagaraj, R., and Banerjee, U. (2007). Combinatorial signaling in the specification of primary pigment cells in the Drosophila eye. Development *134*, 825–831. https://doi.org/10.1242/dev.02788.

56. Udan, R.S., Kango-Singh, M., Nolo, R., Tao, C., and Halder, G. (2003). Hippo promotes proliferation arrest and apoptosis in the Salvador/Warts pathway. Nat. Cell Biol. *5*, 914–920. https://doi.org/10.1038/ncb1050.

57. Hamaratoglu, F., Willecke, M., Kango-Singh, M., Nolo, R., Hyun, E., Tao, C., Jafar-Nejad, H., and Halder, G. (2006). The tumour-suppressor genes NF2/Merlin and Expanded act through Hippo signalling to regulate cell proliferation and apoptosis. Nat. Cell Biol. *8*, 27–36. https://doi.org/10.1038/ncb1339.

58. Wernet, M.F., Labhart, T., Baumann, F., Mazzoni, E.O., Pichaud, F., and Desplan, C. (2003). Homothorax switches function of Drosophila photoreceptors from color to polarized light sensors. Cell *115*, 267–279. https://doi.org/10.1016/s0092-8674(03)00848-1.

59. Lim, H.Y., and Tomlinson, A. (2006). Organization of the peripheral fly eye: the roles of Snail family transcription factors in peripheral retinal apoptosis. Development *133*, 3529–3537. https://doi.org/10.1242/dev.02524.

60. Pai, C.Y., Kuo, T.S., Jaw, T.J., Kurant, E., Chen, C.T., Bessarab, D.A., Salzberg, A., and Sun, Y.H. (1998). The Homothorax homeoprotein activates the nuclear localization of another homeoprotein, extradenticle, and suppresses eye development in Drosophila. Genes Dev. *12*, 435–446. https://doi.org/10.1101/gad.12.3.435.

61. Blochlinger, K., Jan, L.Y., and Jan, Y.N. (1993). Postembryonic patterns of expression of cut, a locus regulating sensory organ identity in Drosophila. Development *117*, 441–450. https://doi.org/10.1242/dev.117.2.441.

62. Seto, E., and Yoshida, M. (2014). Erasers of histone acetylation: the histone deacetylase enzymes. Cold Spring Harb. Perspect. Biol. *6*, a018713. https://doi.org/10.1101/cshperspect.a018713.

63. Hari, K.L., Cook, K.R., and Karpen, G.H. (2001). The Drosophila Su(var)2–10 locus regulates chromosome structure and function and encodes a member of the PIAS protein family. Genes Dev. *15*, 1334–1348. https://doi.org/10.1101/gad.877901.

64. Betz, A., Lampen, N., Martinek, S., Young, M.W., and Darnell, J.E., Jr. (2001). A Drosophila PIAS homologue negatively regulates stat92E. Proc. Natl. Acad. Sci. USA *98*, 9563–9568. https://doi.org/10.1073/pnas.171302098.

65. Ninova, M., Chen, Y.A., Godneeva, B., Rogers, A.K., Luo, Y., Fejes Tóth, K., and Aravin, A.A. (2020). Su(var)2–10 and the SUMO pathway link piRNA-guided target recognition to chromatin silencing. Mol. Cell *77*, 556–570.e6. https://doi.org/10.1016/j.molcel.2019.11.012.

66. Goodrich, J.S., Clouse, K.N., and Schüpbach, T. (2004). Hrb27C, Sqd and Otu cooperatively regulate gurken RNA localization and mediate nurse cell chromosome dispersion in Drosophila oogenesis. Development *131*, 1949–1958. https://doi.org/10.1242/dev.01078.

67. Mach, J., Atkins, M., Gajewski, K.M., Mottier-Pavie, V., Sansores-Garcia, L., Xie, J., Mills, R.A., Kowalczyk, W., Van Huffel, L., Mills, G.B., et al. (2018). Modulation of the Hippo pathway and organ growth by RNA processing proteins. Proc. Natl. Acad. Sci. USA *115*, 10684–10689. https://doi.org/10.1073/pnas.1807325115.

68. Yano, T., López de Quinto, S., Matsui, Y., Shevchenko, A., Shevchenko, A., and Ephrussi, A. (2004). Hrp48, a Drosophila hnRNPA/B homolog, binds and regulates translation of oskar mRNA. Dev. Cell *6*, 637–648. https://doi.org/10.1016/s1534-5807(04)00132-7.

69. Chanut-Delalande, H., Fernandes, I., Roch, F., Payre, F., and Plaza, S. (2006). Shavenbaby couples patterning to epidermal cell shape control. PLoS Biol. *4*, e290. https://doi.org/10.1371/journal.pbio.0040290.

70. Bohère, J., Mancheno-Ferris, A., Al Hayek, S., Zanet, J., Valenti, P., Akino, K., Yamabe, Y., Inagaki, S., Chanut-Delalande, H., Plaza, S., et al. (2018). Shavenbaby and Yorkie mediate Hippo signaling to protect adult stem cells from apoptosis. Nat. Commun. *9*, 5123. https://doi.org/10.1038/s41467-018-07569-0.

71. Andrews, J., Garcia-Estefania, D., Delon, I., Lü, J., Mével-Ninio, M., Spierer, A., Payre, F., Pauli, D., and Oliver, B. (2000). OVO transcription factors function antagonistically in the Drosophila female germline. Development *127*, 881–892.

72. Tare, M., Puli, O.R., Moran, M.T., Kango-Singh, M., and Singh, A. (2013). Domain specific genetic mosaic system in the Drosophila eye. Genesis *51*, 68–74. https://doi.org/10.1002/dvg.22355.

73. Love, M.I., Huber, W., and Anders, S. (2014). Moderated estimation of fold change and dispersion for RNA-seq data with DESeq2. Genome Biol. *15*, 550. https://doi.org/10.1186/s13059-014-0550-8.

74. Oh, H., Slattery, M., Ma, L., Crofts, A., White, K.P., Mann, R.S., and Irvine, K.D. (2013). Genome-wide association of Yorkie with chromatin and chromatin-remodeling complexes. Cell Rep. *3*, 309–318. https://doi.org/10.1016/j.celrep.2013.01.008.

75. Nègre, N., Brown, C.D., Ma, L., Bristow, C.A., Miller, S.W., Wagner, U., Kheradpour, P., Eaton, M.L., Loriaux, P., Sealfon, R., et al. (2011). A cis-regulatory map of the Drosophila genome. Nature *471*, 527–531. https://doi.org/10.1038/nature09990.

76. Vissers, J.H.A., Froldi, F., Schröder, J., Papenfuss, A.T., Cheng, L.Y., and Harvey, K.F. (2018). The scalloped and Nerfin-1 transcription factors cooperate to maintain neuronal cell fate. Cell Rep. *25*, 1561–1576.e7. https://doi.org/10.1016/j.celrep.2018.10.038.

77. Deng, H., Yang, L., Wen, P., Lei, H., Blount, P., and Pan, D. (2020). Spectrin couples cell shape, cortical tension, and Hippo signaling in retinal epithelial morphogenesis. J. Cell Biol. *219*. https://doi.org/10.1083/jcb.201907018.

78. Fernandes, I., Chanut-Delalande, H., Ferrer, P., Latapie, Y., Waltzer, L., Affolter, M., Payre, F., and Plaza, S. (2010). Zona pellucida domain proteins remodel the apical compartment for localized cell shape changes. Dev. Cell *18*, 64–76. https://doi.org/10.1016/j.devcel.2009.11.009.

79. Lai, E.C., Bodner, R., and Posakony, J.W. (2000). The enhancer of split complex of Drosophila includes four Notch-regulated members of the bearded gene family. Development *127*, 3441–3455.

80. Knust, E., Schrons, H., Grawe, F., and Campos-Ortega, J.A. (1992). Seven genes of the Enhancer of split complex of Drosophila melanogaster encode helix-loop-helix proteins. Genetics *132*, 505–518.

81. Kerber, B., Monge, I., Mueller, M., Mitchell, P.J., and Cohen, S.M. (2001). The AP-2 transcription factor is required for joint formation and cell survival in Drosophila leg development. Development *128*, 1231–1238.

82. Micchelli, C.A., Rulifson, E.J., and Blair, S.S. (1997). The function and regulation of cut expression on the wing margin of Drosophila: notch, Wingless and a dominant negative role for Delta and Serrate. Development *124*, 1485–1495.

83. Lai, E.C., and Rubin, G.M. (2001). Neuralized is essential for a subset of Notch pathway-dependent cell fate decisions during Drosophila eye development. Proc. Natl. Acad. Sci. USA *98*, 5637–5642. https://doi.org/10.1073/pnas.101135498.

84. Monge, I., Krishnamurthy, R., Sims, D., Hirth, F., Spengler, M., Kammermeier, L., Reichert, H., and Mitchell, P.J. (2001). Drosophila

transcription factor AP-2 in proboscis, leg and brain central complex development. Development *128*, 1239–1252.

85. Cagan, R.L., and Ready, D.F. (1989). Notch is required for successive cell decisions in the developing Drosophila retina. Genes Dev. *3*, 1099–1112. https://doi.org/10.1101/gad.3.8.1099.

86. Kurata, S., Go, M.J., Artavanis-Tsakonas, S., and Gehring, W.J. (2000). Notch signaling and the determination of appendage identity. Proc. Natl. Acad. Sci. USA *97*, 2117–2122. https://doi.org/10.1073/pnas.040556497.

87. Vosshall, L.B. (2001). The molecular logic of olfaction in Drosophila. Chem. Senses *26*, 207–213. https://doi.org/10.1093/chemse/26.2.207.

88. Barish, S., Li, Q., Pan, J.W., Soeder, C., Jones, C., and Volkan, P.C. (2017). Transcriptional profiling of olfactory system development identifies distal antenna as a regulator of subset of neuronal fates. Sci. Rep. *7*, 40873. https://doi.org/10.1038/srep40873.

89. Fujii, S., Yavuz, A., Slone, J., Jagge, C., Song, X., and Amrein, H. (2015). Drosophila sugar receptors in sweet taste perception, olfaction, and internal nutrient sensing. Curr. Biol. *25*, 621–627. https://doi.org/10.1016/j.cub.2014.12.058.

90. Menuz, K., Larter, N.K., Park, J., and Carlson, J.R. (2014). An RNA-seq screen of the Drosophila antenna identifies a transporter necessary for ammonia detection. PLOS Genet. *10*, e1004810. https://doi.org/10.1371/journal.pgen.1004810.

91. Couturier, L., Mazouni, K., Corson, F., and Schweisguth, F. (2019). Regulation of Notch output dynamics via specific E(spl)-HLH factors during bristle patterning in Drosophila. Nat. Commun. *10*, 3486. https://doi.org/10.1038/s41467-019-11477-2.

92. Morrison, C.M., and Halder, G. (2010). Characterization of a dorsal-eye Gal4 Line in Drosophila. Genesis *48*, 3–7. https://doi.org/10.1002/dvg.20571.

93. Jin, M., Eblimit, A., Pulikkathara, M., Corr, S., Chen, R., and Mardon, G. (2016). Conditional knockout of retinal determination genes in differentiating cells in Drosophila. FEBS J. *283*, 2754–2766. https://doi.org/10.1111/febs.13772.

94. Buschbeck, E.K. (2005). The compound lens eye of Strepsiptera: morphological development of larvae and pupae. Arthropod Struct. Dev. *34*, 315–326. https://doi.org/10.1016/j.asd.2005.04.002.

95. Yeh, E., Gustafson, K., and Boulianne, G.L. (1995). Green fluorescent protein as a vital marker and reporter of gene expression in Drosophila. Proc. Natl. Acad. Sci. USA *92*, 7036–7040. https://doi.org/10.1073/pnas.92.15.7036.

96. Reddy, B.V., Rauskolb, C., and Irvine, K.D. (2010). Influence of fat-hippo and notch signaling on the proliferation and differentiation of Drosophila optic neuroepithelia. Development *137*, 2397–2408. https://doi.org/10.1242/dev.050013.

97. Totaro, A., Castellan, M., Battilana, G., Zanconato, F., Azzolin, L., Giulitti, S., Cordenonsi, M., and Piccolo, S. (2017). YAP/TAZ link cell mechanics to Notch signalling to control epidermal stem cell fate. Nat. Commun. *8*, 15206. https://doi.org/10.1038/ncomms15206.

98. Yimlamai, D., Christodoulou, C., Galli, G.G., Yanger, K., Pepe-Mooney, B., Gurung, B., Shrestha, K., Cahan, P., Stanger, B.Z., and Camargo, F.D. (2014). Hippo pathway activity influences liver cell fate. Cell *157*, 1324–1338. https://doi.org/10.1016/j.cell.2014.03.060.

99. Ligoxygakis, P., Bray, S.J., Apidianakis, Y., and Delidakis, C. (1999). Ectopic expression of individual E(spl) genes has differential effects on different cell fate decisions and underscores the biphasic requirement for notch activity in wing margin establishment in Drosophila. Development *126*, 2205–2214.

100. Peng, H.W., Slattery, M., and Mann, R.S. (2009). Transcription factor choice in the Hippo signaling pathway: homothorax and yorkie regulation of the microRNA bantam in the progenitor domain of the Drosophila eye imaginal disc. Genes Dev. *23*, 2307–2319. https://doi.org/10.1101/gad.1820009.

101. Beyer, T.A., Weiss, A., Khomchuk, Y., Huang, K., Ogunjimi, A.A., Varelas, X., and Wrana, J.L. (2013). Switch enhancers interpret TGF-beta and Hippo signaling to control cell fate in human embryonic stem cells. Cell Rep. *5*, 1611–1624. https://doi.org/10.1016/j.celrep.2013.11.021.

102. Kim, M., Kim, T., Johnson, R.L., and Lim, D.S. (2015). Transcriptional co-repressor function of the hippo pathway transducers YAP and TAZ. Cell Rep. *11*, 270–282. https://doi.org/10.1016/j.celrep.2015.03.015.

103. He, L., Yuan, L., Yu, W., Sun, Y., Jiang, D., Wang, X., Feng, X., Wang, Z., Xu, J., Yang, R., et al. (2020). A regulation loop between YAP and NR4A1 balances cell proliferation and apoptosis. Cell Rep. *33*, 108284. https://doi.org/10.1016/j.celrep.2020.108284.

104. Borggrefe, T., and Oswald, F. (2009). The Notch signaling pathway: transcriptional regulation at Notch target genes. Cell. Mol. Life Sci. *66*, 1631–1646. https://doi.org/10.1007/s00018-009-8668-7.

105. Rossmann, M.P., Hoi, K., Chan, V., Abraham, B.J., Yang, S., Mullahoo, J., Papanastasiou, M., Wang, Y., Elia, I., Perlin, J.R., et al. (2021). Cell-specific transcriptional control of mitochondrial metabolism by TIF1gamma drives erythropoiesis. Science *372*, 716–721. https://doi.org/10.1126/science.aaz2740.

106. Milton, C.C., Grusche, F.A., Degoutin, J.L., Yu, E., Dai, Q., Lai, E.C., and Harvey, K.F. (2014). The Hippo pathway regulates hematopoiesis in Drosophila melanogaster. Curr. Biol. *24*, 2673–2680. https://doi.org/10.1016/j.cub.2014.10.031.

107. Lundin, V., Sugden, W.W., Theodore, L.N., Sousa, P.M., Han, A., Chou, S., Wrighton, P.J., Cox, A.G., Ingber, D.E., Goessling, W., et al. (2020). YAP regulates hematopoietic stem cell formation in response to the biomechanical forces of blood flow. Dev. Cell *52*, 446–460.e5. https://doi.org/10.1016/j.devcel.2020.01.006.

108. Lee, M., Goraya, N., Kim, S., and Cho, S.H. (2018). Hippo-yap signaling in ocular development and disease. Dev. Dyn. *247*, 794–806. https://doi.org/10.1002/dvdy.24628.

109. Özel, M.N., Simon, F., Jafari, S., Holguera, I., Chen, Y.C., Benhra, N., El-Danaf, R.N., Kapuralin, K., Malin, J.A., Konstantinides, N., et al. (2021). Neuronal diversity and convergence in a visual system developmental atlas. Nature *589*, 88–95. https://doi.org/10.1038/s41586-020-2879-3.

110. Kang, J., Yeom, E., Lim, J., and Choi, K.W. (2014). Bar represses dPax2 and decapentaplegic to regulate cell fate and morphogenetic cell death in Drosophila eye. PLoS One *9*, e88171. https://doi.org/10.1371/journal.pone.0088171.

111. Yang, L., and Veraksa, A. (2017). Single-step affinity purification of ERK signaling complexes using the streptavidin-binding peptide (SBP) tag. Methods Mol. Biol. *1487*, 113–126. https://doi.org/10.1007/978-1-4939-6424-6_8.

112. Bischof, J., Maeda, R.K., Hediger, M., Karch, F., and Basler, K. (2007). An optimized transgenesis system for Drosophila using germ-line-specific phiC31 integrases. Proc. Natl. Acad. Sci. USA *104*, 3312–3317. https://doi.org/10.1073/pnas.0611511104.

113. Shannon, P., Markiel, A., Ozier, O., Baliga, N.S., Wang, J.T., Ramage, D., Amin, N., Schwikowski, B., and Ideker, T. (2003). Cytoscape: a software environment for integrated models of biomolecular interaction networks. Genome Res. *13*, 2498–2504. https://doi.org/10.1101/gr.1239303.

114. Schindelin, J., Arganda-Carreras, I., Frise, E., Kaynig, V., Longair, M., Pietzsch, T., Preibisch, S., Rueden, C., Saalfeld, S., Schmid, B., et al. (2012). Fiji: an open-source platform for biological-image analysis. Nat. Methods *9*, 676–682. https://doi.org/10.1038/nmeth.2019.

115. Wickham, H. (2016). ggplot2: Elegant Graphics for Data Analysis (Springer-Verlag New York).

116. Martin, M. (2011). Cutadapt removes adapter sequences from high-throughput sequencing reads. EMBnet J. *17*, 10–12. https://doi.org/10.14806/ej.17.1.200.

117. Langmead, B., and Salzberg, S.L. (2012). Fast gapped-read alignment with Bowtie 2. Nat. Methods *9*, 357–359. https://doi.org/10.1038/nmeth.1923.

118. Dobin, A., Davis, C.A., Schlesinger, F., Drenkow, J., Zaleski, C., Jha, S., Batut, P., Chaisson, M., and Gingeras, T.R. (2013). STAR: ultrafast universal RNA-seq aligner. Bioinformatics *29*, 15–21. https://doi.org/10.1093/bioinformatics/bts635.

119. Liao, Y., Smyth, G.K., and Shi, W. (2014). featureCounts: an efficient general purpose program for assigning sequence reads to genomic features. Bioinformatics *30*, 923–930. https://doi.org/10.1093/bioinformatics/btt656.

120. Kucukural, A., Yukselen, O., Ozata, D.M., Moore, M.J., and Garber, M. (2019). DEBrowser: interactive differential expression analysis and visualization tool for count data. BMC Genomics *20*, 6. https://doi.org/10.1186/s12864-018-5362-x.

121. Huang, da W., Sherman, B.T., and Lempicki, R.A. (2009). Systematic and integrative analysis of large gene lists using DAVID bioinformatics resources. Nat. Protoc. *4*, 44–57. https://doi.org/10.1038/nprot.2008.211.

122. Zhu, L.J., Gazin, C., Lawson, N.D., Pagès, H., Lin, S.M., Lapointe, D.S., and Green, M.R. (2010). ChIPpeakAnno: a Bioconductor package to annotate ChIP-seq and ChIP-chip data. BMC Bioinformatics *11*, 237. https://doi.org/10.1186/1471-2105-11-237.

123. Robinson, J.T., Thorvaldsdóttir, H., Winckler, W., Guttman, M., Lander, E.S., Getz, G., and Mesirov, J.P. (2011). Integrative genomics viewer. Nat. Biotechnol. *29*, 24–26. https://doi.org/10.1038/nbt.1754.

124. Edgar, R., Domrachev, M., and Lash, A.E. (2002). Gene Expression Omnibus: NCBI gene expression and hybridization array data repository. Nucleic Acids Res. *30*, 207–210. https://doi.org/10.1093/nar/30.1.207.

125. Perez-Riverol, Y., Csordas, A., Bai, J., Bernal-Llinares, M., Hewapathirana, S., Kundu, D.J., Inuganti, A., Griss, J., Mayer, G., Eisenacher, M., et al. (2019). The PRIDE database and related tools and resources in 2019: improving support for quantification data. Nucleic Acids Res. *47*, D442–D450. https://doi.org/10.1093/nar/gky1106.

126. Yang, L., Paul, S., DuBois-Coyne, S., Kyriakakis, P., and Veraksa, A. (2017). Medium-scale preparation of drosophila embryo extracts for proteomic experiments. J. Vis. Exp. *123*. https://doi.org/10.3791/55804.

127. Bean, D.M., Heimbach, J., Ficorella, L., Micklem, G., Oliver, S.G., and Favrin, G. (2014). esyN: network building, sharing and publishing. PLoS One *9*, e106035. https://doi.org/10.1371/journal.pone.0106035.

128. Gouge, C.A., and Christensen, T.W. (2010). Drosophila Sld5 is essential for normal cell cycle progression and maintenance of genomic integrity. Biochem. Biophys. Res. Commun. *400*, 145–150. https://doi.org/10.1016/j.bbrc.2010.08.033.

129. Hsiao, H.Y., Johnston, R.J., Jr., Jukam, D., Vasiliauskas, D., Desplan, C., and Rister, J. (2012). Dissection and immunohistochemistry of larval, pupal and adult Drosophila retinas. J. Vis. Exp. *69*, 4347.

130. Walther, R.F., and Pichaud, F. (2006). Immunofluorescent staining and imaging of the pupal and adult Drosophila visual system. Nat. Protoc. *1*, 2635–2642. https://doi.org/10.1038/nprot.2006.379.

131. Beam, C.K., and Moberg, K. (2010). The gang of four gene regulates growth and patterning of the developing Drosophila eye. Fly (Austin) *4*, 104–116. https://doi.org/10.4161/fly.4.2.11890.

132. Cadigan, K.M., and Nusse, R. (1996). Wingless signaling in the Drosophila eye and embryonic epidermis. Development *122*, 2801–2812. https://doi.org/10.1242/dev.122.9.2801.

133. Pepple, K.L., Anderson, A.E., Frankfort, B.J., and Mardon, G. (2007). A genetic screen in Drosophila for genes interacting with senseless during neuronal development identifies the importin moleskin. Genetics *175*, 125–141. https://doi.org/10.1534/genetics.106.065680.

134. Wolff, T. (2011). Preparation of Drosophila eye specimens for scanning electron microscopy. Cold Spring Harb. Protoc. *2011*, 1383–1385. https://doi.org/10.1101/pdb.prot066506.

135. Flicek, P., Amode, M.R., Barrell, D., Beal, K., Billis, K., Brent, S., Carvalho-Silva, D., Clapham, P., Coates, G., Fitzgerald, S., et al. (2014). Ensembl 2014. Nucleic Acids Res. *42*, D749–D755. https://doi.org/10.1093/nar/gkt1196.

136. Maza, E., Frasse, P., Senin, P., Bouzayen, M., and Zouine, M. (2013). Comparison of normalization methods for differential gene expression analysis in RNA-Seq experiments: A matter of relative size of studied transcriptomes. Commun. Integr. Biol. *6*, e25849. https://doi.org/10.4161/cib.25849.

137. Yuan, J.S., Reed, A., Chen, F., and Stewart, C.N., Jr. (2006). Statistical analysis of real-time PCR data. BMC Bioinformatics *7*, 85. https://doi.org/10.1186/1471-2105-7-85.

138. dos Santos, G., Schroeder, A.J., Goodman, J.L., Strelets, V.B., Crosby, M.A., Thurmond, J., Emmert, D.B., and Gelbart, W.M.; FlyBase Consortium (2015). FlyBase: introduction of the Drosophila melanogaster Release 6 reference genome assembly and large-scale migration of genome annotations. Nucleic Acids Res. *43*, D690–D697. Release 6. https://doi.org/10.1093/nar/gku1099.

## STAR★METHODS

### KEY RESOURCES TABLE

| REAGENT or RESOURCE | SOURCE | IDENTIFIER |
|---|---|---|
| Antibodies | | |
| Mouse Monoclonal anti-SBP Tag (SB19-C4) | Santa Cruz Biotechnology | Cat# sc-101595; RRID: AB_1128239 |
| Mouse Monoclonal anti-V5 | MilliporeSigma | Cat# V8012; RRID: AB_261888 |
| Rabbit Polyclonal anti-HA | MilliporeSigma | Cat# H6908; RRID: AB_260070 |
| Mouse Anti-Myc-Tag Monoclonal Antibody | Cell Signaling Technology | Cat# 2276; RRID: AB_331783 |
| Mouse Anti-β-Galactosidase mAb | Promega | Cat# Z3783; RRID: AB_430878 |
| Mouse Monoclonal anti-futsch (22C10) supernatant | DSHB | Cat# 22c10; RRID: AB_528403 |
| Mouse Monoclonal anti-discs large (Dlg) supernatant | DSHB | DSHB Cat# 4F3 anti-discs large; RRID: AB_528203 |
| Mouse Monoclonal anti-Cut homeobox supernatant | DSHB | Cat# 2b10; RRID: AB_528186 |
| Rat Monoclonal anti-Elav supernatant | DSHB | Cat# Rat-Elav-7E8A10 anti-elav; RRID: AB_528218 |
| Rat Monoclonal anti-E-caderin supernatant | DSHB | Cat# DCAD2; RRID: AB_528120 |
| Rabbit anti-GFP Polyclonal Antibody | Thermo Fisher Scientific | Cat# A-11122; RRID: AB_221569 |
| Guinea Pig anti-Bon | Gift from Hugo Bellen: Beckstead et al.[25] | N/A |
| Guinea Pig anti-Hth | Gift from Claude Desplan: Ozel et al.[109] | N/A |
| Rabbit anti-BarH1 | Gift from Kwang-Wook Choi: Kang et al.[110] | N/A |
| Goat anti-Mouse IgG, IRDye 680RD | LI-COR Biosciences | Cat# 926-68070; RRID: AB_10956588 |
| Donkey anti-Rabbit IgG, IRDye 800CW | LI-COR Biosciences | Cat# 926-32213; RRID: AB_621848 |
| Goat anti-Guinea Pig IgG (H+L) Highly Cross-Adsorbed Secondary Antibody, Alexa Fluor 488 | Thermo Fisher Scientific | Cat# A-11073; RRID: AB_2534117 |
| Goat anti-Guinea Pig IgG (H+L) Highly Cross-Adsorbed Secondary Antibody, Alexa Fluor 555 | Thermo Fisher Scientific | Cat# A-21435; RRID: AB_2535856 |
| Donkey anti-Mouse IgG (H+L) Highly Cross-Adsorbed Secondary Antibody, Alexa Fluor 647 | Thermo Fisher Scientific | Cat# A-31571; RRID: AB_162542 |
| Goat anti-Mouse IgG (H+L) Cross-Adsorbed Secondary Antibody, Alexa Fluor 555 | Thermo Fisher Scientific | Cat# A-21422; RRID: AB_2535844 |
| Donkey anti-Mouse IgG (H+L) Highly Cross-Adsorbed Secondary Antibody, Alexa Fluor 488 | Thermo Fisher Scientific | Cat# A-21202; RRID: AB_141607 |
| Goat anti-Rat IgG (H+L) Cross-Adsorbed Secondary Antibody, Alexa Fluor 647 | Thermo Fisher Scientific | Cat# A-21247; RRID: AB_141778 |
| Goat anti-Rat IgG (H+L) Cross-Adsorbed Secondary Antibody, Alexa Fluor 555 | Thermo Fisher Scientific | Cat# A-21434; RRID: AB_2535855 |
| Goat anti-Rat IgG (H+L) Cross-Adsorbed Secondary Antibody, Alexa Fluor 488 | Thermo Fisher Scientific | Cat# A-11006; RRID: AB_2534074 |
| Donkey anti-Rabbit IgG (H+L) Highly Cross-Adsorbed Secondary Antibody, Alexa Fluor Plus 647 | Thermo Fisher Scientific | Cat# A32795; RRID: AB_2762835 |

(*Continued on next page*)

*Continued*

| REAGENT or RESOURCE | SOURCE | IDENTIFIER |
|---|---|---|
| Donkey anti-Rabbit IgG (H+L) Highly Cross-Adsorbed Secondary Antibody, Alexa Fluor 488 | Thermo Fisher Scientific | Cat# A-21206; RRID: AB_2535792 |
| **Chemicals, peptides, and recombinant proteins** | | |
| Pierce Streptavidin Plus UltraLink Resin | Thermo Fisher Scientific | Cat# 53117 |
| Pierce Control Agarose Resin | Thermo Fisher Scientific | Cat# 26150 |
| GFP-Trap Agarose | Bulldog Bio | Cat# GTA020 |
| RFP-Trap Agarose | Bulldog Bio | Cat# RTA020 |
| Anti-V5 Agarose Affinity Gel | MilliporeSigma | Cat# A7345 |
| EZview Red Anti-HA Affinity Gel | MilliporeSigma | Cat# E6779 |
| Odyssey Blocking Buffer (PBS) | LI-COR Biosciences | Cat# 927-40003 |
| Western Blocking Reagent, Solution | MilliporeSigma (Roche) | Cat# 11921681001 |
| cOmplete Protease Inhibitor Cocktail | MilliporeSigma (Roche) | Cat# 11836145001 |
| cOmplete, Mini, EDTA-free Protease Inhibitor Cocktail | MilliporeSigma (Roche) | Cat# 11836170001 |
| Hexamethyldisilazane (HMDS) | Electron Microscopy Sciences | Cat# 16700 |
| Formaldehyde solution | MilliporeSigma | Cat# F8775 |
| 16% Paraformaldehyde (formaldehyde) aqueous solution | Electron Microscopy Sciences | Cat# 15710 |
| Pierce 16% Formaldehyde (w/v), Methanol-free | Thermo Fisher Scientific | Cat# 28906 |
| ProLong Gold Antifade Mountant with DAPI | Thermo Fisher Scientific | Cat# P36931 |
| ProLong Gold Antifade Mountant | Thermo Fisher Scientific | Cat# P10144 |
| Gibco Schneider's *Drosophila* Medium | Thermo Fisher Scientific | Cat# 21720001 |
| Gibco Fetal Bovine Serum, US certified, heat inactivated | Thermo Fisher Scientific | Cat# 10082147 |
| Gibco Penicillin-Streptomycin (10,000 U/mL) | Thermo Fisher Scientific | Cat# 15140122 |
| Hygromycin B | MilliporeSigma | Cat# H3274 |
| IGEPAL CA-630 | MilliporeSigma | Cat# I8896 |
| Bovine Serum Albumin (BSA) | VWR | Cat# RLBSA50 |
| Phalloidin, Alexa Fluor 488 | Thermo Fisher Scientific | Cat# A12379 |
| Phalloidin, Alexa Fluor 594 | Thermo Fisher Scientific | Cat# A12381 |
| Phalloidin, CF405M | Biotium | Cat# 00034-T |
| Invitrogen TRIzol Reagent | Thermo Fisher Scientific | Cat# 15596026 |
| Trichloroacetic Acid (Flakes or Crystals) | Fisher Scientific | Cat# BP555-500 |
| MG-132 - CAS 133407-82-6 – Calbiochem | MilliporeSigma | Cat# 474790 |
| Indicating Drierite | W.A. Hammond | Cat# 23005 |
| 10x PBS | Fisher Scientific | Cat# BP3994 |
| UltraPure DNase/RNase-Free Distilled Water | Thermo Fisher Scientific | Cat# 10977015 |
| RNase A, DNase and protease-free | Thermo Fisher Scientific | Cat# EN0531 |
| Proteinase K Solution, ChIP grade | Thermo Fisher Scientific | Cat# 26160 |
| CMCP-10 High viscosity mountant | Polysciences, Inc. | Cat# 16300-250 |
| **Critical commercial assays** | | |
| Q5 Site-Directed Mutagenesis Kit | NEB | Cat# E0554S |
| NEBuilder HiFi DNA Assembly Cloning Kit | NEB | Cat# E5520S |
| Effectene transfection reagent | QIAGEN | Cat# 301427 |

(*Continued on next page*)

*Continued*

| REAGENT or RESOURCE | SOURCE | IDENTIFIER |
|---|---|---|
| NuPAGE 4-12% Bis-Tris Protein Gel | Thermo Fisher Scientific | Cat# NP0335 |
| SilverQuest Silver Staining Kit | Thermo Fisher Scientific | Cat# LC6070 |
| Click-iT™ EdU Imaging Kit with Alexa Fluor™ 488, 594, and 647 Azides | Thermo Fisher Scientific | Cat# C10086 |
| RNeasy Mini Kit | QIAGEN | Cat# 74104 |
| RNase-Free DNase Set | QIAGEN | Cat# 79254 |
| SuperScript III First-Strand Synthesis System | Thermo Fisher Scientific | Cat# 18080051 |
| PowerUp SYBR Green Master Mix | Thermo Fisher Scientific | Cat# A25742 |
| NEBNext Ultra II RNA Library Prep with Sample Purification Beads | NEB | Cat# E7775S |
| NEBNext Poly(A) mRNA Magnetic Isolation Module | NEB | Cat# E7490S |
| NEBNext Multiplex Oligos for Illumina (Index Primers Set 2) | NEB | Cat# E7500S |
| Chromatin Immunoprecipitation (ChIP) Assay Kit | MilliporeSigma | Cat# 17-295 |
| Aluminum Mount, Carbon Adhesive Tape, and Mount Holder | Electron Microscopy Sciences | Cat# 75220, 77816 and 76510 |
| **Deposited data** | | |
| RNA-seq | Gene Expression Omnibus (GEO) | GEO: GSE181299 |
| Proteomics | Proteomics Identification Database (PRIDE) | PRIDE: PXD027934 |
| Mendeley Data | Mendeley Data | Mendeley Data: https://doi.org/10.17632/v2v9n9tbfp.1 |
| **Experimental models: Cell lines** | | |
| *D. melanogaster* S2 cell line | Gift from Spyros Artavanis-Tsakonas (Harvard Medical School) | N/A |
| *D. melanogaster* S2-*yki-SBP* | This study | N/A |
| *D. melanogaster* S2-*bon-SBP* | This study | N/A |
| **Experimental models: Organisms/strains** | | |
| *D. melanogaster: w*; UAS-yki-EGFP attP2* | This study | N/A |
| *D. melanogaster: w; UAS-bon-mCherry attP40* | This study | N/A |
| *D. melanogaster: w; UAS-bon-PPxA-mCherry attP40* | This study | N/A |
| *D. melanogaster: y[1], w[*]* | Gift from Alexei Tulin (University of North Dakota) | N/A |
| *D. melanogaster: Oregon R* | Bloomington Drosophila Stock Center | BDSC: 25211 |
| *D. melanogaster: UAS-GFP* | Bloomington Drosophila Stock Center | BDSC: 5430 |
| *D. melanogaster: da-GAL4* | Wodarz et al.[35] | N/A |
| *D. melanogaster: GMR-Gal4, UAS-yki$^{S168A}$: YFP/ TM6B, Tb, Hu* (used in Figure S1A only) | Gift from Duojia Pan (UT Southwestern Medical Center) | N/A |
| *D. melanogaster: en-GAL4, UAS-GFP/ Cyo, tub-GAL80; UAS-Yki/ TM6B, Tb* (used in Figure S1C only) | Gift from Duojia Pan | N/A |

(*Continued on next page*)

*Continued*

| REAGENT or RESOURCE | SOURCE | IDENTIFIER |
|---|---|---|
| *D. melanogaster: GMR-GAL4* | Freeman[47] and Hay et al.[45] | N/A |
| *D. melanogaster: en-GAL4* | Bloomington Drosophila Stock Center | BDSC: 30564 |
| *D. melanogaster: en-GAL4, ex-lacZ/ CyO, twi>GFP* | Derivative of BDSC: 44248 | BDSC: 44248 |
| *D. melanogaster: en-GAL4/ CyO, Dfd-GFP; Diap1-lacZ/ TM6B* | Derivative of BDSC: 12093 | BDSC: 12093 |
| *D. melanogaster: UAS-bon-RNAi-1* $w^{1118}$*; P{GD1388}v44283* | Vienna Drosophila Resource Center | VDRC: 44283 |
| *D. melanogaster: UAS-bon-RNAi-2* $w^{1118}$*; P{GD1388}v44284* | Vienna Drosophila Resource Center | VDRC: 44284 |
| *D. melanogaster: UAS-bon-RNAi-3* y[1] sc[*] v[1] sev[21]; P{y[+t7.7] v[+t1.8]= TRiP.HMS01657}attP40 | Bloomington Drosophila Stock Center | BDSC: 37515 |
| *D. melanogaster: UAS-bon-RNAi-4* y[1] v[1]; P{y[+t7.7] v[+t1.8]=TRiP.JF02373}attP2 | Bloomington Drosophila Stock Center | BDSC: 27047 |
| *D. melanogaster:* $bon^{21B}$ null allele *P{ry[+t7.2]=hsFLP}22, y[1] w[*]; P{ry[+t7.2]= neoFRT}82B bon[21B]/TM3, Sb[1]* | Bloomington Drosophila Stock Center | BDSC: 43660 |
| *D. melanogaster:* $bon^{487}$ hypomorphic allele *y[1] w[67c23]; P{w[+mC]=lacW}bon[S048706]/ TM3, Sb[1] Ser[1]* | Bloomington Drosophila Stock Center | BDSC: 4543s |
| *D. melanogaster:* $wts^{X1}$ null allele *w[*]; wts[x1] P{ry[+t7.2]= neoFRT}82B/TM6B, Tb[1]* | Bloomington Drosophila Stock Center | BDSC: 44251 |
| *D. melanogaster:* $yki^{B5}$ null allele $yki^{B5}$*/Cyo: twi>GFP* | Gift from Duojia Pan: Huang et al.[44] | N/A |
| *D. melanogaster: UAS-w-RNAi-1* y[1] v[1]; P{y[+t7.7] v[+t1.8]= TRiP.HMS00004}attP2/TM3, Sb[1] | Bloomington Drosophila Stock Center | BDSC: 33613 |
| *D. melanogaster: UAS-w-RNAi-2* y[1] v[1]; P{y[+t7.7] v[+t1.8]= TRiP.JF02387}attP2 | Bloomington Drosophila Stock Center | BDSC: 33762 |
| *D. melanogaster: UAS-yki-RNAi-1* y[1] v[1]; P{y[+t7.7] v[+t1.8]=TRiP.HMS00041}attP2 | Bloomington Drosophila Stock Center | BDSC: 34067 |
| *D. melanogaster: UAS-yki-RNAi-2* P{KK109756}VIE-260B (@40D and 30B) | Vienna Drosophila Resource Center | VDRC: 104523 |
| *D. melanogaster: UAS-sd-RNAi* | Gift from Jin Jiang: Zhang et al.[51] | N/A |
| *D. melanogaster: UAS-wts-RNAi* P{KK101055}VIE-260B (inserted at 30B only) | Vienna Drosophila Resource Center | VDRC: 111002 |
| *D. melanogaster: UAS-yki-S168A-1* y[1] w[*]; P{w[+mC]=UAS-yki.S168A.GFP.HA}10-7-Y | Bloomington Drosophila Stock Center | BDSC: 28816 |
| *D. melanogaster: UAS-yki-S168A-2* y[1] w[*]; P{w[+mC]=UAS-yki.S168A.GFP.HA}10-12-1 | Bloomington Drosophila Stock Center | BDSC: 28836 |
| *D. melanogaster: UAS-mCherry y[1] sc[*] v[1] sev[21]; P{y[+t7.7] v[+t1.8]= UAS-mCherry.VALIUM10}attP2* | Bloomington Drosophila Stock Center | BDSC: 35787 |
| *D. melanogaster: w; FRT82B* | Gift from Spyros Artavanis-Tsakonas | N/A |
| *D. melanogaster: y w hsFLP122; FRT82B Ubi-GFP* | Gift from Spyros Artavanis-Tsakonas | N/A |

(*Continued on next page*)

*Continued*

| REAGENT or RESOURCE | SOURCE | IDENTIFIER |
|---|---|---|
| *D. melanogaster: y w eyFLP; FRT82B Ubi-GFP/TM6B* | Gift from Iswar Hariharan (UC Berkeley) | N/A |
| *D. melanogaster: Ubx-FLP, y w; FRT40A/CyO; FRT82B Sb[63b] /TM3, Ser* | Bloomington Drosophila Stock Center | BDSC: 43337 |
| *D. melanogaster: eyFLP* | Bloomington Drosophila Stock Center | BDSC: 5580 |
| *D. melanogaster: y w hsFLP122; TM3Sb/ TM6B* | Gift from Naoto Ito | N/A |
| *D. melanogaster: w; FRT82B Ubi-mRFP* | Bloomington Drosophila Stock Center | BDSC: 30555 |
| *D. melanogaster: UAS-ovoA w[*]; P{w[+mC]=UAS-ovo.A}1M* | Bloomington Drosophila Stock Center | BDSC: 38428 |
| *D. melanogaster: UAS-ovoB w[*]; P{w[+mC]=UASp-ovo.B}Cmm* | Bloomington Drosophila Stock Center | BDSC: 38429 |
| *D. melanogaster: UAS-svb-RNAi $w^{1118}$; P{GD9026}v41584* | Vienna Drosophila Resource Center | VDRC: 41584 |
| *D. melanogaster: UAS-HDAC1 y[1] w[*]; P{w[+mC]=UAS-HDAC1.V5}A2a* | Bloomington Drosophila Stock Center | BDSC: 32242 |
| *D. melanogaster: UAS-HDAC1-RNAi-1 $w^{1118}$; P{GD4513}v30600* | Vienna Drosophila Resource Center | VDRC: 30600 |
| *D. melanogaster: UAS-HDAC1-RNAi-2 y[1] sc[*] v[1] sev[21]; P{y[+t7.7] v[+t1.8]= TRiP.HMS00164}attP2* | Bloomington Drosophila Stock Center | BDSC: 34846 |
| *D. melanogaster: UAS-Su(var)2-10-RNAi-1 y[1] sc[*] v[1] sev[21]; P{y[+t7.7] v[+t1.8]= TRiP.HMS00705}attP2/TM3, Sb[1]* | Bloomington Drosophila Stock Center | BDSC: 32915 |
| *D. melanogaster: UAS-Su(var)2-10-RNAi-2 y[1] sc[*] v[1] sev[21]; P{y[+t7.7] v[+t1.8]= TRiP.HMS00750}attP2* | Bloomington Drosophila Stock Center | BDSC: 32956 |
| *D. melanogaster: UAS-Hrb27C-RNAi-1 $w^{1118}$; P{GD6964}v16040* | Vienna Drosophila Resource Center | VDRC: 16040 |
| *D. melanogaster: UAS-Hrb27C-RNAi-2 y[1] sc[*] v[1] sev[21]; P{y[+t7.7] v[+t1.8]= TRiP.HMS00597}attP2* | Bloomington Drosophila Stock Center | BDSC: 33716 |
| *D. melanogaster: UAS-sha w[*]; P{w[+mC]=UAS-sha.GFP}3* | Bloomington Drosophila Stock Center | BDSC: 32096 |
| *D. melanogaster: UAS-f-RNAi-1 $w^{1118}$; P{GD1443}v33200* | Vienna Drosophila Resource Center | VDRC: 33200 |
| *D. melanogaster: UAS-f-RNAi-2 y[1] sc[*] v[1] sev[21]; P{y[+t7.7] v[+t1.8]= TRiP.HMS02251}attP2* | Bloomington Drosophila Stock Center | BDSC: 41687 |
| *D. melanogaster: UAS-E(spl)mdelta-HLH y[1] w[*]; P{w[+mC]=UAS-mdelta}h8* | Bloomington Drosophila Stock Center | BDSC: 26677 |
| *D. melanogaster: UAS-E(spl)m3-HLH* | Gift from Eric Lai (Sloan Kettering Institute) | N/A |
| *D. melanogaster: (y) w; M[p3xP3-RFP floxed out), E(spl)-C GFP-mdelta]51D/Cyo* | Gift from François Schweisguth: Couturier et al.[91] | N/A |
| *D. melanogaster: $w^{1118}$; M[p3xP3-RFP floxed out), E(spl)-C m3-sfGFP]51D/Cyo* | Gift from François Schweisguth: Couturier et al.[91] | N/A |
| *D. melanogaster: y; DE-GAL4/TM6B* | Derivative of BDSC: 29650 | BDSC: 29650 |
| *D. melanogaster: ey-GAL4 w[*]; P{w[+m*]=GAL4-ey.H}3-8* | Bloomington Drosophila Stock Center | BDSC: 5534 |

(*Continued on next page*)

*Continued*

| REAGENT or RESOURCE | SOURCE | IDENTIFIER |
|---|---|---|
| *D. melanogaster: ey-GAL4-2 w[*]; P{w[+m*]=GAL4-ey.H}4-8/CyO* | Bloomington Drosophila Stock Center | BDSC: 5535 |
| *D. melanogaster: Hth-GAL4/TM3Sb* | Gift from Claude Desplan: Wernet et al.[58] | N/A |
| *D. melanogaster: UAS-GFP, bi-GAL4* | Bloomington Drosophila Stock Center | BDSC: 58815 |
| *D. melanogaster: C5-GAL4* | Yeh et al.[95] | N/A |
| **Oligonucleotides** | | |
| qRT-PCR primers for *rp49* (normalizing control): Fwd: CGGATCGATATGCTAAGCTGT; Rev: GCGCTTGTTCGATCCGTA | Zhang et al.[42] | N/A |
| qRT-PCR primers for *sha*: Fwd: TCGCTGTGAAATCGAACAAG; Rev: GCCGCCATAGTGACAAACTT | This study | N/A |
| qRT-PCR primers for *f*: Fwd: GAAGGTACCGAAGCCCTACC; Rev: CTTCTTGATGCCCGGTATGT | This study | N/A |
| qRT-PCR primers for *E(spl)m3-HLH*: Fwd: CAGGGAGTAGTGGCTGGTGT; Rev: GGTAATCTGATCGGCAGCAT | This study | N/A |
| qRT-PCR primers for *E(spl)m2-BFM*: Fwd: CATGCGTAACGTGTGGAAAC; Rev: TCAATGAGCAACTCCTGCTG | This study | N/A |
| qRT-PCR primers for *E(*spl*)mdelta-HLH*: Fwd: ACTCAGCATTACCGCAAGGT; Rev: CTTTCTCCAGCTTGCTGACC | This study | N/A |
| ChIP-qPCR primers for *E(*spl*)mdelta-HLH-P1*: Fwd: ATCCCCGAATACCCAATCTC; Rev: GCATGTGCATCGTGAGAAAG | This study | N/A |
| ChIP-qPCR primers for *E(*spl*)mdelta-HLH-P2*: Fwd: TCTTTTCTCGAGGGAAGTGG; Rev: AAGAGTCGGAGCAATCAACC | This study | N/A |
| **Recombinant DNA** | | |
| pMT-yki-V5 | Zhang et al.[42] | N/A |
| pMK33-SBP-C | Yang and Veraksa[111] | N/A |
| pUASTattB | Bischof et al.[112] | N/A |
| pMT-V5-His | Invitrogen | Cat# V412020 |
| pMK33-yki-SBP | This study | N/A |
| pUASTattB-yki-EGFP | This study | N/A |
| pMT-yki-HA | This study | N/A |
| pMT-yki-Y281A-HA | This study | N/A |
| pMT-yki-Y350A-HA | This study | N/A |
| pMT-yki-Y281A Y350A-HA | This study | N/A |
| pFlc-1-bon | Drosophila Genomics Resource Center | DGRC: RE48191 |
| pMT-bon-V5 | This study | N/A |
| pMT-bon-Y507A-V5 | This study | N/A |
| pMT-bon-Y585A-V5 | This study | N/A |
| pMT-bon-Y507A Y585A-V5 | This study | N/A |
| pMK33-bon-SBP | This study | N/A |
| pUASTattB-bon-mCherry | This study | N/A |
| pUASTattB-bon-Y507A Y585A-mCherry | This study | N/A |

(*Continued on next page*)

*Continued*

| REAGENT or RESOURCE | SOURCE | IDENTIFIER |
|---|---|---|
| pFlag-wts | Gift from Maxim Frolov (University of Illinois at Chicago) | N/A |
| pMT-Myc-wts | This study | N/A |
| Software and algorithms | | |
| Significance Analysis of INTeractome (SAINT) (v2.5.0) | Choi et al.[36] | http://saint-apms.sourceforge.net/Main.html |
| Cytoscape (v3.8.0) | Shannon et al.[113] | https://cytoscape.org/; RRID: SCR_003032 |
| STRING (v11.0) | Szklarczyk et al.[37] | https://string-db.org/ |
| Fiji (v2.1.0) | Schindelin et al.[114] | https://imagej.net/Fiji; RRID:SCR_002285 |
| GraphPad Prism (v9.1.0) | GraphPad | https://www.graphpad.com/; RRID:SCR_002798 |
| R (v4.0.0) | R Core Team | https://www.r-project.org/; RRID:SCR_001905 |
| RStudio (v1.2.5042) | RStudio, Inc. | https://www.rstudio.com/; RRID: SCR_000432 |
| ggplot2 (v3.3.2) | Wickham[115] | https://ggplot2.tidyverse.org/ |
| ggpubr (v0.4.0) | Alboukadel Kassambara | https://rpkgs.datanovia.com/ggpubr/ |
| Cutadapt (v2.9) | Martin[116] | https://cutadapt.readthedocs.io/en/stable/; RRID:SCR_011841 |
| Bowtie 2 (v2.3.5.1) | Langmead and Salzberg[117] | http://bowtie-bio.sourceforge.net/bowtie2/index.shtml; RRID:SCR_016368 |
| STAR (v2.7.0e) | Dobin et al.[118] | https://github.com/alexdobin/STAR; RRID:SCR_004463 |
| featureCounts (Subread v1.6.2) | Liao et al.[119] | https://rnnh.github.io/bioinfo-notebook/docs/featureCounts.html; RRID:SCR_012919 |
| DESeq2 (v1.30.1) | Love et al.[73] | https://bioconductor.org/packages/release/bioc/html/DESeq2.html; RRID:SCR_015687 |
| DEBrowser (v1.16.3) | Kucukural et al.[120] | https://www.bioconductor.org/packages/release/bioc/html/debrowser.html |
| DAVID Bioinformatics Resources (v6.8) | Huang da et al.[121] | https://david.ncifcrf.gov/; RRID:SCR_001881 |
| ChIPpeakAnno (v3.30.1) | Zhu et al.[122] | https://bioconductor.org/packages/release/bioc/html/ChIPpeakAnno.html; RRID: SCR_012828 |
| Integrative Genomics Viewer (IGV) (v2.8.2) | Robinson et al.[123] | https://software.broadinstitute.org/software/igv/; RRID:SCR_011793 |

## RESOURCE AVAILABILITY

### Lead contact

Further information and requests for resources and reagents should be directed to and will be fulfilled by the lead contact, Alexey Veraksa (alexey.veraksa@umb.edu).

### Materials availability

Plasmids, cell lines, and transgenic *Drosophila* strains generated in this study are available upon request.

### Data and code availability

The RNA-seq dataset generated in this study has been deposited in NCBI's Gene Expression Omnibus[124] and is accessible through accession number GEO: GSE181299. Mass spectrometry data have been deposited to the ProteomeXchange Consortium via the

PRIDE[125] partner repository with the dataset identifier PRIDE: PXD027934. Raw images of Western blots have been deposited to Mendeley Data: https://doi.org/10.17632/v2v9n9tbfp.1. Any additional information required to reanalyze the data reported in this paper is available from the lead contact upon request.

## EXPERIMENTAL MODEL AND SUBJECT DETAILS

### Cell lines

*Drosophila* S2 cells were cultured in Schneider's *Drosophila* Medium supplemented with 10% (v/v) heat-inactivated fetal bovine serum and 100 unit/ml of penicillin/streptomycin at 25°C. Stable cell lines with recombinant DNA were selected by culturing the cells in the medium supplemented with 300 μg/ml Hygromycin.

### Drosophila strains

*Drosophila melanogaster* stocks were maintained at 18°C or room temperature (RT, 22°C) on standard medium containing cornmeal, molasses, yeast and agar. Genetic crosses were carried out at 25°C unless otherwise indicated. Both male and female animals were used unless otherwise noted.

## METHOD DETAILS

### Plasmid construction

pMK33-yki-SBP, pUASTattB-yki-EGFP and pMT-yki-HA were generated by cloning *yki-RG* isoform from pMT-yki-V5[42] into pMK33-SBP-C vector,[111] pUASTattB vector,[112] and pMT-V5-His vector (Invitrogen, Cat# V412020), respectively. The numbering of the key tyrosine residues for Yki corresponds to the first reported *yki* sequence (*yki-RH*) which has a stretch of additional 23 amino acids at the N-terminus.[44] pMT-bon-V5, pMK33-bon-SBP, and pUASTattB-bon-mCherry were generated by cloning *bon-RB* isoform from pFlc-1-bon (DGRC, RE48191). All tags for Yki and Bon were added to the C-terminus. Mutagenesis in WW domains of Yki and PPxY motifs of Bon was done by Q5 Site-Directed Mutagenesis Kit (NEB, Cat# E0554S). pMT-Myc-wts was generated by cloning the coding sequence of *wts* from pFlag-wts plasmid kindly offered by Maxim Frolov Lab. Myc tag for Wts was added to the N-terminus.

### Stable cell lines

S2 cells were transfected with pMK33-yki-SBP and pMK33-bon-SBP constructs using the Effectene transfection reagent (Qiagen, Cat# 301427). Stable cell lines were selected with medium containing 300 μg/ml of Hygromycin B (MilliporeSigma, Cat# H3274). Yki-SBP and Bon-SBP stable cells were induced overnight with 0.07 mM $CuSO_4$, and protein expression was verified by western blot using anti-SBP antibody (1:1000, Santa Cruz, Cat# sc-101595).

### Transgenic fly lines

pUASTattB-yki-EGFP plasmid was injected into the attP2 site in *D. melanogaster* embryos (Genetic Services, Inc). pUASTattB-bon-mCherry and pUASTattB-bon-Y507A Y585A-mCherry plasmids were injected into the attP40 site in *D. melanogaster* embryos (Rainbow Transgenic Flies, Inc). *yw*, Chr. 2 and Chr. 3 balancer stocks were used in standard crossing schemes to establish the homozygous transgenic lines.

### Genetic crosses

To score the trichome phenotype, *UAS-bon-mCherry*, *UAS-yki-EGFP*, *UAS-yki-S168A-1* (*UAS-yki.S168A.GFP.HA*, BDSC: 28816) and *UAS-wts*-RNAi (VDRC: 111002) were combined with the eye driver *GMR-GAL4* to generate *UAS-bon-mCherry/CyO wg-lacZ; GMR-GAL4/TM6B*, *GMR-GAL4 UAS-yki-EGFP/TM6B*, *GMR-GAL4 UAS-yki-S168A-GFP-1/TM6B* and *UAS-wts*-RNAi/*CyO wg-lacZ; GMR-GAL4/TM6B* fly lines, respectively. *GFP*, *w*-RNAi-1, or *w*-RNAi-2 were coexpressed for transgene dosage compensation.

To achieve higher GAL4 activity, all crosses with *GMR-GAL4 UAS-yki-EGFP*, *GMR-GAL4 UAS-yki-S168A-GFP-1*, and *UAS-wts*-RNAi *GMR-GAL4* were set up at 25°C and shifted to 29°C after the emergence of first instar larvae. All the crosses with *UAS-bon-mCherry; GMR-GAL4* were carried out at 25°C.

All the crosses using *ey-GAL4* and *ey-GAL4-2* were carried out at 29°C except for the cross of *ey-GAL4* and *UAS-wts*-RNAi which was carried out at 25°C. The cross of *da-GAL4* and *UAS-yki-EGFP* for embryo collection and affinity purification was carried out at RT. All other crosses were carried out at 25°C.

Mosaic clones with hsFLP/FRT were generated by heat-shocking first instar larvae with indicated time (figure legends) after egg deposition (AED) at 37°C for 1 hr. Genotypes used for clones are as follows:

3E: *hsFLP;; FRT82B/FRT82B Ubi-GFP*
3F and 3G: *hsFLP;; FRT82B* $wts^{X1}$*/FRT82B Ubi-GFP*
3H: *hsFLP;; FRT82B* $wts^{X1}$*/FRT82B* $Sb^{63b}$
3I ctrl: *eyFLP;; FRT82B/FRT82B Ubi-GFP*
3I $bon^{21B}$: *eyFLP;; FRT82B* $bon^{21B}$*/FRT82B Ubi-GFP*

S3L: *hsFLP;; FRT82B/FRT82B Sb$^{63b}$*
S3M: *hsFLP;; FRT82B bon$^{21B}$/FRT82B Sb$^{63b}$*
6H ctrl: *eyFLP;; GFPmδ/+; FRT82B/FRT82B Ubi-mRFP*
6H *wts$^{X1}$*: *eyFLP;; GFPmδ/+; FRT82B wts$^{X1}$/FRT82B Ubi-mRFP*
6I *bon$^{21B}$*: *eyFLP;; GFPmδ/+; FRT82B bon$^{21B}$/FRT82B Ubi-mRFP*
S6D ctrl: *eyFLP;; m3-GFP/+; FRT82B/FRT82B Ubi-mRFP*
S6D *wts$^{X1}$*: *eyFLP;; m3-GFP/+; FRT82B wts$^{X1}$/FRT82B Ubi-mRFP*

## Affinity Purification

### *Affinity purification from S2 cells*

Blank S2 cells (control) and stable cell lines with 50 ml dense culture were induced overnight (~16 hrs) with 0.07 mM $CuSO_4$ at 25°C. Cells were collected and lysed on ice for 20 min using 1 ml of ice-cold Default Lysis Buffer (DLB) (50 mM Tris pH 7.5, 125 mM NaCl, 5% (v/v) glycerol, 0.2% (v/v) IGEPAL, 1.5 mM $MgCl_2$, 25 mM NaF, 1 mM $Na_3VO_4$, 1 mM DTT, and 2x cOmplete Protease Inhibitor (MilliporeSigma, Cat# 11836145001, 1 tablet per 25 ml lysis buffer)). The lysate was centrifugated at 16,000 rcf for 20 min at 4°C, and the supernatant was incubated with 50 μl of packed Streptavidin beads (Thermo Fisher Scientific, Cat# 53117) for 2 hrs at 4°C with rotation. The beads were then washed 5 times with 1 ml DLB. Proteins on the beads were eluted with 300 μl DLB containing 2 mM biotin and precipitated by adding 1/10 volume of 8.74 M Trichloroacetic acid solution (TCA, Fisher Scientific, Cat# BP555-500). Precipitated proteins were washed once with 500 μl of 0.874 M TCA and four times with ice-cold acetone. The protein pellet was dried overnight at RT and incubated in 40 μl of 2x SDS sample buffer at 95°C for 5 min. Samples were assessed by silver staining using NuPAGE 4-12% Bis-Tris Protein Gel (Thermo Fisher Scientific, Cat# NP0335) and SilverQuest Silver Staining Kit (Thermo Fisher Scientific, Cat# LC6070). The protein samples for mass spectrometry were separated on a short SDS-PAGE gel (8% Tris-Glycine) followed by Coomassie blue staining. Two gel pieces (>75 kDa and < 75 kDa) for each sample were submitted to Taplin Mass Spectrometry Facility at Harvard Medical School for mass spectrometry analysis.

### *Affinity purification from embryos*

5 L fly cages with apple juice plates[126] were set up for *yw* (control) and the cross *da-GAL4* x *UAS-yki-EGFP*. Flies were allowed to lay eggs for 15 hrs at RT, then the apple juice plates containing the embryos were incubated for 3 hrs at 25°C. Approximately 1 g embryos were dechorionated with 50% (v/v) Clorox bleach and washed with water. Collected embryos were then mixed with 6 ml of ice-cold DLB containing 0.5% (v/v) IGEPAL and 10 μM MG132 in a glass homogenizer and lysed on ice with 20-30 strokes using a tight pestle. The lysate was kept on ice for 20 min and centrifuged at 16,000 rcf for 20 min at 4°C. The supernatant was filtered with pre-chilled 0.45 μm filter and incubated with 50 μl of packed Pierce Control Agarose Resin (Thermo Fisher Scientific, Cat# 26150) for 30 min at 4°C with rotation to preclear unspecific binding. The lysate was then incubated with 20 μl of packed GFP-Trap Agarose (Bulldog Bio, Cat# GTA020) for 2 hrs at 4°C with rotation. After binding, the GFP beads were washed 5 times with 1 ml DLB containing 0.5% (v/v) IGEPAL and 10 μM MG132, followed by addition of 40 μl of 4x SDS sample buffer and heating at 95°C for 6 min. The samples were then assessed by silver staining and the protein samples for mass spectrometry were prepared and submitted as above.

## Mass Spectrometry and data analysis

In-gel trypsin digestion and liquid chromatography/tandem mass spectrometry (nanoLC-MS/MS) were performed by Taplin Mass Spectrometry Facility at Harvard Medical School. Mass spectrometry results from two gel pieces for each sample were combined, and the results from the experimental and control samples were analyzed with Significance Analysis of INTeractome (SAINT) (v2.5.0) using the total peptides identified for each protein.[36] Any protein with the SAINT score (average probability) $\geq$ 0.8 was considered as a high-confidence interactor and was included in the interactome. SAINT analysis included the following numbers of samples: Yki-SBP, four experiments and four controls; Yki-EGFP, three experiments and five controls; Bon-SBP, two experiments and three controls.

### *Yki protein interactome*

Yki protein interactors with SAINT score $\geq$ 0.8 either in S2 cells or in embryos were included in the Yki protein interactome. The Yki protein interactome was further populated with the interactions incorporated from the STRING database (v11.0) and FlyBase (vFB2020_04).[37,38] All proteins in the Yki interactome from the current study were imported into the STRING database and analyzed with default settings: full network, medium confidence 0.4 and all active interaction sources (Textmining, Experiments, Databases, Co-expression, Neighborhood, Gene Fusion and Co-occurrence). The summary of physical interactions of Yki in FlyBase was selected to show neighbor-neighbor interactions, and the summary of genetic interactions was selected to show both suppression and enhancement. The interaction data from FlyBase were exported through esyN,[127] while only the interactions between the proteins that were identified as components of the Yki protein interactome from the current study were incorporated into the Yki protein interactome. The Yki protein interactome was visualized with Cytoscape.[113] Nodes represent Yki and Yki interactors identified in the current study. Edges represent the interactions incorporated from STRING and FlyBase. Clustering was done manually based on FlyBase annotations and publications.[38] Gene symbols were updated to FlyBase version FB2020_04, released Aug 18, 2020.

### Bon protein interactome

Bon protein interactors with SAINT score ≥ 0.8 from S2 cells were included in the Bon protein interactome which was visualized with Cytoscape. The nodes and edges represent the interactors and interactions identified in the current study, respectively. Gene symbols were updated to FlyBase version FB2020_04, released Aug 18, 2020.

## Co-immunoprecipitation

S2 cells were transfected with indicated plasmids or blank pMT-V5-His vector using the Effectene transfection reagent. 24 hrs after transfection, cells were induced with 0.35 mM $CuSO_4$ overnight at 25°C, collected and lysed on ice for 20 min with 600 μl of ice-cold DLB. The lysate was centrifuged at 16,000 rcf for 20 min at 4°C. 40 μl supernatant was mixed with 20 μl of 4x SDS sample buffer and heated at 95°C for 6 min to generate lysate samples. The rest of the lysate was incubated with 20 μl of packed anti-V5 beads (MilliporeSigma, Cat# A7345) or anti-HA beads (MilliporeSigma, Cat# E6779) for 2 hrs at 4°C. The beads were then washed 3 times (or 4 times for co-IP with Myc-wts) with 1 ml DLB, mixed with 40 μl of 4x SDS sample buffer, and heated at 95°C for 6 min to generate IP samples. The lysate samples and IP samples were subjected to SDS-PAGE followed by western blot using Odyssey Blocking Buffer (PBS) (LI-COR Biosciences, Cat# 927-40003) as blocking buffer, mouse anti-V5 antibody (1:1000, MilliporeSigma, Cat# V8012), Rabbit anti-HA antibody (1:1000, MilliporeSigma, Cat# H6908) and Mouse anti-Myc antibody (1:1000, Cell Signaling, Cat# 2276S) as primary antibody, and Goat anti-Mouse IgG (1:20,000, LI-COR Biosciences, Cat# 926-68070) and Donkey anti-Rabbit IgG (1:20,000, LI-COR Biosciences, Cat# 926-32213) as secondary antibodies. Blotting membranes were scanned with LI-COR Odyssey CLx Imaging Systems.

## EdU incorporation assay

EdU incorporation assay was performed using Click-iT® EdU Imaging Kit (Thermo Fisher Scientific, C10086) with adapted procedures from.[128] Eye discs were dissected in unsupplemented Schneider's *Drosophila* Medium and incubated in 100 μM EdU for 20 min in the dark at RT. Discs were then washed three times with 1x PBS, fixed in 3.7% (v/v) Formaldehyde (MilliporeSigma, Cat# F8775) in 1x PBS for 15 min in the dark at RT, followed by three washes with 1x PBS and permeabilization in PB-Triton (1x PBS containing 0.3% (v/v) Triton X-100) for 20 min at RT. Discs were then washed twice with 3% BSA (m/v, VWR, Cat# RLBSA50) in 1x PBS and incubated in Click-iT reaction cocktail containing Alexa Fluor 488 (for *bon-mCherry*) or 594 (for *yki-S168A-GFP*) for 30 min in the dark at RT. After washing once with 3% BSA in 1x PBS and once with 1x PBS, discs were mounted in ProLong Gold Antifade Mountant with DAPI (Thermo Fisher Scientific, Cat# P36931). All Incubation and washing were carried out on a platform shaker with mild shaking.

## Tissue staining

### Antibodies and phalloidin

All antibodies and phalloidin reagents used in this study are listed in the key resources table. All primary antibodies from DSHB were used at 1:50 (v/v) dilution. All primary and secondary antibodies and phalloidin from Thermo Fisher Scientific were used at 1:500 (v/v) dilution. Mouse anti-β-Gal antibody (Promega, Cat# Z3783) was used at 1:100 (v/v) dilution. Guinea Pig anti-Bon antibody was used at 1: 5000 (v/v) dilution.[25] Guinea Pig anti-Hth antibody was used at 1:1000 (v/v) dilution.[109] Rabbit anti-BarH1 was used at 1:500 (v/v) dilution.[110] Phalloidin 405 (Biotium, Cat# 00034-T) was used at 1:100 (v/v) dilution.

### Embryo staining

Stage 16 embryos were collected and dechorionated with 50% (v/v) Clorox bleach, rinsed with water, and fixed in 20 ml of fixative containing 4% (v/v) paraformaldehyde (Electron Microscopy Sciences, Cat# 15710), 25% (v/v) Heptane and 1x PBS for 20 min at RT. 8 ml of methanol was added to remove the vitelline membrane. Fixed and devitellinized embryos were washed three times with 1.4 ml methanol, four times with 1.4 ml ethanol and twice with PBT (1x PBS containing 0.1% (v/v) Tween 20). Embryos were subsequently incubated in 1 ml of blocking solution (1:1 (v/v) of Western Blocking Reagent (Roche, Cat#11921681001) and PBT) for 2 hrs at RT and incubated overnight in 500 μl of blocking solution containing primary antibody at 4°C. Embryos were then washed five times with 0.1% BSA (m/v in PBT) and incubated in 1 ml of blocking solution for 1 hr at RT. The embryos were then incubated in secondary antibody diluted in blocking solution for 2 hrs in the dark at RT, washed sequentially in 0.1% BSA, PBT and 1x PBS, and mounted with ProLong Gold Antifade Mountant with DAPI. All incubation and washing were carried out on a nutator.

### L3 imaginal disc staining

3rd instar larval wing discs and eye-antennal discs were dissected in ice-cold 1x PBS and were fixed in 3.7% (v/v) formaldehyde (MilliporeSigma, Cat# F8775) for 15-20 min at RT. The discs were washed three times with 1x PBS, permeabilized with PB-Triton for 20 min at RT and were incubated in primary antibodies diluted in blocking solution (1:1 (v/v) of Western Blocking Reagent and PBT) overnight at RT. The discs were then washed four times with PBT, incubated in secondary antibodies diluted in blocking solution for 2-3 hrs in the dark at RT, washed four times with PBT, and mounted with ProLong Gold Antifade Mountant with DAPI. All incubation and washing were carried out on a platform shaker with mild shaking.

### Pupal eye staining

Pupal eye staging, dissection and staining procedures were adapted from.[129,130] Newly formed white pupae were circled on the fly vial. 32-46 hrs later, pupal eyes were dissected with forceps in ice-cold 1x PBS, transferred to 3.7% (v/v) formaldehyde (MilliporeSigma, Cat# F8775) and fixed for 15-20 min at RT. Fixative was replaced with 1x PBS and washed three times followed by permeabilizing with PB-Triton for 30 min. The pupal eyes were then incubated in primary antibodies diluted in PB-Triton overnight at RT, washed four times with PB-Triton, and incubated in secondary antibody or Phalloidin diluted in PB-Triton for 3 hrs in the dark at

RT. The pupal eyes were then washed four times with PB-Triton and mounted with ProLong Gold Antifade Mountant (Thermo Fisher Scientific, Cat# P10144). All incubation and washing were carried out on a platform shaker with mild shaking.

### Fluorescence and bright-field microscopy

Fluorescent images were acquired using Zeiss LSM 880 Confocal Microscope. For embryos, 20x objective and 1 Airy Unit (AU) pinhole were used. For L3 wing discs, 20x objective was used to take a z stack, and maximum intensity projection of the entire disc proper was performed to generate final images. For L3 eye-antennal discs, 20x or 63x objective was used to take z stacks with optimal step size, and maximum intensity projection was performed for the entire disc proper, except for the anti-Ct staining which was focused on the disc proper while minimizing the inclusion of the cone cell focal plane, or for the orthogonal sections and their corresponding 2D views which are indicated in the figures and legends. For pupal eyes, 63x objective and z stack were used with focal plane set to the corresponding cell type, except for the final images of *GFPmδ* and anti-Elav staining which were generated by maximum intensity projection of the entire depth of pupal eye unless indicated otherwise. In mispatterned pupal eyes overexpressing Bon, Ct-positive cone cells and BarH1-positive primary pigment cells were distinguished from bristle groups which have both Ct and BarH1 expression in the basal nuclei by not having both signals.[15,131,132] Bright-field images of adult eyes were taken under Zeiss Stemi 2000-C Microscope with an attached camera at 50x magnification. Adult wings were separated, immersed briefly in isopropanol, mounted with 3:1 (v/v) CMCP-10 (Polysciences, Inc., Cat# 16300-250) and lactic acid, and imaged with Olympus BX60 Microscope under 4x and 40x objectives for the entire wing and wing trichomes, respectively. Due to the difference in size, only images from female adult flies were analyzed. All images were processed with Fiji.[114]

### Scanning electron microscopy (SEM)

Preparation of adult flies for SEM was adapted from.[133,134] 1-2 days old adult flies were sequentially dehydrated in 1 ml of 25%, 50%, 75%, 100%, 100% and 100% ethanol (v/v in water) for 8-16 hrs per step at RT (overnight for the first step). The flies were then chemically dried in 500 μl of 25%, 50%, 75%, 100%, 100% and 100% Hexamethyldisilazane (v/v in ethanol) (HMDS, Electron Microscopy Sciences, Cat# 16700) for 30 min per step at RT. Most of the HMDS was then removed and the remaining HMDS was allowed to be dried under vacuum in a desiccator containing Indicating Drierite (W.A. Hammond, Cat# 23005) overnight at RT. The samples were then mounted on Aluminum Mount using Carbon Adhesive Tape, and stored in Mount Holder (Electron Microscopy Sciences, Cat# 75220, 77816 and 76510). The samples were subsequently coated with gold at 50 mAmps for 150 secs with Denton Vacuum Desk V sputter coater for most samples or coated with platinum for 8 nm with Denton Vacuum 502-B for samples in Figures S2O–S2T. Most images were acquired with JEOL JSM-6010LA IntouchScope Scanning Electron Microscope using 20 kV voltage, 10 mm working distance, 40-50 spot size, and 150x, 300x, 500x, 1000x, and 3000x magnifications as needed. Images in Figures S2O–S2T were acquired with FEI Quanta 200 FEG MK II Scanning Electron Microscope using 10 kV voltage, 10 mm working distance, 2.5 spot size, and 150x and 1000x magnifications as needed. Due to the difference in size, only images from female adult flies were analyzed. Images were processed with Fiji. The numbers of trichomes were counted with Fiji in an area of 1306 $\mu m^2$ (41.73 μm x 31.30 μm) per image for all genotypes.

### Total RNA preparation

Total RNA preparation method was adapted from.[42] Pupal eyes were dissected from 40-41 hrs APF pupae (newly formed white pupae were staged for 40 hrs at 25°C and dissected within 1 hr at RT) in ice cold RNase-free 1x PBS diluted from RNase-free 10x PBS (Fisher Scientific, Cat# BP3994) with RNase-free water (Thermo Fisher Scientific, Cat# 10977015). Dissected pupal eyes were immediately transferred to 100 μl of TRIzol (Thermo Fisher Scientific, Cat# 15596026) and kept at RT for 5 min to lyse. Samples in TRIzol were stored at -80°C until 60 pupal eyes for each genotype were collected. All TRIzol samples for each genotype were then thawed and combined, and the volume was brought up to 500 μl per sample. Total RNA was extracted twice by adding 100 μl of chloroform, vigorously shaking for 15 secs, incubating at RT for 3 min, centrifuging at 11,000 rcf at 4°C for 15 min, and collecting the aqueous phase. The total RNA was then precipitated by adding 1 volume of 70% ethanol (v/v in RNase-free water), and purified with RNeasy Mini Kit (QIAGEN, Cat# 74104, 79254).

### RNA-sequencing, data analysis, and qRT-PCR validation

The RNA-seq libraries were prepared from 100 ng of total RNA per genotype with NEBNext Ultra II RNA Library Prep Kit mRNA Isolation Module (NEB, Cat# E7775S, E7490S, E7500S). Quality control and sequencing of the RNA-seq libraries were performed by GENEWIZ, Inc. using Agilent TapeStation and Illumina HiSeq 4000 with a 2x150 paired-end configuration.

The adapter sequences were trimmed from raw reads, and reads shorter than 18 nt were removed by Cutadapt (v2.9).[116] The reads mapped to tRNAs, rRNA, snRNA and snoRNA were removed by mapping through Bowtie 2 (v2.3.5.1) with very sensitive setting and maximum fragment size of 1000 in addition to default setting.[117] The tRNA, rRNA, snRNA and snoRNA reference sequences (dmel-all-tRNA-r6.33.fasta and dmel-all-miscRNA-r6.33.fasta) were obtained from FlyBase.[38] The remaining reads were mapped to *D. melanogaster* genome Ensembl_BDGP6[135] by STAR (v2.7.0e)[118] with default parameters. Gene counting was achieved by featureCounts (Subread v1.6.2) with overlapping or polycistronic genes counted as a fraction.[119] Differential gene expression analysis was performed with DESeq2 (v1.30.1) through DEBrowser (v1.16.3) with default settings,[73,120] and genes with maximum count fewer than

10 were filtered out. Normalization method used in DESeq2 was Median Ratio Normalization (MRN).[136] The Pearson Correlation Coefficient analysis was performed by ggpubr R package. Plots were generated using ggplot2.[115] The Gene Ontology (GO) analysis was performed with DAVID Bioinformatics Resources (v6.8).[121]

cDNA was generated from total RNA using SuperScript III First-Strand Synthesis System (Thermo Fisher Scientific, Cat# 18080051). qPCR was performed with biological and technical triplicates using PowerUp SYBR Green Master Mix (Thermo Fisher Scientific, Cat# A25742) on QuantStudio 3 Real-Time PCR System. Gene expression was normalized to ribosomal protein *rp49*. P values were calculated using the values of ΔCq (Cq (gene of interest) - Cq(rp49)).[137] The sequences of the primers are listed in the key resources table.

### DNA binding analysis and ChIP-qPCR

Overlap in the DNA binding locus for Yki, Bon, and Sd was analyzed and visualized by ChIPpeakAnno[122] using published ChIP-seq datasets of Yki (GSE38594)[74] and Bon (GSE25921)[75] after converting to dm6 coordinates, and DamID-seq dataset of Sd (GSE120731).[76] The p values between every two datasets were determined by the hypergeometric test using totalTest number for number of potential peaks.[122] The totalTest number here (89144) was calculated by dividing the *Drosophila* genome (143.7 Mb)[138] with the largest mean peak width from three datasets (1612 bp for Sd DamID), assuming that these three proteins can potentially bind anywhere in the genome. The presence of ChIP peaks and DamID peaks at Bon-Yki jointly regulated genes was analyzed using IGV.[123]

ChIP assay was performed using Chromatin Immunoprecipitation (ChIP) Assay Kit (MilliporeSigma, Cat# 17-295) with adaptations based on the application notes on GFP- and RFP-Trap by ChromoTek. 100 L3 eye-antennal discs for each replicate were dissected in ice-cold 1x PBS. Protein and DNA were crosslinked by incubating the discs in 1.8% (v/v) formaldehyde (Thermo Fisher Scientific, Cat# 28906) in 1x PBS for 15 min at RT and quenched with 225 mM Glycine for 5 min at RT.[74] Discs were washed three time with 1x PBS, transferred to 200 μl SDS lysis buffer containing 2.5 x EDTA-free mini cOmplete Protease Inhibitor (MilliporeSigma, Cat# 11836170001, 1 tablet per 4 ml SDS lysis buffer), homogenized with Pellet Pestle for 30 secs on ice, and incubated for 10 min on ice. The lysate was sonicated using Bioruptor sonicator for 15 min (30 secs on and 30 secs rest at high power) in 4°C water bath to shear the DNA. Samples were centrifuged at 16,000 rcf for 10 min at 4°C, and the supernatant was diluted 10-fold in ChIP Dilution Buffer containing 2.5 x mini cOmplete inhibitor. Samples were pre-cleared with 75 μl (50% slurry) of Pierce Control Agarose Resin for 1 hr at 4°C with rotation, and after a brief centrifugation, 5% sample was saved as input sample. The supernatant was then incubated with 25 μl (50% slurry) of RFP-Trap agarose overnight at 4°C with rotation. The agarose beads were washed as indicated in the kit. The protein-DNA complex was eluted twice with 250 μl elution buffer for 15 min, first at RT on a nutator and second on a 65°C shaker. Input samples and elutes were reverse cross-linked with 0.2 M NaCl at 65°C overnight, digested with RNase A (Thermo Fisher Scientific, Cat# EN0531) for 30 min at 37°C and Proteinase K (Thermo Fisher Scientific, Cat# 26160) as indicated in the kit. DNA was recovered by phenol/chloroform extraction and ethanol precipitation.

qPCR was performed with biological triplicates and technical duplicates using PowerUp SYBR Green Master Mix on QuantStudio 3 Real-Time PCR System. Ratio to the input was presented. P values were calculated using the values of ΔCq (Cq (ChIPped) - Cq(input)). The sequences of the primers are listed in the key resources table.

## QUANTIFICATION AND STATISTICAL ANALYSIS

Statistical significance of categorical variables was determined by Fisher's exact test with two-sided p value calculation using GraphPad Prism (v9.1.0). Unless indicated otherwise, in all other statistical analyses, data were presented as mean ± SD of at least three replicates, and the significance was determined by unpaired t-test with Welch's correction using GraphPad Prism (v9.1.0). The numbers (n) and values of each sample used per experiment are provided in Table S5. The p values are presented as follows: ns ($p > 0.05$, not significant), * ($p \leq 0.05$), ** ($p \leq 0.01$), *** ($p \leq 0.001$), **** ($p \leq 0.0001$).

**Developmental Cell, Volume *58***

## Supplemental information

# Hippo pathway and Bonus control developmental cell fate decisions in the *Drosophila* eye

**Heya Zhao, Kenneth H. Moberg, and Alexey Veraksa**

# Figure S1

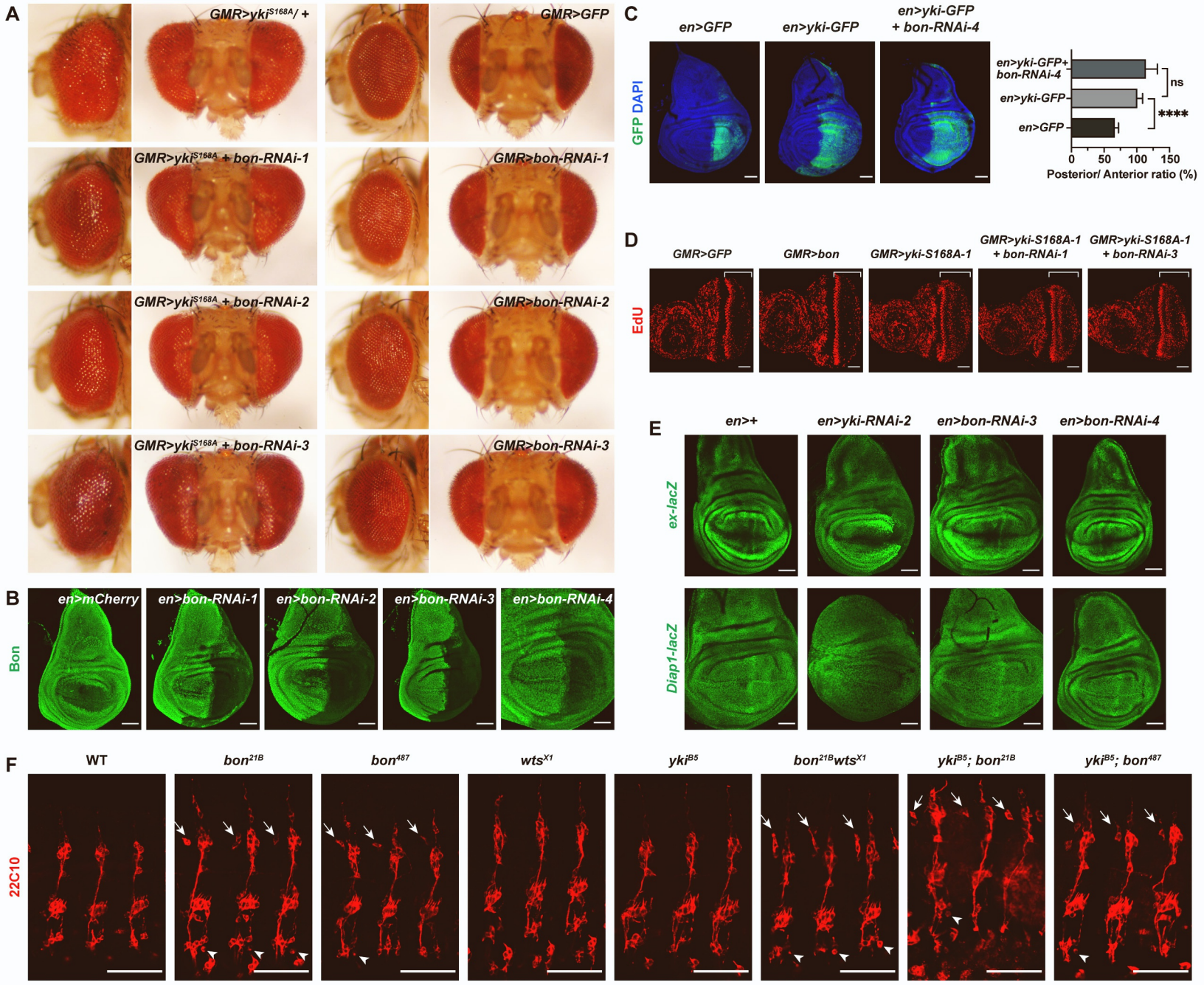
A
GMR>yki$^{S168A}$/ +
GMR>GFP
GMR>yki$^{S168A}$ + bon-RNAi-1
GMR>bon-RNAi-1
GMR>yki$^{S168A}$ + bon-RNAi-2
GMR>bon-RNAi-2
GMR>yki$^{S168A}$ + bon-RNAi-3
GMR>bon-RNAi-3
B
Bon
en>mCherry
en>bon-RNAi-1
en>bon-RNAi-2
en>bon-RNAi-3
en>bon-RNAi-4
C
en>GFP
en>yki-GFP
en>yki-GFP + bon-RNAi-4
GFP DAPI
en>yki-GFP+ bon-RNAi-4
en>yki-GFP
en>GFP
ns
****
0
50
100
150
Posterior/ Anterior ratio (%)
D
EdU
GMR>GFP
GMR>bon
GMR>yki-S168A-1
GMR>yki-S168A-1 + bon-RNAi-1
GMR>yki-S168A-1 + bon-RNAi-3
E
en>+
en>yki-RNAi-2
en>bon-RNAi-3
en>bon-RNAi-4
ex-lacZ
Diap1-lacZ
F
22C10
WT
bon$^{21B}$
bon$^{487}$
wts$^{X1}$
yki$^{B5}$
bon$^{21B}$wts$^{X1}$
yki$^{B5}$; bon$^{21B}$
yki$^{B5}$; bon$^{487}$

**Figure S1. Independent functions of Yki and Bon in growth regulation and embryonic peripheral nervous system (PNS) development (related to Figure 2).**

(A) Adult eyes expressing indicated *UAS* transgenes with *GMR-GAL4* were examined for growth phenotypes. Knockdown of *bon* with different RNAi lines did not modify Yki-S168A-induced eye overgrowth (left panels) and did not affect eye size when expressed alone (right panels).

(B) Third instar larval (L3) wing discs expressing indicated *UAS* transgenes with the posterior compartment driver *en-GAL4* were immunostained with anti-Bon antibody, confirming the effectiveness of all four Bon RNAi lines. Anterior is on the left. Scale bars: 50 μm.

(C) L3 wing discs expressing indicated *UAS* transgenes with *en-GAL4* were examined for the effect of *bon-RNAi* on Yki-induced overgrowth. Quantification was based on the ratio of the area of the posterior compartment (GFP) to the area of the anterior compartment (non-GFP) of the wing discs. Data shown as mean ± SD of ≥4 wing discs. Details of quantification are provided in Table S5. Scale bars: 50 μm.

(D) L3 eye-antennal discs expressing indicated *UAS* transgenes with *GMR-GAL4* were examined for cell proliferation using EdU incorporation assay. Brackets: from the second mitotic wave (SMW) to the posterior end. Overexpression of Bon did not affect EdU incorporation, and the ectopic DNA synthesis posterior to the SMW with Yki-S168A overexpression was not affected by knockdown of *bon*. Scale bars: 50 μm.

(E) L3 wing discs expressing indicated *UAS* transgenes with *en-GAL4* were examined for the effect of *bon-RNAi* on the reporters of canonical Yki targets, *ex-lacZ* and *Diap1-lacZ*. Scale bars: 50 μm.

(F) Stage 16 embryos of the indicated genotypes were immunostained with neuronal antibody 22C10 to examine the PNS. Oregon R was used as wild-type (WT) control. All mutants were homozygous. Second to fourth abdominal segments (A2-A4) are shown in all images, with anterior to the left and dorsal up. Arrows and arrowheads indicate the ectopic neurons anterior to the dorsal clusters and posterior to the v' clusters, respectively. Scale bars: 50 μm.

**Figure S2**

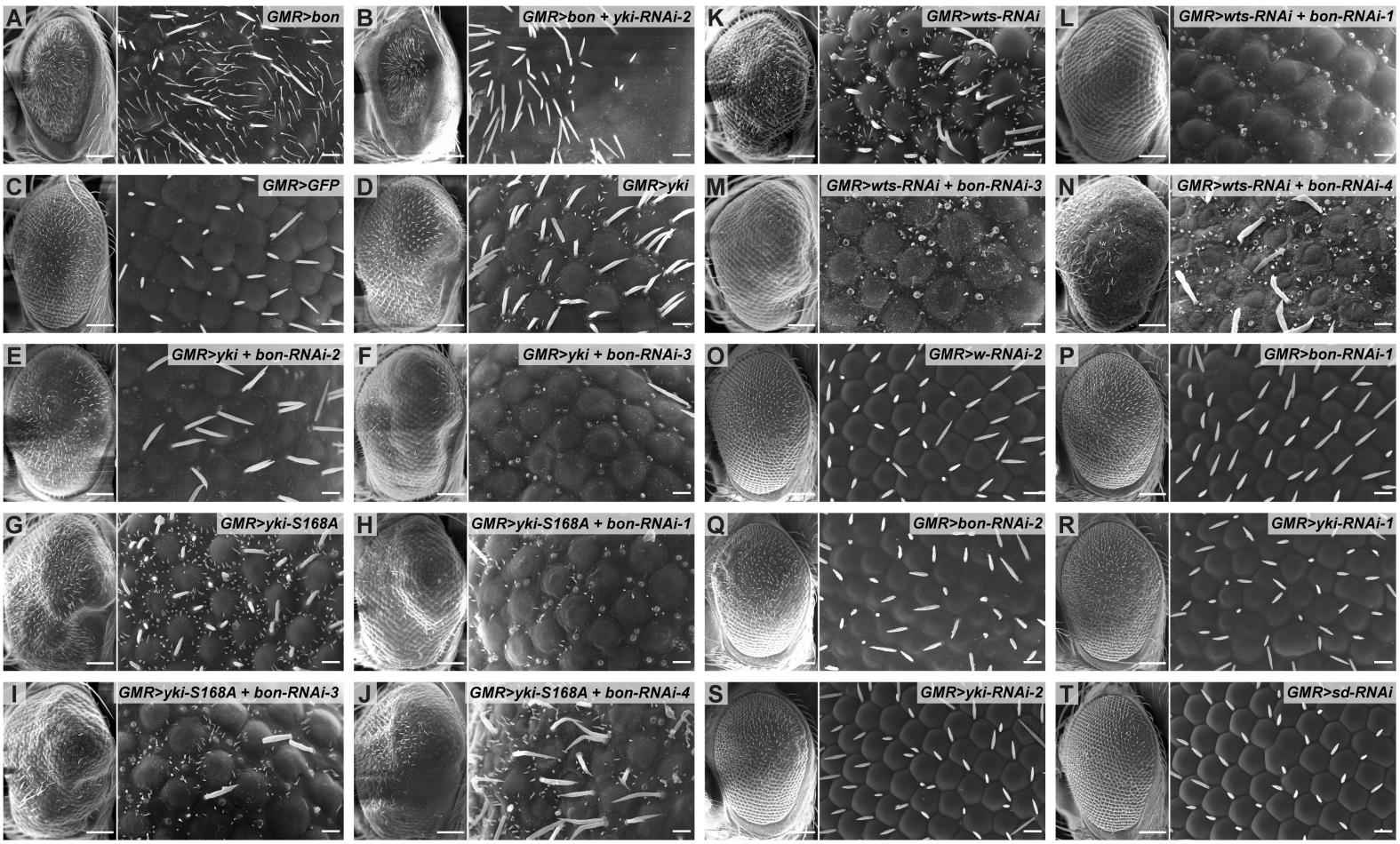
A
GMR>bon
B
GMR>bon + yki-RNAi-2
K
GMR>wts-RNAi
L
GMR>wts-RNAi + bon-RNAi-1
C
GMR>GFP
D
GMR>yki
M
GMR>wts-RNAi + bon-RNAi-3
N
GMR>wts-RNAi + bon-RNAi-4
E
GMR>yki + bon-RNAi-2
F
GMR>yki + bon-RNAi-3
O
GMR>w-RNAi-2
P
GMR>bon-RNAi-1
G
GMR>yki-S168A
H
GMR>yki-S168A + bon-RNAi-1
Q
GMR>bon-RNAi-2
R
GMR>yki-RNAi-1
I
GMR>yki-S168A + bon-RNAi-3
J
GMR>yki-S168A + bon-RNAi-4
S
GMR>yki-RNAi-2
T
GMR>sd-RNAi

**Figure S2. Bon and Yki are mutually dependent for trichome formation in adult eyes (related to Figure 2).**

(A-B) Scanning Electron Microscope (SEM) images of adult eyes with the indicated genotypes, quantified in Figure 2H. Scales bars in left panels: 100 μm; in enlarged views in right panels: 10 μm.

(C-N) SEM images of adult eyes with the indicated genotypes, quantified in Figures 2O-2R or Table S5, showing that *bon-RNAi*s significantly suppressed wild-type Yki (C-F), Yki-S168A (G-J), and *wts* knockdown (K-N) induced trichomes in adult eyes. Crosses were set up at 25°C and shifted to 29°C after the emergence of first instar larvae. Scales bars in left panels: 100 μm; in enlarged views in right panels: 10 μm.

(O-T) SEM images of adult eyes with individual knockdown of *bon*, *yki*, or *sd* with *GMR-GAL4*. *w-RNAi-2* was used as a control. Scales bars in left panels: 100 μm; in enlarged views in right panels: 10 μm.

# Figure S3

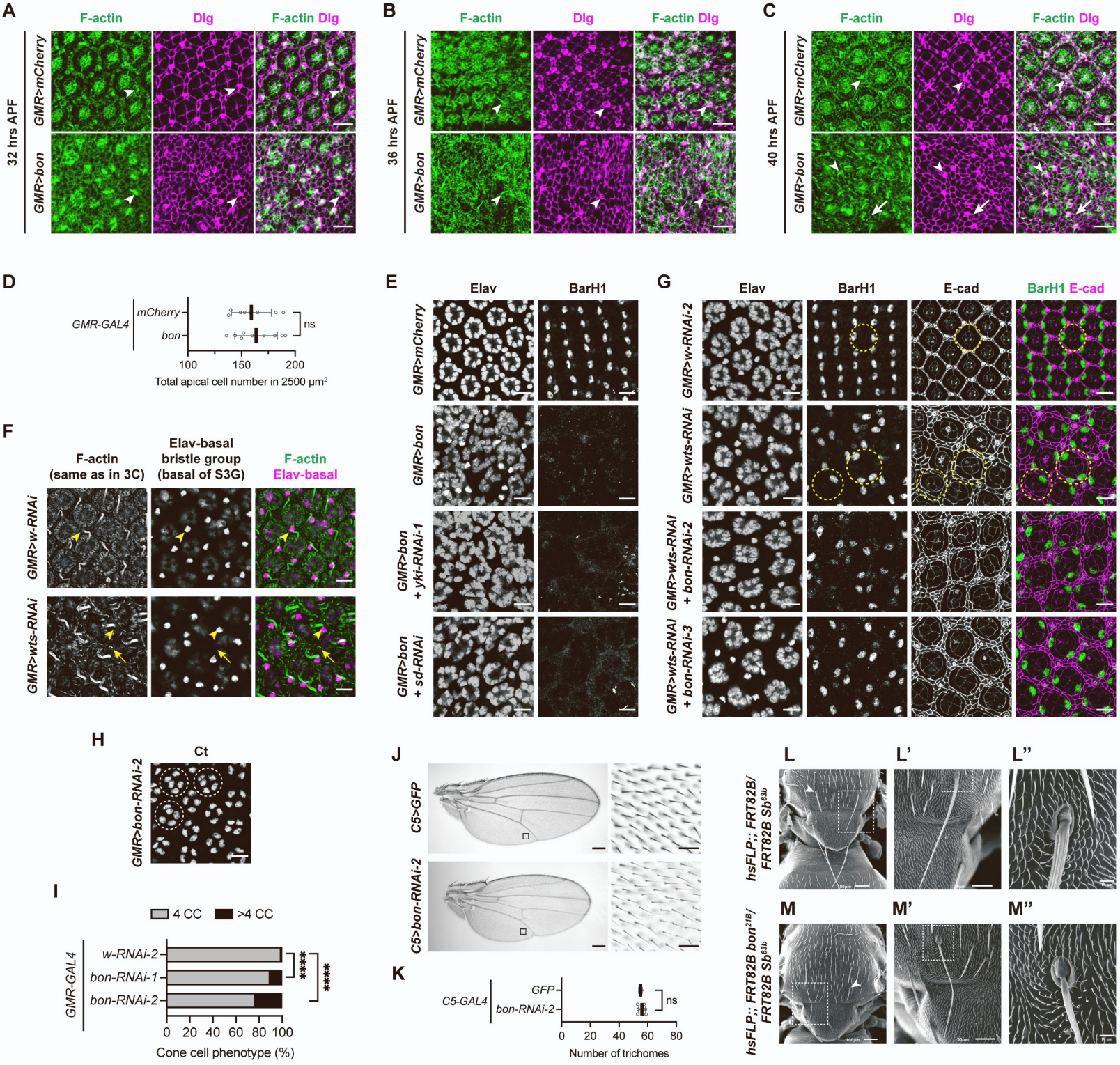
A
F-actin
Dlg
F-actin Dlg
32 hrs APF
GMR>mCherry
GMR>bon
B
36 hrs APF
C
40 hrs APF
D
GMR-GAL4
mCherry
bon
ns
100
150
200
Total apical cell number in 2500 µm²
E
Elav
BarH1
GMR>mCherry
GMR>bon
GMR>bon + yki-RNAi-1
GMR>bon + sd-RNAi
F
F-actin (same as in 3C)
Elav-basal bristle group (basal of S3G)
F-actin Elav-basal
GMR>w-RNAi
GMR>wts-RNAi
G
E-cad
BarH1 E-cad
GMR>w-RNAi-2
GMR>wts-RNAi
GMR>wts-RNAi + bon-RNAi-2
GMR>wts-RNAi + bon-RNAi-3
H
Ct
GMR>bon-RNAi-2
I
4 CC
>4 CC
GMR-GAL4
w-RNAi-2
bon-RNAi-1
bon-RNAi-2
****
****
0 20 40 60 80 100
Cone cell phenotype (%)
J
C5>GFP
C5>bon-RNAi-2
K
C5-GAL4
GFP
bon-RNAi-2
ns
0 20 40 60 80
Number of trichomes
L
L'
L''
hsFLP;; FRT82B/ FRT82B Sb63b
M
M'
M''
hsFLP;; FRT82B bon21B/ FRT82B Sb63b

**Figure S3. Bon and Yki promote epidermal trichomes at the expense of retinal cells (related to Figure 3 and Discussion).**

(A-C) Bon induced trichomes are initiated at 40 hrs after puparium formation (APF). Pupal eyes expressing the indicated *UAS* transgenes with *GMR-GAL4* were collected at the indicated time points and stained with phalloidin for F-actin and anti-disc large antibody (Dlg) for cell boundaries. Arrowheads: interommatidial bristles and sockets; arrows: trichomes and the corresponding cells. Scale bars: 10 μm.

(D) Quantification of the total cell numbers in an apical area of 2500 $\mu m^2$ for pupal eyes at 44 hrs APF of the indicated genotypes shown in Figure 3A. All cells outlined by the anti-Dlg staining at the apical surface were counted (photoreceptor cells were not clearly outlined thus not included), including all the cone cells, primary pigment cells, secondary pigment cells, tertiary pigment cells, undifferentiated cells, and bristle groups which were counted as one cell each. Data shown as mean ± SD of ≥8 pupal eyes. Detailed numbers are provided in Table S5.

(E) Pupal eyes at 44 hrs APF expressing the indicated *UAS* transgenes with *GMR-GAL4* were immunostained with anti-Elav antibody for photoreceptors and bristle groups, or anti-BarH1 antibody for primary pigment cells. Scale bars: 10 μm.

(F) Images of pupal eyes with the indicated genotypes (from Figures 3C and S3G) co-stained for F-actin and Elav were analyzed for the difference between trichomes and interommatidial bristles. Elav is expressed in the interommatidial bristle groups (arrowheads) but not in trichomes (arrows). Scale bars: 10 μm.

(G) Pupal eyes at 40 hrs APF grown at 29°C (equivalent to 48 hrs APF at 25°C) expressing the indicated *UAS* transgenes with *GMR-GAL4* were immunostained with anti-Elav antibody for photoreceptors and bristle groups, or co-stained with anti-BarH1 and anti-E-cad antibodies for primary pigment cells and cell boundaries, respectively. Dashed circles: individual primary pigment cell clusters or the corresponding ommatidia. Scale bars: 10 μm.

(H) Pupal eye at 44 hrs APF with *bon* knocked down using *GMR-GAL4* was immunostained with anti-Cut (Ct) antibody for cone cells. Dashed circles: individual cone cell clusters per ommatidium. Scale bars: 10 μm.

(I) Quantification of the cone cell numbers per ommatidium for the indicated genotypes, including the one shown in H. The *p* values were determined using Fisher's exact test for ommatidia with 4 cone cells (CC) per ommatidium and those with >4 CC per ommatidium. Number of the cone cell clusters quantified: n≥280 from ≥3 pupal eyes per genotype. See also Table S5 for details.

(J) Adult wings expressing indicated transgenes with a wing blade driver *C5-GAL4* were examined for the morphology and the number of trichomes. Knockdown of *bon* showed thinner trichomes.

Right panels: enlarged ventral views of the boxed areas on the left. Scale bars: left, 200 μm; enlarged views, 20 μm.

(K) Quantification of trichome numbers in the wing blade of the indicated genotypes shown in J. Knockdown of *bon* did not affect the number of trichomes. Data shown as mean ± SD of ≥3 adult wings. Detailed numbers are provided in Table S5.

(L-M'') SEM images of adult notum with indicated genotypes. The mosaic clones were generated by heat shock at 112 hrs after egg deposition (AED) and were marked by the absence of $Sb^{63b}$. Arrowheads indicate short bristles that are positive for $Sb^{63b}$. Only the clone areas had normal-length, non-*Sb* bristles. The bristles in $bon^{21B}$ clones were thinner compared to wild type control clones, while the surrounding trichomes were not affected. However, the extent of the clone area beyond the bristle could not be determined in this experiment, as *Sb* does not affect trichomes. L' and M': enlarged views of boxed areas in L and M, respectively. L'' and M'': enlarged views around the socket of bristles boxed in L' and M', respectively. Scale bars: L/M, 100 μm; L'/M', 50 μm; L''/M'', 10 μm.

**Figure S4**

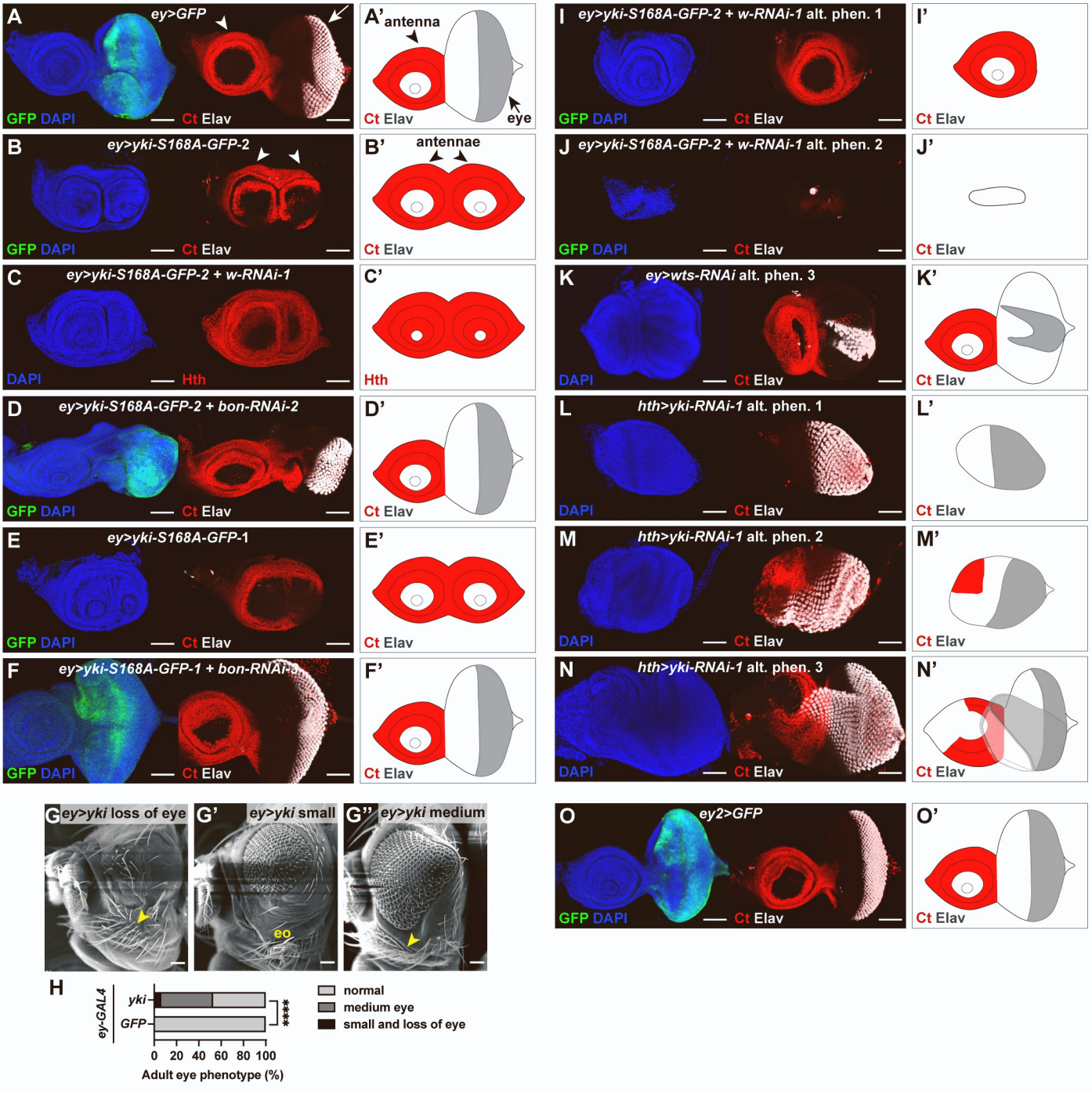
A
ey>GFP
GFP DAPI
Ct Elav
A'
antenna
eye
B
ey>yki-S168A-GFP-2
B'
antennae
C
ey>yki-S168A-GFP-2 + w-RNAi-1
DAPI
Hth
C'
D
ey>yki-S168A-GFP-2 + bon-RNAi-2
D'
E
ey>yki-S168A-GFP-1
E'
F
ey>yki-S168A-GFP-1 + bon-RNAi-2
F'
I
ey>yki-S168A-GFP-2 + w-RNAi-1 alt. phen. 1
I'
J
ey>yki-S168A-GFP-2 + w-RNAi-1 alt. phen. 2
J'
K
ey>wts-RNAi alt. phen. 3
K'
L
hth>yki-RNAi-1 alt. phen. 1
L'
M
hth>yki-RNAi-1 alt. phen. 2
M'
N
hth>yki-RNAi-1 alt. phen. 3
N'
G
ey>yki loss of eye
G'
ey>yki small
eo
G''
ey>yki medium
H
ey-GAL4
yki
GFP
****
0 20 40 60 80 100
Adult eye phenotype (%)
normal
medium eye
small and loss of eye
O
ey2>GFP
O'

**Figure S4. Yki and Bon promote antennal fate and epidermal fate while suppressing eye fate (related to Figure 4).**

(A-F') L3 eye-antennal discs with the indicated genotypes (quantified in Figure 4I) were immunostained with anti-Ct or anti-Hth antibody for the antennal compartment and anti-Elav antibody for the neuronal eye fate. (A'-F') Schematic illustrations of A-F. Arrows: eye discs, arrowheads: antennal discs. Scale bars: 50 μm.

(G-G'') SEM images of adult eyes expressing wild-type Yki with *ey-GAL4*. Representative images are shown for loss of eye (G), small eye (G') and medium eye (G'') phenotypes. eo, epidermal outgrowth. Arrowheads: extra vibrissae. Scale bars: 50 μm.

(H) Quantification of the phenotypes in G-G''. *p* value was determined using Fisher's exact test for normal and abnormal eye populations. Number of adult eyes quantified: n≥100. See also Table S5 for details.

(I-K') Representative alternative eye disc phenotypes quantified in Figure 4I. (I'-K') Schematic illustrations of I-K. Scale bars: 50 μm.

(L-N') Representative alternative loss of antenna phenotypes quantified in Figure 4P. (L'-N') Schematic illustrations of L-N. Scale bars: 50 μm.

(O-O') L3 eye-antennal disc expressing GFP with *ey-GAL4*-2 (*ey2*) was immunostained with anti-Ct and anti-Elav antibodies and used as a control for *ey2>bon-mCherry* (Figure 4J). (O') Schematic illustration of O. Scale bars: 50 μm.

**Figure S5**

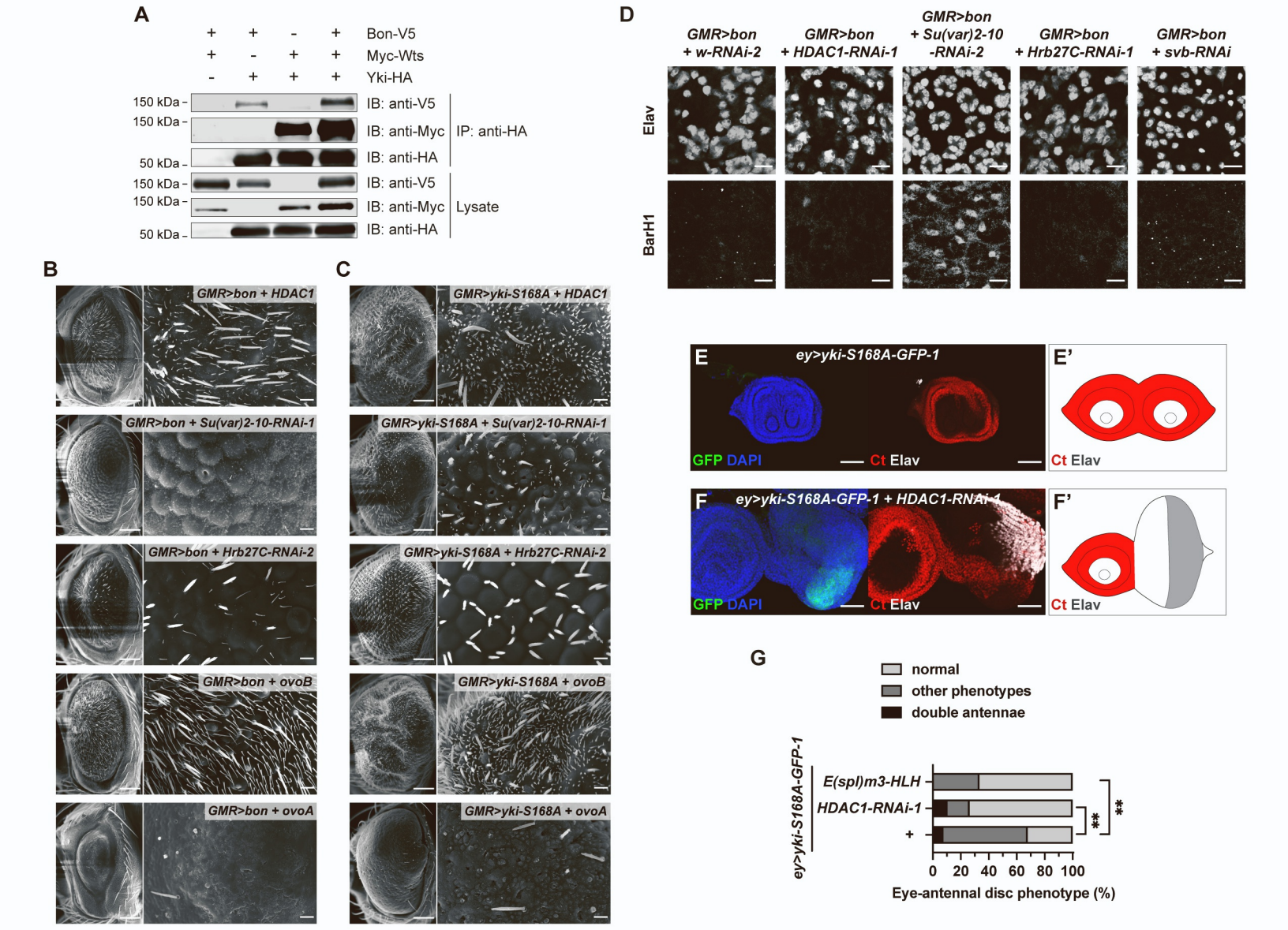
A
+ + - + Bon-V5
+ - + + Myc-Wts
- + + + Yki-HA
150 kDa
150 kDa
50 kDa
IB: anti-V5
IB: anti-Myc
IB: anti-HA
IP: anti-HA
150 kDa
150 kDa
50 kDa
IB: anti-V5
IB: anti-Myc
IB: anti-HA
Lysate
B
GMR>bon + HDAC1
GMR>bon + Su(var)2-10-RNAi-1
GMR>bon + Hrb27C-RNAi-2
GMR>bon + ovoB
GMR>bon + ovoA
C
GMR>yki-S168A + HDAC1
GMR>yki-S168A + Su(var)2-10-RNAi-1
GMR>yki-S168A + Hrb27C-RNAi-2
GMR>yki-S168A + ovoB
GMR>yki-S168A + ovoA
D
GMR>bon + w-RNAi-2
GMR>bon + HDAC1-RNAi-1
GMR>bon + Su(var)2-10 -RNAi-2
GMR>bon + Hrb27C-RNAi-1
GMR>bon + svb-RNAi
Elav
BarH1
E
ey>yki-S168A-GFP-1
GFP DAPI
Ct Elav
E'
Ct Elav
F
ey>yki-S168A-GFP-1 + HDAC1-RNAi-1
GFP DAPI
Ct Elav
F'
Ct Elav
G
normal
other phenotypes
double antennae
ey>yki-S168A-GFP-1
E(spl)m3-HLH
HDAC1-RNAi-1
+
**
**
0 20 40 60 80 100
Eye-antennal disc phenotype (%)

**Figure S5. Bon and Yki control eye-epidermal fate determination through cofactors (related to Figures 5 and 7).**

(A) Co-IP of Bon-V5, Myc-Wts, and Yki-HA expressed in S2 cells, pulling down with Yki-HA.

(B-C) SEM images of adult eyes with the indicated genotypes quantified in Figure 5L. Crosses with Bon were kept at 25°C (B), and crosses with Yki-S168A were set up at 25°C and shifted to 29°C after the emergence of first instar larvae (C). Scale bars in left panels: 100 μm; in enlarged views in right panels: 10 μm.

(D) Pupal eyes at 44 hrs APF expressing the indicated *UAS* transgenes with *GMR-GAL4* were immunostained with anti-Elav antibody for photoreceptors and bristle groups, or anti-BarH1 antibody for primary pigment cells. Scale bars: 10 μm.

(E-F') L3 eye-antennal discs expressing the indicated *UAS* transgenes with *ey-GAL4* were immunostained with anti-Ct antibody for the antennal compartment and anti-Elav antibody for the neuronal eye fate. (E'-F') Schematic illustrations of E-F. Scale bars: 50 μm.

(G) Quantification of the phenotypes for genotypes in E-F and Figures 7J-K. *p* values were determined using Fisher's exact test for normal and abnormal eye disc populations. Number of discs quantified: n≥19. Detailed numbers are provided in Table S5.

# Figure S6

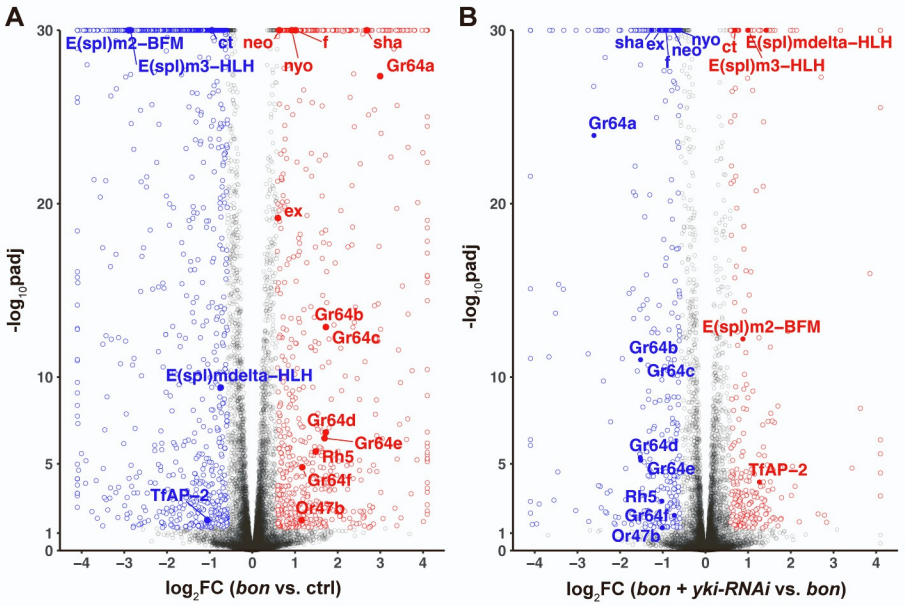


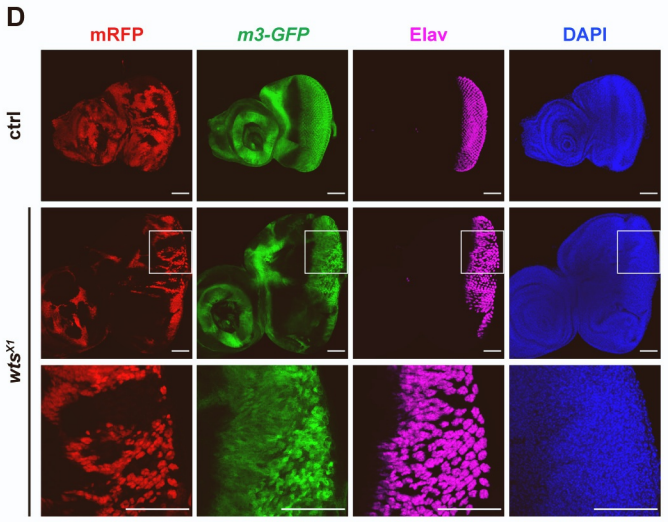


C

| | Yki ChIP peak embryo[1] | Yki ChIP peak wing disc[1] | Sd DamID peak L3 CNS[2] | Bon ChIP peak embryo[3] |
|---|---|---|---|---|
| *sha* | No | No | No | No |
| *f* | No | No | No | No |
| *neo* | No | Yes | No | No |
| *nyo* | No | No | No | No |
| *Gr64s* | No | No | No | No |
| *Or47b* | No | No | No | No |
| *E(spl)mdelta-HLH* | Yes | Yes | Yes | One peak in this region |
| *E(spl)m2-BFM* | No | Yes | Yes | |
| *E(spl)m3-HLH* | Yes | Yes | No | |
| *ct* | Yes | Yes | Yes | No |
| *TfAP-2* | Yes | Yes | Yes | No |

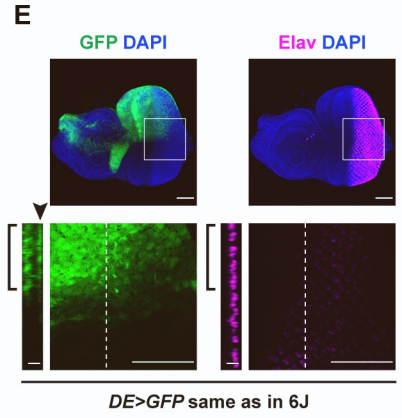


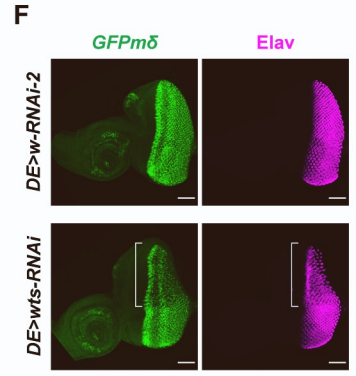


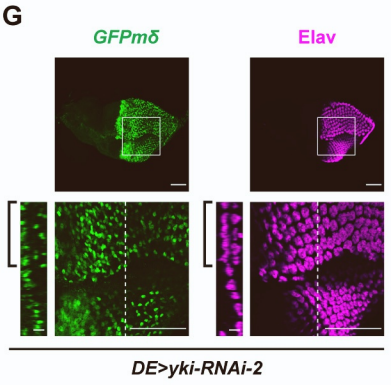


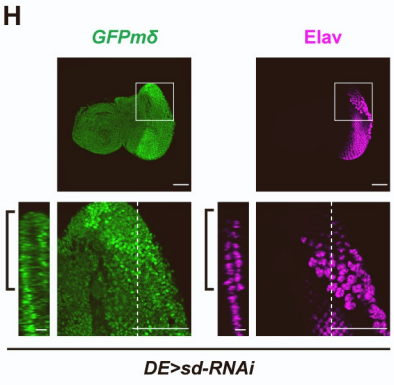


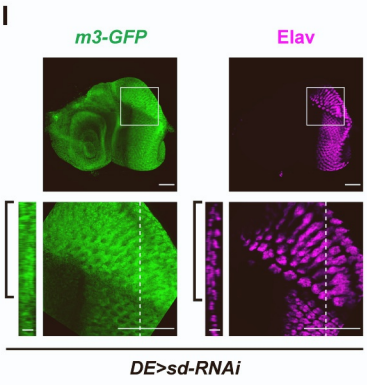


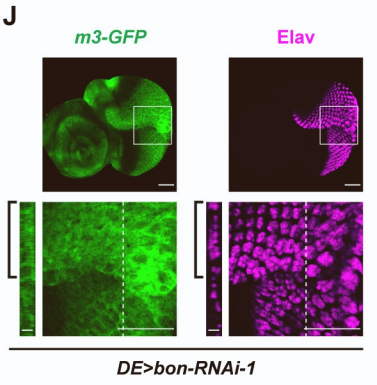


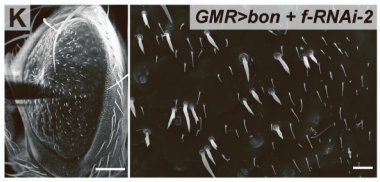


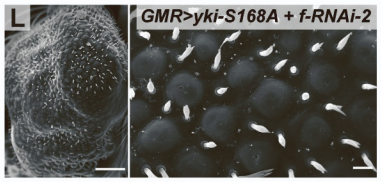


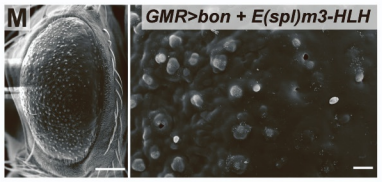


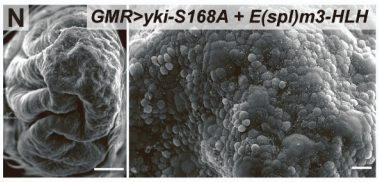

**Figure S6. Bon and Yki control the eye-antenna-epidermis fate determination through their joint transcriptional targets (related to Figures 6 and 7).**

(A-B) Volcano plots showing differentially expressed genes in *GMR>bon-mCherry* compared to *GMR>mCherry* (ctrl) (A) and *GMR>bon-mCherry + yki-RNAi-1* compared to *GMR>bon-mCherry* (B). Colored circles: significantly regulated genes with fold change (FC) ≥ 1.5 in both directions and *p* adj. ≤ 0.05. Red circles: significantly upregulated genes. Blue circles: significantly downregulated genes. Solid circles with labels: genes of interest.

(C) Analysis of published ChIP-seq and DamID-seq datasets for genes of interest jointly regulated by Bon and Yki. Bon-activated/Yki-dependent genes are in red, and Bon-repressed/Yki-dependent genes are in blue. The assignment of Yes or No was based on the presence of a called peak from 1 kb upstream of the transcription start site to the end of the gene body. The following datasets are indicated with superscript numbers: 1. Yki ChIP-seq from 8-16 hrs embryos and L3 wing discs (GSE38594) [S1]. 2. DamID-seq of Sd from L3 central nervous system (GSE120731) [S2]. 3. Bon ChIP-seq from 16-24 hrs embryos (GSE25921) [S3].

(D) L3 eye-antennal discs with mosaic clones were immunostained with anti-GFP antibody for *m3-GFP* reporter and anti-Elav antibody for neuronal eye fate. DAPI was used to ensure that the loss of reporter and Elav was not due to the loss of cells. Mutant clones were generated with *eyFLP* and marked by loss of mRFP. The exact genotypes are given in Method Details. Bottom panels: enlarged views of the boxed regions in $wts^{X1}$ clones. Scale bars: 50 μm.

(E) L3 eye-antennal disc expressing *UAS-GFP* with *DE-GAL4* (same as the one in Figure 6J) was used to reveal the expression pattern of the *DE-GAL4* driver and was immunostained with anti-Elav antibody for the normal pattern of this neuronal eye fate marker. Bottom-right panels: enlarged views of the boxed regions with focus set at the peripodial epithelium (PE), bottom-left panels: orthogonal sections at the dashed lines. Brackets: dorsal compartment expressing GFP in both disc proper (DP) and PE. Arrowhead: PE layer. The orthogonal sections and their scale bars were scaled 2x along the z axis for easier visualization. Scale bars: 5 μm in orthogonal views and 50 μm in others.

(F) L3 eye-antennal discs expressing indicated *UAS* transgenes with *DE-GAL4* were immunostained with anti-GFP antibody for *GFPmδ* reporter and anti-Elav antibody for neuronal eye fate. Brackets: loss of *GFPmδ* and Elav in the dorsal compartment with *DE>wts-RNAi*. Scale bars: 50 μm.

(G-J) L3 eye-antennal discs expressing indicated transgenes with *DE-GAL4* were immunostained with anti-GFP antibody for *GFPmδ* or *m3-GFP* reporter and anti-Elav antibody for neuronal eye fate. Penetrance for S6J: 12.5% (n=8). Top and bottom-right panels are focused at the PE.

Bottom-right panels: enlarged views of the boxed regions, bottom-left panels: orthogonal sections at the dashed lines, brackets: gain of *GFPmδ*, *m3-GFP*, and Elav in the PE layer of the dorsal compartment. The orthogonal sections and their scale bars were scaled 2x along the z axis for easier visualization. Scale bars: 5 μm in orthogonal views and 50 μm in others.

(K-N) SEM images of adult eyes with indicated genotypes quantified in Figure 7I. Crosses with Bon were kept at 25°C (K and M), and crosses with Yki-S168A were set up at 25°C and shifted to 29°C after the emergence of first instar larvae (L and N). Scale bars in left panels: 100 μm; in enlarged views in right panels: 10 μm.

Figure S7

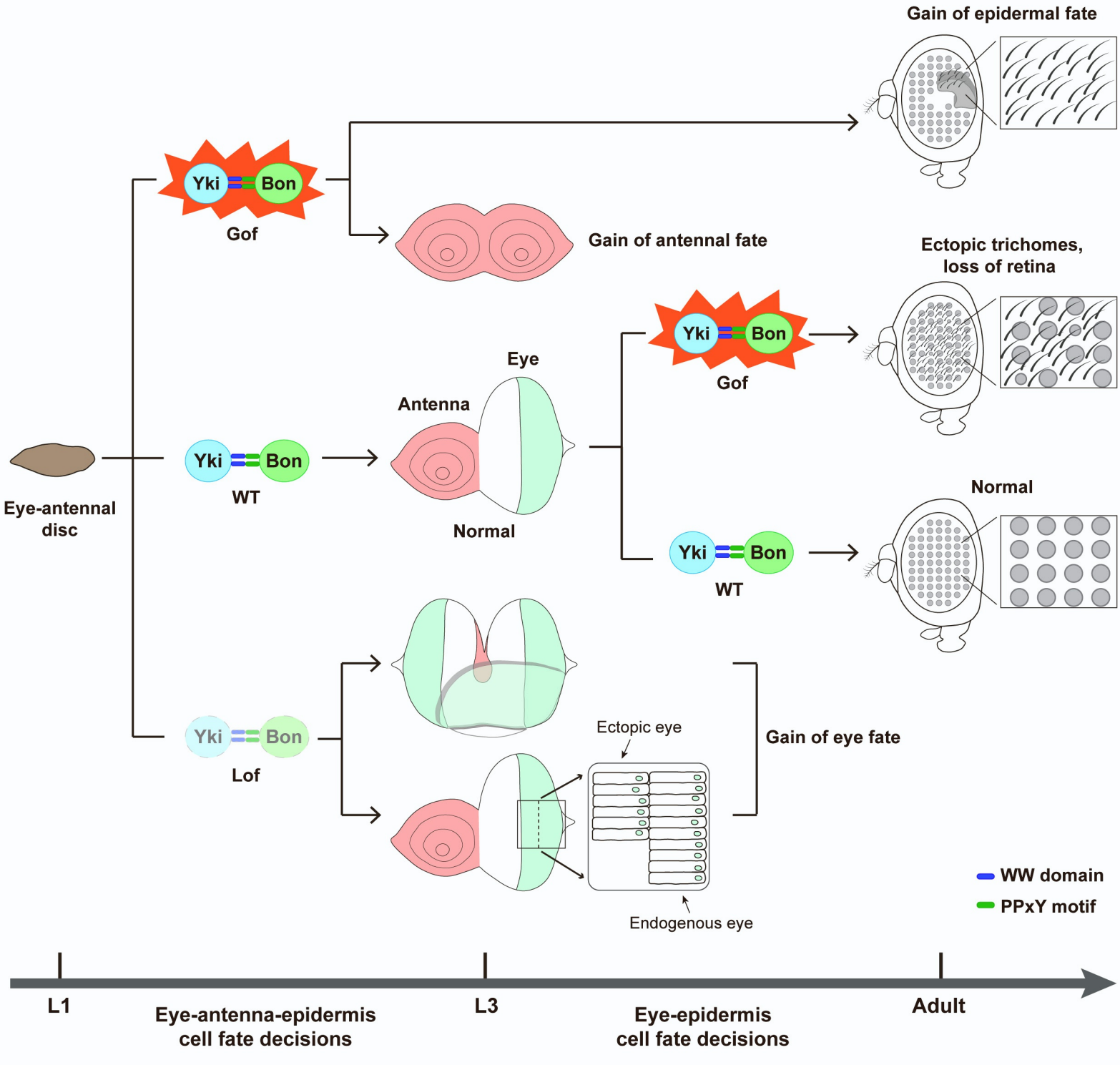
Gain of epidermal fate
Yki
Bon
Gof
Gain of antennal fate
Ectopic trichomes,
loss of retina
Yki
Bon
Gof
Eye
Antenna
Eye-antennal
disc
Yki
Bon
WT
Normal
Normal
Yki
Bon
WT
Ectopic eye
Yki
Bon
Lof
Gain of eye fate
Endogenous eye
WW domain
PPxY motif
L1
Eye-antenna-epidermis
cell fate decisions
L3
Eye-epidermis
cell fate decisions
Adult

**Figure S7. The Yki-Bon complex regulates cell fate decisions in the eye at two levels during *Drosophila* eye development (related to Figure 7 and Discussion).**

First, the Yki-Bon complex promotes antennal and epidermal fates and inhibits the eye fate during the early eye field specification, before the L3 larval stage, whereas Wts counteracts this activity. When the Yki-Bon complex is activated early (Gof, gain of function), it results in eye-to-antenna transformation and/or epidermal outgrowth. Early inactivation of the complex (Lof, loss of function) results in ectopic eye fate seen as antenna-to-eye transformation or induction of ectopic eye markers in the eye discs at L3. Second, after the segregation of the eye/antenna/epidermis fields and the start of MF in L3, the Yki-Bon complex promotes the epidermal cell fate while suppressing the retinal fate, whereas Wts ensures the proper differentiation of the retina by inhibiting Yki. When the Yki-Bon complex is activated late (Gof after L3), it induces ectopic epidermal cells with trichomes at the expense of the retinal cells.

**Supplemental References:**


[S1]. Oh, H., Slattery, M., Ma, L., Crofts, A., White, K.P., Mann, R.S., and Irvine, K.D. (2013). Genome-wide association of Yorkie with chromatin and chromatin-remodeling complexes. Cell Rep *3*, 309-318. 10.1016/j.celrep.2013.01.008.

[S2]. Vissers, J.H.A., Froldi, F., Schroder, J., Papenfuss, A.T., Cheng, L.Y., and Harvey, K.F. (2018). The Scalloped and Nerfin-1 Transcription Factors Cooperate to Maintain Neuronal Cell Fate. Cell Rep *25*, 1561-1576 e1567. 10.1016/j.celrep.2018.10.038.

[S3]. Negre, N., Brown, C.D., Ma, L., Bristow, C.A., Miller, S.W., Wagner, U., Kheradpour, P., Eaton, M.L., Loriaux, P., Sealfon, R., et al. (2011). A cis-regulatory map of the Drosophila genome. Nature *471*, 527-531. 10.1038/nature09990.